NOVEMBER 1959 VOLUME 5 (1959) No. 5

GREGG M. SINCLAIR LIBRARY
UNIVERSITY OF HAWAII
8-7-63

NUCLEAR INSTRUMENTS & METHODS

A JOURNAL ON ACCELERATORS, INSTRUMENTATION AND TECHNIQUES IN NUCLEAR PHYSICS

EDITOR: K. SIEGBAHN - UPPSALA

CONTENTS

K. A. DOLMATOVA and V. M. KELMAN, A longitudinal β-spectrometer with compensated spherical aberration . . . 269
FRANK KRIENEN, The tuningfork frequency modulator of the CERN synchro-cyclotron. Part I. General design . . . 280
FRANK KRIENEN, The tuningfork frequency modulator of the CERN synchro-cyclotron. Part II. Mechanics of tuningfork . . . 292
J. APTER, J. ROUSSEL, J. M. TISSIER et R. WAHL, Selecteur 1000 canaux temps de vol . . . 300
RICHARD L. CALDWELL and WILLIAM R. MILLS JR., Activation analysis in petroleum exploration research . . . 312
K. H. LAUTERJUNG und W. GRUHLE, Ein Gerät zur schnellen Registrierung ausgedehnter radioaktiver Strahler . . . 323
W. M. JONES, A. C. L. BARNARD, K. M. YOUNG, E. D. TAYLOR, D. G. WATERS and H. B. MUNDY, Nuclear plate cameras for the measurement of proton energies emitted from a toroidal discharge in deuterium . . . 327
J. C. BARTON, Simple core scaling circuits . . . 332
V. I. DANILOV, YU. N. DENISOV, V. P. DMITRIEVSKY, V. P. DZHELEPOV, A. A. GLAZOV, V. V. KOLGA, A. A. KROPIN, LU NE-CHUAN, V. S. RYBALKO, L. A. SARKISYAN, A. L. SAVENKOV, D. P. VASILEVSKAYA, B. I. ZAMOLODCHIKOV and N. L. ZAPLATIN, Starting up of the cyclotron with space variation of the magnetic field . . . 335
A. A. VOROBJEV and L. S. SOKOLOV, Withdrawal of a beam of accelerated electrons out of the chamber of a cyclical accelerator without the application of a lead-out device . . . 337
Book Reviews . . . 339
Author Index . . . 341
Subject Index . . . 343
Book Reviews Index . . . 344

LAST NUMBER OF THIS VOLUME

NORTH-HOLLAND PUBLISHING COMPANY - AMSTERDAM

NUCLEAR INSTRUMENTS AND METHODS

A journal on accelerators, instrumentation and techniques in nuclear physics

EDITOR: K. SIEGBAHN, UPPSALA

EDITORIAL BOARD:

J. B. ADAMS (CERN)
F. A. ALSINA (Buenos Aires)
E. AMALDI (Rome)
H. L. ANDERSON (Chicago)
K. T. BAINBRIDGE (Cambridge, Mass.)
C. J. BAKKER (CERN)
P. R. BELL (Oak Ridge)
R. E. BELL (Montreal)
A. BERTHELOT (Saclay)
H. BRINKMAN (Groningen)
E. H. COOKE–YARBOROUGH (Harwell)
S. DE BENEDETTI (Pittsburgh)
M. DE HEMPTINNE (Louvain)
A. DE-SHALIT (Rehovoth)
M. DEUTSCH (Cambridge, Mass.)
S. DU TOIT (Pretoria)
B. S. DŽELEPOV (Leningrad)
W. GENTNER (Heidelberg)
P. C. GUGELOT (Amsterdam)
H. HALBAN (Paris)
O. HAXEL (Heidelberg)
P. HUBER (Basel)
D. J. HUGHES (Brookhaven)
S. KIKUCHI (Tokyo)
J. KOCH (Copenhagen)
M. S. KOZODAEV (Moscow)
S. LIVINGSTON (Cambridge, Mass.)
E. M. MCMILLAN (Berkeley)
M. G. MEŠČERJAKOV (Moscow)
P. B. MOON (Birmingham)
M. L. OLIPHANT (Canberra)
W. PAUL (Bonn)
A. S. RAO (Bombay)
G. SALVANI (Rome)
P. SAVIČ (Belgrade)
P. SCHERRER (Zürich)
CH. SCHMELZER (CERN)
H. W. B. SKINNER (Liverpool)
R. TANGEN (Oslo)
D. TAYLOR (Northampton)
V. I. VEKSLER (Moscow)
O. WERNHOLM (Stockholm)
G. VON DARDEL (CERN)
R. R. WILSON (Cornell)
S. D. WINTER (Saclay)

INSTRUCTIONS FOR CONTRIBUTORS

Contributions may be sent to the Editor, Professor K. Siegbahn, Institute of Physics, University of Uppsala, Sweden, either directly or through the intermediation of one of the members of the Editorial Board. Contributions may be written in English, French or German but should always, except for very short papers, be supplied with a brief abstract in English. Figures should be in inked original drawings or glossy prints and they should be sufficiently large. Contributors should make sure that important details in drawings and photographs will show up clearly in the diminished copy used by the publisher.

Books for review should be sent to Professor Siegbahn.

Objective and descriptive material on endeavours and product developments from the industry for the section "Spotlight on Industry" should be sent directly to the publishers, North-Holland Publishing Company, P.O. Box 103, Amsterdam.

Nuclear Instruments and Methods is published monthly. The subscription price of a volume of 360 pages is $ 17.00 (130 s), postage free.

Subscription should be sent to the publishers, North-Holland Publishing Company. P.O. Box 103. Amsterdam or to any subscription-agent.

No part of this issue may be reproduced in any form, by print, photoprint, microfilm or any other means without written permission from the publisher. Reprints, photoprints or microfilms are obtainable at cost from the publisher.

PHILIPS

equipment for

Nuclear Physics and

Atomic Energy

- Synchro-cyclotrons for various final energies.
- Cockcroft-Walton accelerators.
- Generators for very high d.c. voltages.
- Linear electron accelerators.
- Reactor control instrumentation.
- Radiation measuring and detection equipment.
- Civil defence instruments.
- Area monitoring instrumentation.
- Geiger counter tubes.
- Photomultipliers.
- Radio-active isotopes.
- Air & gas liquefiers.
- Vacuum measuring equipment.

Generally low-level beta-counting involves the use of relatively cumbersome and heavy equipment, which occupies quite a lot of laboratory space. Thanks to the introduction of a new type of guard counter, an invention of the Philips Research Laboratories, it was found possible to solve space and weight problems in a neat way. Shown here is the Low-Level Beta-Counting Arrangement, type PW 4127, and its corresponding measuring equipment. Background-reduction to less than 1.3 c.p.m. is obtained with a thin end-window counter used for measuring low-energy betas, and to less than 1.5 c.p.m. with an end-window counter for general low-intensity work.
The shielding comprises 30 mm of special lead, some 250 years old, with an extremely low specific activity, and 100 mm of iron.

PHILIPS

PHILIPS

Nuclear Equipment

For further information please apply to one of the following addresses:

N.V. PHILIPS' GLOEILAMPENFABRIEKEN, Scientific Equipment Department, Eindhoven-Holland
RESEARCH & CONTROL INSTRUMENTS LTD., Instrument House, 207/215, King's Cross Road, London WC1
PHILIPS ELECTRONICS INC., Instruments Division, 750, South Fulton Avenue, Mount Vernon N.Y. U.S.A.

Elcor inc.
1225 W. BROAD ST.,
FALLS CHURCH, VA.

MODEL A 309
CURRENT INDICATOR AND INTEGRATOR

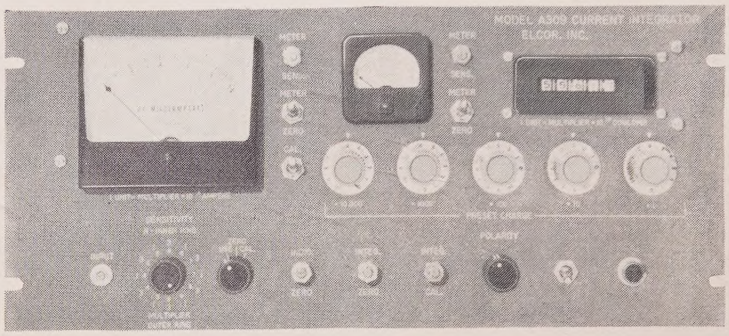

MODEL A 309 A

FEATURES

- Wide current range: 1 x 10^{-3} to 3 x 10^{-9} amp. in 12 switch settings.
- High accuracy: 1% of full scale.
- Internal calibrating current source to check proper operation.
- Front panel switch allows instrument to be used with current of either polarity.
- Pre-setting feature provides means of safeguarding against over-exposure.
- Developed especially for use with Van de Graaff and other high-voltage accelerators.
- Permits many experiments with particle accelerators that would otherwise be difficult or impossible.
- Register readout gives digital accuracy on charge measurement.

The versatility and accuracy of two instruments in one!

1. Measures currents from 1 milliampere to 3 milli-microamperes.
2. Integrates input current and registers accumulated charge.

GENERAL DESCRIPTION—The Model A309 Current Indicator and Integrator is a sensitive current indicator that also measures the total charge collected in a given length of time. Developed especially for use with high-voltage particle accelerators such as the Van de Graaff generator, the instrument is also ideally suited for other applications requiring the measurement of accumulated charge or the integration of a variable current.

The full-scale sensitivity of the instrument can be varied from 1 milliampere to 3 milli-microamperes in twelve ranges. For convenience in checking the performance and accuracy of the instrument, an internal calibrating current source is provided for each range. The accumulated charge is indicated on a 5-decimal digit register. Any number up to 99,999 can be preset into the instrument, and upon reaching the corresponding charge a relay closes to actuate a warning device or control auxiliary equipment. In applications where X-rays are being generated, this feature affords protection against accidental over-exposure.

Input current of either polarity can be measured and integrated, and a front panel switch enables the instrument to be immediately changed from one polarity to the other. Advanced circuit techniques have been employed to achieve low input impedance, negligible drift, and a high overall accuracy and reliability.

Two models are available with the same specifications except for the method of presetting. In the Model A309A the presetting means consists of five front-panel switches. Presetting in the Model A309B is accomplished by manual adjustment of five presetting wheels that are accessible through the hinged cover of the register used in this model.

SPECIFICATIONS

1. Input current for full-scale meter deflection — 1 x 10^{-3} to 3 x 10^{-9} ampere in twelve switch settings.
2. Polarity of input current — positive or negative, controlled by front-panel switch.
3. Current indicating means — 4½" meter.
4. Charge indicating means — 5-decimal-digit register and 2½" meter
5. Maximum charge indicating capacity — 99,999 units.
   Note: Each unit is equal to one coulomb multiplied by the numerical value of the full-scale current.
6. Maximum integrating time — 28 hours.
7. Integrating rate for full-scale current — 1 unit per second.
8. Method of presetting:
   Model A309A — five front-panel switches.
   Model A309B — five presetting wheels in register.
9. Accuracy (Indicating and integrating accuracy, based on full-scale current) — 1%.
10. Maximum drift — .01% per hour.
11. Maximum input voltage for full-scale current — 2 millivolts.
12. Minimum signal-source impedance for 1% accuracy — 1 ohm divided by numerical value of full-scale current.
13. Calibration — Internal reference current provided for each current range.
14. Power Input — 110–125 volts, 50-60 cps.
15. Dimensions — 19" wide x 8¾" high x 13¼" deep.
16. Mounting — standard 19" relay rack.
17. Weight — approximately 25 lbs.
18. Price: Model A309A — $1674.00,
    Model A309B — $1524.00.

ELCOR,—INC. • 1225 W. BROAD STREET • FALLS CHURCH, VA.

Telephone JEfferson 2-7718 A subsidiary of Fairfax Manufacturing Co., Inc. Bulletin No. 24-1258

PRACTICAL ACCURACY

The portable CN-110 256-channel pulse analysis system — can be changed from pulse height analysis to time-of-flight to pulsed neutron measurement — or to some special program — simply by interchanging the compact plug-in logic units in the front panel. The basic computer with plug-in weighs only 30 lbs., and can be bench or rack-mounted or carried anywhere in a portable case for laboratory or field work. Power consumption is only 25 watts — needs no auxiliary cooling . . . can be set up for analog, digital or binary readout of various methods.

. . . new portability in TMC instruments

These new instruments from TMC, with completely transistorized circuits and efficient, straightforward design, are the most practical answer to the need for portable yet accurate pulse measurement instruments. Whether in a laboratory or in the field, the extreme reliability, accuracy and compactness of these instruments combine to provide convenient, dependable operation wherever they are set up.

The SG-10A Serviscaler is an extremely economical and portable instrument designed for training or general laboratory use. All-transistor circuits are housed in a 12 lb., 12¾" x 9" x 5⅛" package. Continuous high voltage, adjustable from 600 to 1600 volts; resolving time better than 200 μsec; power consumption of only 20 watts. Price is $350.

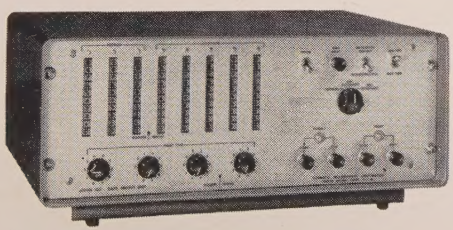

The No. 220 Data Handling Unit — a logical companion to the CN-110, is both a timer and data-handling unit. During the CN-110's accumulation cycle the 220 can be used for true or live timing, then instantly switched to a manual, semi-, or fully-automatic digital readout cycle (destructive or non-destructive). The compact 220 may be used with various paper tape punching and printing machines.

TMC also manufactures a complete line of single instruments, systems and related equipment for radiation measurement. Complete details are available on request.

TMC

TECHNICAL MEASUREMENT CORPORATION

441 WASHINGTON AVENUE, NORTH HAVEN, CONNECTICUT

COMPACT 100 CHANNEL PULSE HEIGHT ANALYZER

The C.D.C. KICKSORTER

developed by Atomic Energy of Canada and manufactured by Computing Devices of Canada Limited

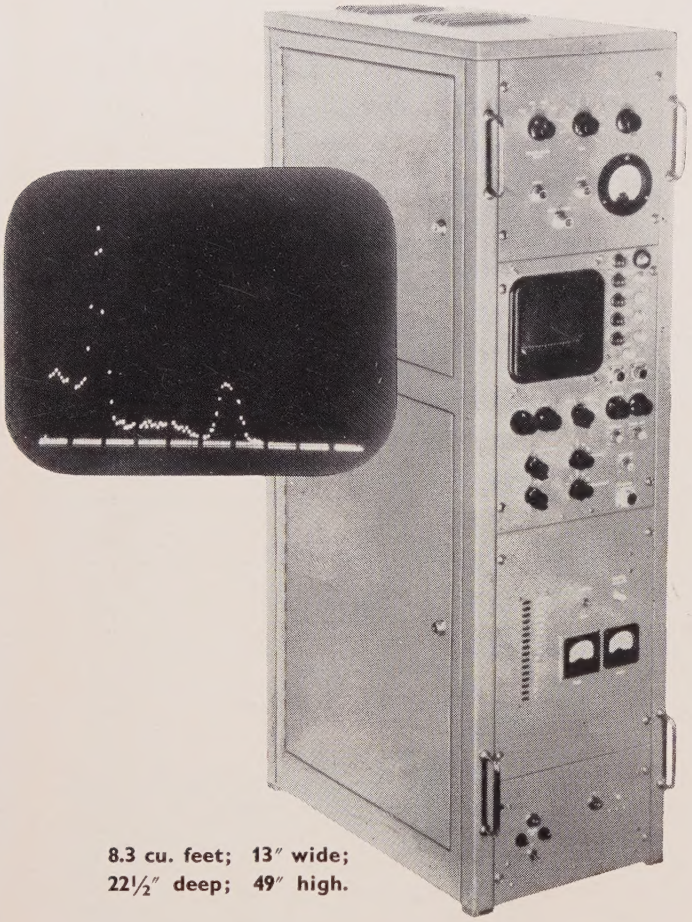

8.3 cu. feet; 13″ wide; 22½″ deep; 49″ high.

88% Transistorized

- Printed Circuitry
- Low Maintenance—High Reliability
- Compact—Semiportable
- Low Power Consumption—120 watts
- No Ventilation or Cooling problems

Highly Versatile

- Oscilloscope display
- Binary manual count readout allows the count on any channel to be displayed in digital form
- Accessory readout devices: photo recording camera, strip chart recorder, punch tape
- Magnetic core memory—65,535 counts can be stored per channel
- Permanent count storage—sixteen magnetic cores for each of the 100 channels

Bendix International

The "Chalk River Kicksorter", recently developed and based on designs and specifications prepared by Atomic Energy of Canada Ltd. is an extremely fast, accurate and versatile instrument.

The "Kicksorter" is designed to span random pulses of various amplitudes and shapes, sort them out according to amplitude into 100 channels, and store a record of the counted pulses in a magnetic core memory. A simple computer with its magnetic core memory and versatile data display system make it possible to observe the pulse amplitude spectrum as it accumulates or after it has accumulated.

In addition to its wide use in gamma spectroscopy, it has many applications in the fields of medical research, neutron time-of-flight studies, radioactive fallout studies, shielding studies, oil well and uranium logging, neutron activation analyses, measuring of radioactivity in humans and other uses.

The analyzer is designed so that information accumulated may be displayed or read out in various ways. Data may be observed on the oscilloscope, or information already accumulated in the memory core may be displayed on the screen, plotted on a strip chart recorder, or printed out in decimal form on an automatic printer.

Since the unit is highly versatile, it can be modified to accommodate most applications which require additional features.

For additional information, wire or write to:

Bendix International

DIVISION OF BENDIX AVIATION CORPORATION

205 E. 42ND ST., NEW YORK 17, N.Y., U.S.A. Cable Address: "BENDIXINT"

Sales Representatives for Great Britain

NUCLEAR ENTERPRISES (G.B.) LTD.

BANKHEAD MEDWAY, SIGHTHILL; EDINBURGH 11, SCOTLAND

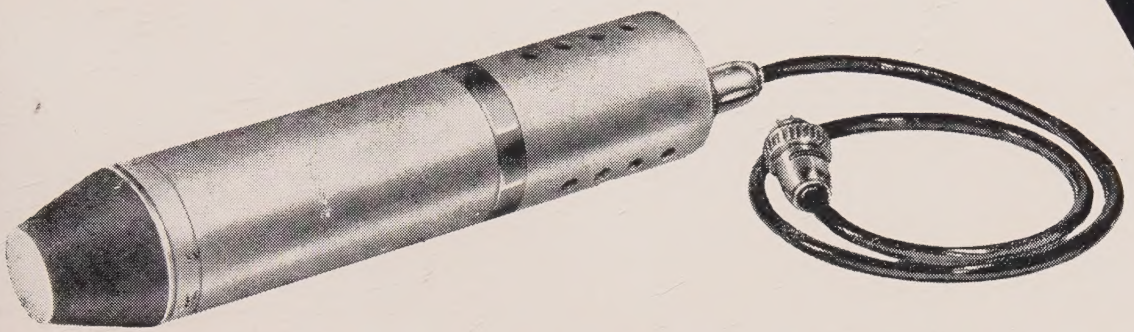

EKAF type 50301 Probe Scintillation Detector

This detector consists of a cylindrical aluminum tube (length 33 cm. x diam. 8 cm.), containing a selected EMI photomultiplier tube type 6097 AF and cathode follower; circuit cooling system incorporated. A 1½" x 1" NaJ (Tl) selected Harshaw scintillation crystal is glued on top of the EMI photomultiplier tube and is held in position by a special threaded locking device of dural. The instrument is fitted with 6 ft. connecting cable and plug. The probe is finished in EKAF blue baked enamel.

EKAF type 50302 Well-Type Probe Scintillation Detector

Same as EKAF type 50301, but length of probe is 34,5 cm. and the instrument is fitted with a 1¾" (diam.) x 2" (depth) NaJ (Tl) selected Harshaw Crystal with a well ¾" (diam.) x 1½" (depth).

EKAF

ELEKTRONISCH-KERNFYSISCHE APPARATEN FABRIEK N.V.,

Hartogstraat 5a
The Hague, Holland
Phone: 070-113959

Sales office: **N.V. NENIMIJ**
Laan Copes van Cattenburch 74
The Hague, Holland
Phone: 070-630977

NORTH-HOLLAND BOOKS

Paul Ehrenfest

COLLECTED SCIENTIFIC PAPERS

XII + 632 pages

Guilders 45,00 (90s.)

This volume makes widely scattered publications readily available. All Dutch articles appear here in English; the German publications are in the original language.

Sole Agency for U.S.A.:

Interscience Publishers Inc. — New York

NORTH-HOLLAND PUBLISHING COMPANY - AMSTERDAM

FOR SCINTILLATION & PROPORTIONAL COUNTING

Non-overloading Linear Amplifiers

MODELS 108 and 108 p

* GAIN–40,000, continuously variable
* RISE TIME–0.2 microsecond
* ACCEPTS + AND — PULSES

Tremendous Dynamic Range

EXCEEDS 1,000,000 (0.1 mV to 100 V)

Excellent linearity for small pulses in the presence of tremendous overloads that paralyze other amplifiers.
Model 108 P includes precision trigger type Pulse-Height Selector.

Model 413 Mercury relay precision sliding Pulser

The one pulser that fills every need of the Nuclear Physics Laboratory
0 to 100 Volts

10 full scale ranges from 1 mV to 100 volts
Fast rise and exponential decay of 1, 3, 10. 30, and 100 microsec simulate pulses from scintillation, proportional and Geiger counters.
Incorporates both manual control and precision motor drive.
The ideal instrument for precise calibration and test of pulse-height analyzers and other nuclear instrumentation.

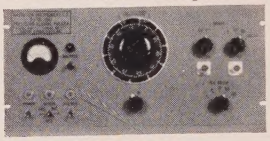

Window widths are determined AUTOMATICALLY, 10 × more ACCURATELY, 40 × FASTER than with conventional pulsers.

Model 108 Amplifier . . . . . $ 545.00
Model 108 P Amplifier (includes pulse-height selector) $ 595.00
Model 413 Precision Sliding Pulser . . . . . $ 630.00
Prices f.o.b. Silver Spring. Md.

RADIATION INSTRUMENT CO.

P.O. BOX 733 SILVERSPRING, MARYLAND, U.S.A.

NORTH-HOLLAND BOOKS

Analytical and Canonical Formalism in Physics

by

ANDRÉ MERCIER

Head of the Department of Theoretical Physics, University of Berne

6 × 9″ VIII + 222 pages Guilders 20.00 (40 s.)

THE CONTENTS

i LAGRANGIAN FORMALISM
ii LAGRANGIAN DENSITY
iii CANONICAL FORMALISM
iv CANONICAL FORM OF ELECTRODYNAMICS
v HAMILTONIAN DENSITIES
vi TRANSFORMATIONS
vii CANONICAL FORMALISM WITH VANISHING JACOBIAN DETERMINANT

Sole Agency for U.S.A.: Interscience Publishers Inc. – New York

NORTH-HOLLAND PUBLISHING COMPANY — AMSTERDAM

NOW BEING DELIVERED!

MODEL 34-8
TRANSISTORIZED 200 CHANNEL ANALYZER

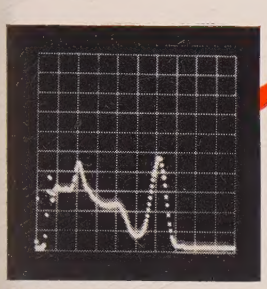

Cesium 137 spectrum photographed from CRT display of Model 34-8.

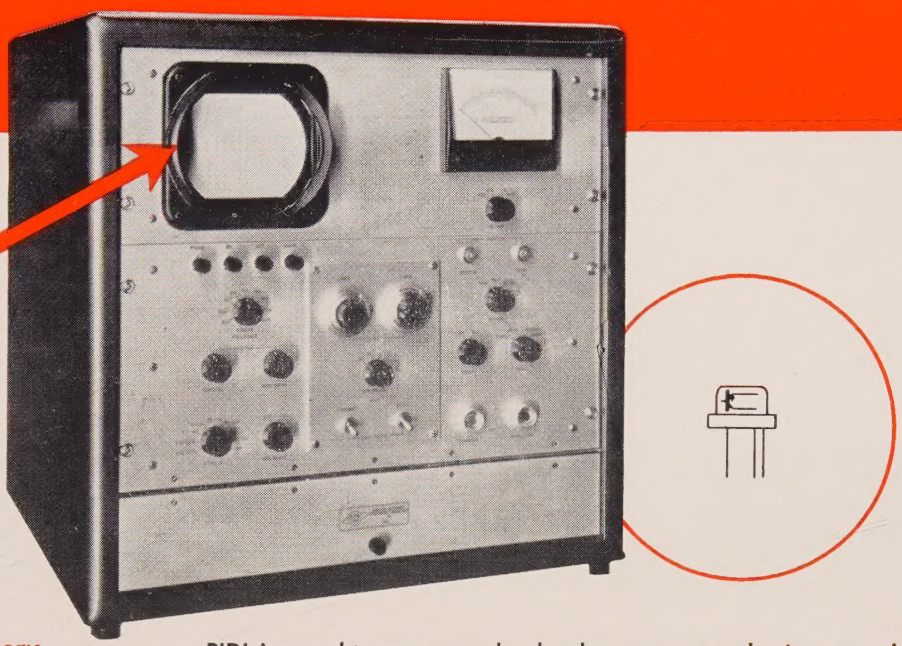

- Ferrite Core Memory
- 200 Channels
- Add-Subtract Logic
- Auto-Print
- Auto-Record
- Automatic Background Subtraction
- Memory Subgrouping
- External Programming
- Spectrum Transfer Circuit
- Coded Decimal Storage
- Parallel Coded Decimal Readout
- Multi-Channel Scaler Operation
- 10^5 Count Capacity
- Installation by Factory Engineer
- Course of Instruction Offered

RIDL is proud to announce the development — production — and delivery of the Model 34-8 Transistorized 200 Channel Analyzer. This unit is a **completely new** approach to the field of multi-channel analysis. This new approach, in conjunction with solid-state techniques — i.e., transistors in place of vacuum tubes, printed circuitry, etc. — allows compactness, low power consumption and heat dissipation and high reliability.

The STANDARD Model 34-8 is capable of operation as either a Multi-Channel *Pulse Height* Analyzer or a Multi-Channel Scaler (*Time* Analyzer). There are no extra plug-in modules to purchase in order to perform these separate functions. The change from one analysis mode to another is accomplished by the use of a single toggle switch.

In the Model 34-8, data is stored in the memory in coded decimal form. This, in conjunction with parallel coded decimal readout directly from the data register to the printer, eliminates the need for a 'Binary-to-Decimal Decoder'. The printout speed is therefore limited only by the particular printer used.

The Model 34-8 is another of the NEW line of instruments designed and developed by RIDL. Whatever your instrumentation problem may be, RIDL has the solution. Our staff is always available to answer your inquiries. Write today to Dept. 57 for complete information.

Available soon!
Model 34-12
Transistorized 400
Channel Analyzer

RIDL INC.

Radiation Instrument Development Laboratory, Inc.

5737 South Halsted Street, Chicago 21, Illinois • Phone TRiangle 3-2345

Representatives in major cities

MILLIMICROSECOND PULSE GENERATOR

Ultra fast rise time (2.5 millimicroseconds) and high frequency for advanced solid state, computer and research applications

MODEL 120B F.O.B. OAKLAND, CALIF. $1275

The 120B offers unique performance advantages over mercury and competing electronic generators. The 2.5 millimicrosecond rise time feature is ahead of the field and offers a new tool for fast, high resolution work. Two independently variable outputs add to its flexibility, as does the wide range of frequencies provided (10 cps to 10 Megacycles). Available also are an advanced scope triggering pulse and a fast, flexible gating input for complex pulse-time and pulse-amplitude selection.

SPECIFICATIONS

RISE TIME (10% to 90%)
Less than 2.5 millimicroseconds

PULSE WIDTH
2.5 to 25 millimicroseconds

REPETITION RATE (External or Internal)
10 cps to 10 Mc

OUTPUTS
(Two Independent Output Channels)
Amplitude, 0 to −8 volts (also 0 to +8)
Impedance, 93 ohms

TRIGGER OUTPUT
Positive 15 volt pulse

CONNECTORS
All BNC type

TRIGGER ADVANCE
120 millimicroseconds

EXTERNAL DRIVE
Delay, 50 millimicroseconds
Amplitude Required, 3 volts rms

ELECTRONIC GATE
Gating Time, less than 100 millimicroseconds
Amplitude Required, positive 20 vo

Write or wire E-H for additional informa

E-H RESEARCH LABORATORIES, INC.
1922 PARK BLVD. • GLENCOURT 2-1314 • OAKLAND 6, CALIFORNIA

NORTH-HOLLAND BOOKS

TURNING POINTS IN PHYSICS

A
Series of Lectures
given at
Oxford University
in
Trinity Term 1958

1959 5 × 7½″
viii + 192 pages
Guilders 10.50
20s.

by
R. J. BLIN-STOYLE
D. TER HAAR
K. MENDELSSOHN
G. TEMPLE
F. WAISMANN
D. H. WILKINSON

with an introduction
by
A. C. CROMBIE

Sole Agency for U.S.A.: Interscience Publishers Inc. – New York

NORTH-HOLLAND PUBLISHING COMPANY — AMSTERDAM

ELECTROMETER AMPLIFIER

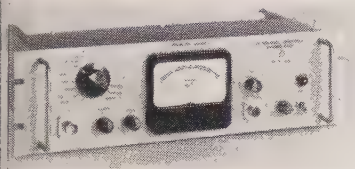

del 201C f.o.b. Oakland, Calif. $650

he 201C makes *both* DC and AC easurements to 10^{-15} ampere in e low current region. Excellent C stability, fast response, low ise and high sensitivity make an outstanding instrument. 16 nges, 10^{-6} to 3 x 10^{-15} ampere, d response to 40 microseconds ve it exceptional flexibility.

ELECTROMETER FOR AUTOMATIC CONTROL

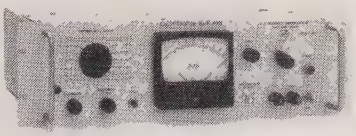

Model No. 202 f.o.b. Oakland, Calif. $775

Fast response time permits applications such as reactor control, radiation level alarms, component gauging and level controls. Measures current between 10^{-6} and 10^{-15} ampere. Ultra-high sensitivity with ultra-low noise. Response time: 200 microseconds for 3 x 10^{-9} ampere full scale. Has presettable high limit for actuation of external devices. Extremely stable; zero drift less than 3% per week.

ELECTROMETER MULTIMETER

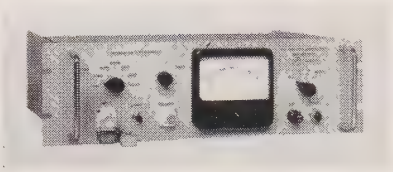

Model No. 215

Excellent stability 30μv/volt line change; high input impedance $10^{15}\Omega$; good sensitivity 200μv; large band pass 5 Kc. Uses — via external R, C, or E: millivoltmeter, 10 mv to 10 v scales, fast response; ammeter, $< 10^{-14}$ amps; ohmmeter, $>10^{16}$ ohms; current integrator, $< 10^{-13}$ coulomb.

E-H instruments are designed to meet the critical requirements of advanced work. Thanks to superior engineering and the finest components, these instruments have a remarkable record for stable performance.

Write or wire E-H for additional information

E-H RESEARCH LABORATORIES, INC.
1922 PARK BLVD. • GLENCOURT 2-1314 • OAKLAND 6, CALIFORNIA

NORTH-HOLLAND BOOKS

Asymptotic methods in Analysis

by

N. G. DE BRUIJN

Professor of Mathematics at the University of Amsterdam

6 × 9″ XII + 200 pages Guilders 20.00 (40s.)

CONTENTS

CH. I. INTRODUCTION
CH. II. IMPLICIT FUNCTIONS
CH. III. SUMMATION
CH. IV. THE LAPLACE METHOD FOR INTEGRALS
CH. V. THE SADDLE POINT METHOD
CH. VI. APPLICATIONS OF THE SADDLE POINT METHOD
CH. VII. INDIRECT ASYMPTOTICS
CH. VIII. ITERATED FUNCTIONS
CH. IX. DIFFERENTIAL EQUATIONS

Sole Agency for U.S.A.: Interscience Publishers Inc. - New York

NORTH-HOLLAND PUBLISHING COMPANY — AMSTERDAM

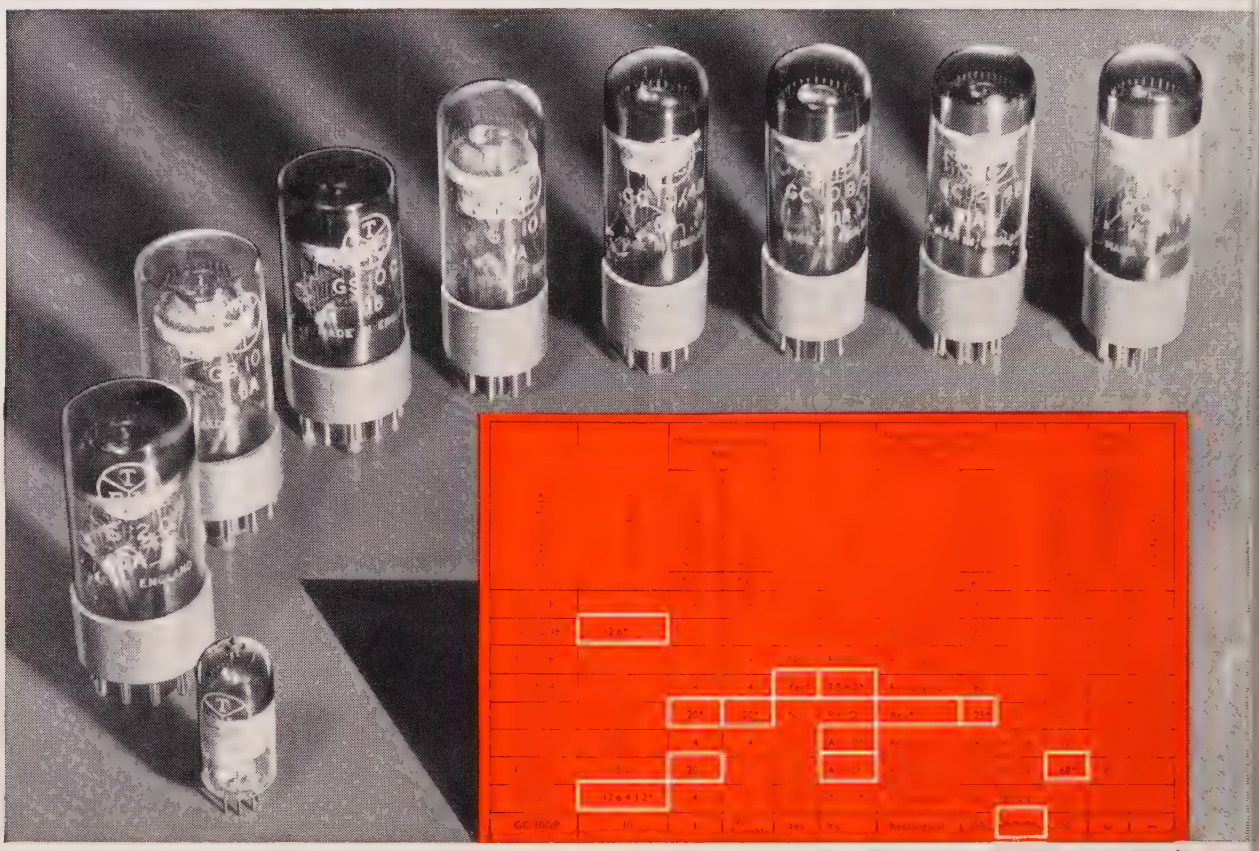

DEKATRONS

The most comprehensive range of glow-transfer scaling tubes in the world

FEATURES INCLUDED IN THIS RANGE

- BI-DIRECTIONAL COUNTING
- SPEEDS UP TO 20,000 COUNTS PER SEC.
- ONLY RANGE TO INCLUDE 10 OR 12 CATHODE TUBES
- ACCESS TO ONE, FOUR OR ALL CATHODES
- NO SHAPING OF INPUT WAVEFORM NECESSARY

Described as the most significant advance in the technique of slow and medium speed counting during the last decade, Dekatron scaling tubes have logged hundreds of thousands of unfailing working hours. Leading manufacturers of counting, timing and measuring instruments prefer these reliable tubes because they allow simplified circuitry, replace a number of thermionic tubes, operate at low current, dissipate negligible heat and are moderately priced. Available in decade and duo-decade types, the Dekatron is the original and the leading counting tube for superior performance. Are *you* taking full advantage of the economy, long life and versatility of these cold-cathode scaling tubes?

If you would like more information please write to:—

THE TECHNICAL SERVICES DEPT.,
TUBE DIVISION
BEESTON · NOTTINGHAM · ENGLAND

ETELCO

DEKATRON IS AN ETELCO TRADE MARK

ETELCO LIMITED, HEAD OFFICE: 22 LINCOLNS INN FIELDS LONDON, W.C.2. Telephone: HOLborn 6936

E115AR/93AR *ORIGINATORS AND SOLE MANUFACTURERS OF DEKATRON SCALING TUBES*

Announcing the Eldorado 4100

A Fast, Stable Pulse Height Analyzer

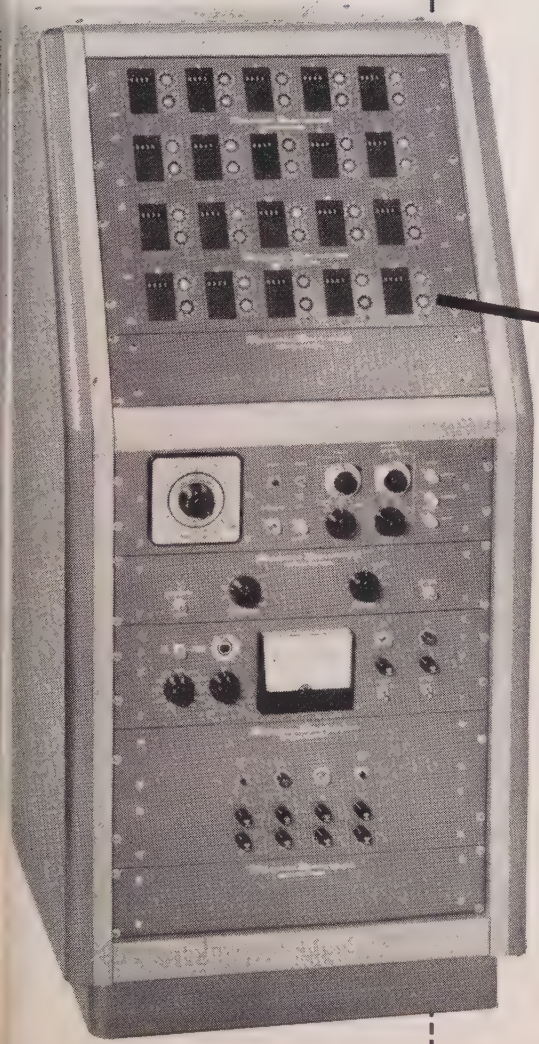

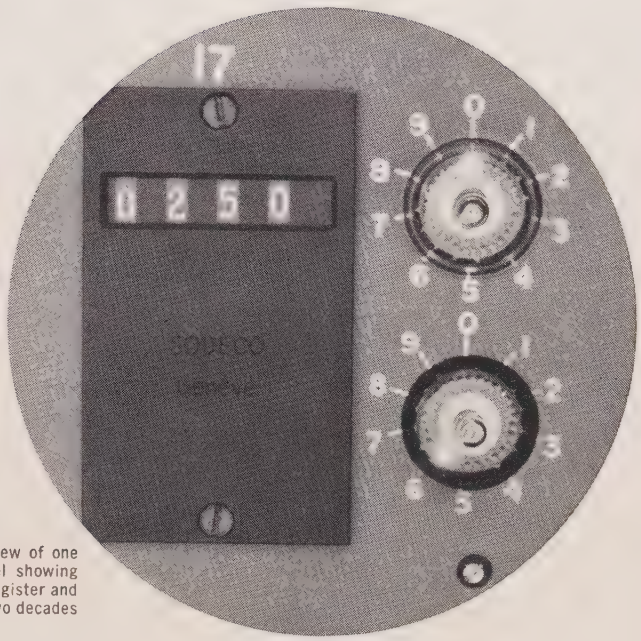

Full size view of one channel showing register and two decades

How Fast?

- ✻ Double pulse resolution better than 0.5 microseconds
- ✻ Dead time less than 0.1 microseconds
- ✻ Average counting rates greater than 10^5 counts per second without baseline distortion or use of temporary storage

How Stable?

- ✻ Channel width less than 1% drift per week
- ✻ Baseline less than 0.1% shift per week
- ✻ Channel triggering level unaffected by changes in input pulse width

For complete details, call your nearby Eldorado Engineering representative or write Dept. H3

…w in production, with 30 day delivery, the …00 is priced at $8950 f.o.b. Berkeley, Cali… …nia. Shown with optional LA-600 Linear …plifier and optional High Voltage …ver Supply PS-530

…IEF SPECIFICATIONS

NUMBER OF CHANNELS	20
CHANNEL WIDTH	1.0V NOMINAL
SCALER CAPACITY	10^6 COUNTS/CHANNEL
…NDOW AMPLIFIER INPUT	20V NOMINAL
…NDOW POSITION RANGE	5-105V

Eldorado Electronics

2821 TENTH STREET · BERKELEY 10, CALIFORNIA

Phone THornwall 1-4613

INTERNATIONAL

advertise

YOUR NUCLEAR PRODUCTS IN

sell

YOUR NUCLEAR PRODUCTS

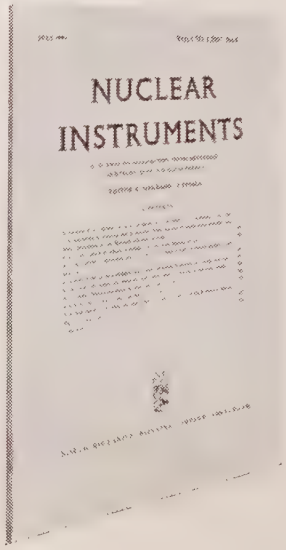

reap

YOUR NUCLEAR SALES
REWARDS

world wide

KEY NUCLEAR MANAGEMENT
NUCLEAR SCIENTISTS
NUCLEAR ENGINEERS
NUCLEAR PRODUCTION
PERSONNEL

SUBSCRIBE TO

you reach

THE WHOLE
NUCLEAR SALES WORLD IN

Entirely international in scope Nuclear Instruments and Methods is the one nuclear scientific journal that has an established subscription clientele throughout the whole world-where-ever nuclear men are at work—they want your nuclear products—they need your nuclear products—advertise in Nuclear Instruments and tell them WHAT – HOW – WHERE they can get your nuclear products

GO INTERNATIONAL WITH YOUR SALES PROGRAM TODAY WRITE

WILLIAM F. BAARS - ADVERTISING MANAGER NORTH-HOLLAND PUBLISHING COMPANY

P.O. BOX 103 – AMSTERDAM, HOLLAND

INTERNATIONAL

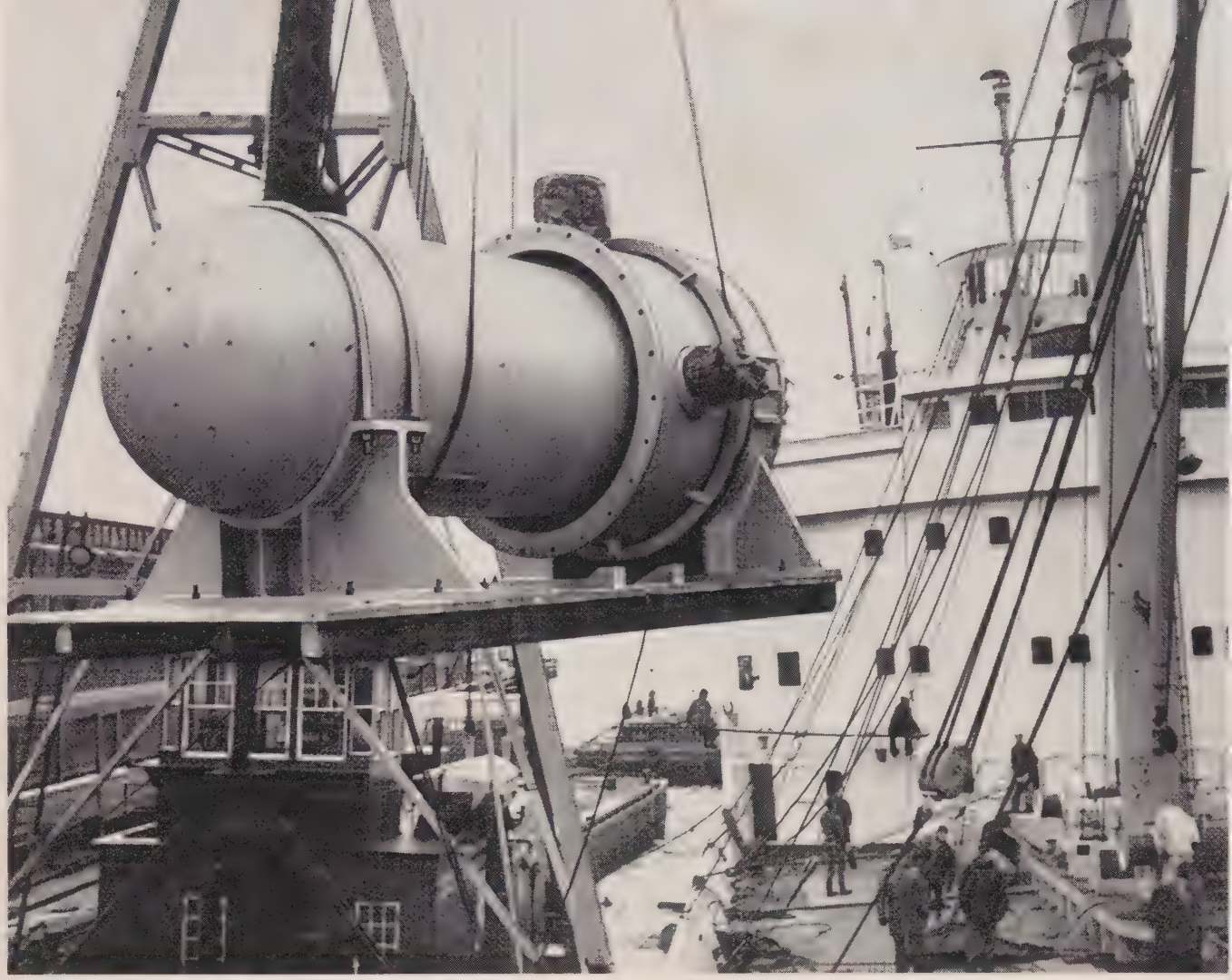

B&W reactor vessel manufactured for the Belgian Thermal Reactor, BR-3, designed by Westinghouse Electric Corporation, Atomic Power Department.

MORE NUCLEAR POWER FOR EUROPE

This is the 14th pressurized water reactor vessel shipped of a total of 34 ordered from The Babcock & Wilcox Company, U.S.A.

B&W's continuing search for improved nuclear products is helping to speed the practical application of nuclear energy throughout the free world. For more information, write The Babcock & Wilcox Company, Export Department, 161 E. 42nd Street, New York 17, N. Y., U.S.A.

Der 14te von 34 bei The Babcock & Wilcox Company, U.S.A., in Auftrag gegebenen Druckwasserreaktor-Tanks wird verladen. Die fortwährende Forschung der B&W nach besseren Atomprodukten befördert die praktische Anwendung der Atomenergie in der ganzen Welt. Für nähere Auskunft, bitte sich zu wenden an The Babcock & Wilcox Company, Export Department, 161 E. 42nd Street, New York 17, N. Y., U.S.A.

Le 14ième vaisseau du réacteur à eau sous pression d'une commande totale de 34 unités, passée à la société The Babcock & Wilcox Company, E.U.A., est embarqué.

La recherche constante de B&W pour améliorer les produits nucléaires contribue à activer l'application pratique de l'énergie nucléaire à travers le monde. Pour plus de détails, écrivez à The Babcock & Wilcox Company, Export Department, 161 E. 42nd Street, New York 17, N. Y., U.S.A.

B&W

THE BABCOCK & WILCOX COMPANY

NUCLEAR ENERGY EQUIPMENT

NC-111

Complete nuclear systems, cores, components, fuel elements, nuclear research and development

VERSATILE ACCELERATORS for fundamental or applied NEUTRON RESEARCH

●

NEUTRON SOURCES now available from High Voltage Engineering Corporation range from compact, low-cost Van de Graaff positive-ion accelerators to large linear electron accelerators for energies up to 100 Mev and higher.

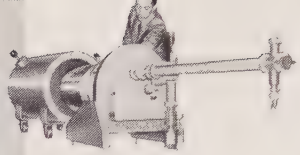

PN-400 Van de Graaff — Lowest cost. Ideal for reactor engineering, nuclear training courses, pulsing subcritical assemblies.

Pulsed or continuous operation.

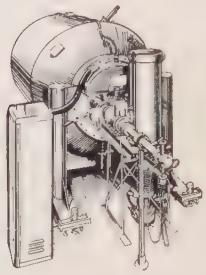

KN Van de Graaff — Powerful and precise for broad research programs including nuclear physics, advanced neutron work, biology, reactor engineering, and activation analysis.

Pulsed or continuous operation.

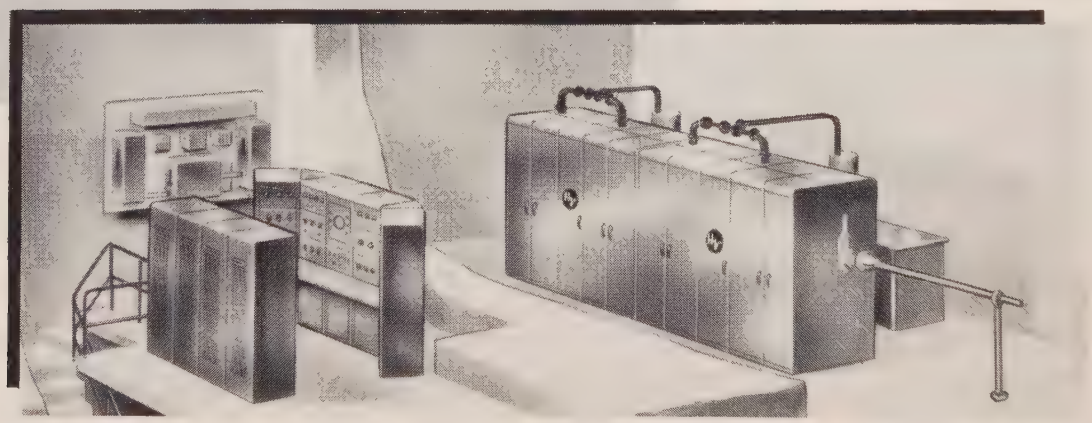

LS Series Linear Accelerators — Electron energies of 6 Mev and above. Optimum neutron yield per kilowatt obtained above 30 Mev. Useful for nuclear physics, neutron-damage studies, time-of-flight research, high-energy radiography. High flux density suitable for isotope production.

Other accelerators rated for operation at intermediate and higher outputs, are also available. Write High Voltage Technical Sales Department for specific performance data

Model	Particle Energy Mev	Pulse Current milliamperes	Total Neutron-yield Rates during Pulse	Pulsing and Repetition Rates
PN-400	0.4	0.10	10^{10} n/sec †	μsec range 1-10,000 pps
KN	3	0.40	2×10^{12} n/sec ‡	millimicrosecond to μsec range; 1-10,000 pps
LS Series Example	40	350	10^{16} n/sec *	0.01-10 μsec 1-2500 pps

† $T(d, n) He^4$ reaction
‡ $Be^9 (d, n) B^{10}$
* Photo-nuclear and photo-fission reactions.

HIGH VOLTAGE SERVICING COMPANY LTD.
LONDON-ENGLAND

HIGH VOLTAGE ENGINEERING (EUROPA) N.V.
AMERSFOORT
THE NETHERLANDS

HIGH VOLTAGE ENGINEERING CORPORATION
BURLINGTON, MASSACHUSETTS, U.S.A.

NUCLEAR INSTRUMENTS AND METHODS 5 (1959) 269–279; NORTH-HOLLAND PUBLISHING CO.

A LONGITUDINAL β-SPECTROMETER WITH COMPENSATED SPHERICAL ABERRATION†

K. A. DOLMATOVA and V. M. KELMAN

Physical-Technical Institute, Academy of Science USSR, Leningrad, USSR

Received 15 January 1959

A new method for the compensation of spherical aberration in a longitudinal beta-ray spectrometer is described. On the homogenous magnetic field is superimposed a correcting field generated by means of an special coil system placed inside the spectrometer. Theoretical and experimental investigations of the focussing properties are given and it is shown that the compensation coils gives a considerable reduction of the spherical aberration. With a 1×1 mm^2 source a relative halfwidth of 1.4 percent and an effective transmission of 5.2 percent was obtained. At a resolution of 1.9 percent the effective transmission was found to be 6.5 percent. A Ø 5 mm source gave a resolution of 3 percent.

The bigger the transmission and resolving power of the used β-spectrometer, the more complete can be the research of electron spectra of radioactive elements. However, due to aberration an increase of transmission means a decrease of resolving power, so that the two requirements are conflicting. One of the most important types of aberration is the aberration which limits the possibilities of a β-spectrometer, which exists even when a correctly arranged point source is used and which depends only on the aperture of the spectrometer. By analogy with the well-known type of aberration in light optics, this aberration is called spherical.

In β-spectrometers with a transversal magnetic field, spherical aberration can be completely corrected for electrons, moving in the median plane of the deflecting magnetic fields. If the source and detector are in the field, spherical aberration can be completely corrected or made much smaller by choosing a special distribution of the magnetic field[2–5]). If they are not in the field, the aberration can be corrected by suitably choosing the form of the field boundaries, the distribution of the intensity of the field, (in the regions where it exists), being more or less arbitrary[6]).

In the indicated ways spherical aberration in transversal fields (strictly speaking, in the median plane of such fields) can not only be corrected, but can be assigned any value—positive or negative. This means, that transversal fields can be used to compensate spherical aberration in an electron—optical system.

It is a different question with lens β-spectrometers. It can be proved in electron optics, that spherical aberration in electron lenses is always positive and that it can not be completely eliminated in a lens with finite optical strength, in the case of practically attainable intensities of magnetic fields. However the magnitude of the spherical aberration can be made much smaller by rationally choosing the distribution of the field[7–9]).

One of the most effective ways of reducing

† A short report about this work is given in [1]).

[1]) K. A. Dolmatova and V. M. Kelman, Doklady Akad. Nauk SSSR **113** (1957) 1244.

[2]) M. Korsunsky, V. Kelman and B. Petrov, JETP **14** (1944) 339.

[3]) B. S. Dželepov and A. A. Bashilov, Izvest. Akad. Nauk SSSR Ser. Fiz. **14** (1950) 263.

[4]) P. P. Pavinsky, Izvest. Akad. Nauk SSSR Ser. Fiz. **18** (1954) 175.

[5]) N. Svartholm and K. Siegbahn, Ark. Mat. Astr. Fys. **33** (1949) No. 21.

[6]) L. Kervin, Rev. Sci. Instr. **20** (1949) 381.

[7]) W. Glaser, Zs. f. Phys. **116** (1940) 19.

[8]) K. Siegbahn, Phil. Mag. **37** (1946) 162.

[9]) H. Slätis and K. Siegbahn, Ark. f. Fys. B I (1949) No. 17, 339.

spherical aberration is to use an annular focus instead of a point focus[10,11]).

Very high values of light power and satisfactory resolution (transmission 2%, line halfwidth 0.4%) were obtained on a β-spectrometer with a longitudinal homogeneous magnetic field, when one worked with an annular focus. However, even when one uses an annular focus, the value of the spherical aberration is still considerable, so that with increase of the aperture ratio a high resolving power cannot be maintain in longitudinal spectrometers. In this paper a method of reducing the spherical aberration of instruments with a longitudinal field is used; the essence of this method is that spherical aberration in these instruments is compensated by superimposing transversal fields with spherical aberration of the opposite sign. This method was employed by Dzhelepov, No Sen Chan and Tishkin to compensate aberration along the axis of a spectrometer with a thin lens[12]).

We constructed an instrument with a homogeneous longitudinal magnetic field and an annular focus, in which the spherical aberration is largely compensated by a transversal magnetic field, the intensity of which is inversely proportional to the distance from the symmetry axis of the instrument; the lines of force are circles with their centre on this axis. The necessary value of the negative aberration is attained by choosing the boundary of the transversal compensating field. We chose this type of β-spectrometer because, as was mentioned above, the β-spectrometer with a homogeneous field and an annular focus is a very good instrument in any case and compensation of its spherical aberration must make its qualities still better. Besides that, the differential equations of the electron trajectories in a homogeneous field, on which a field, changing according to the law $H = H_1/r$ is superimposed, reduces to quadratures[13]) and this makes the calculations much easier.

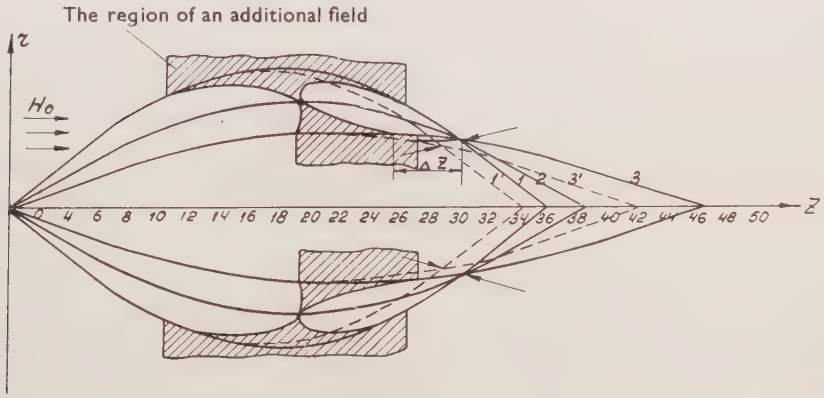

Fig. 1a

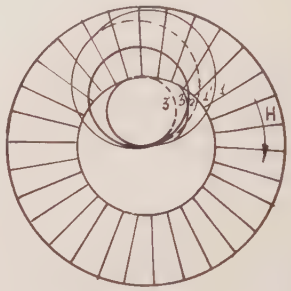

Fig. 1b

Fig. 1. Relations $r = r(z)$. 1', 2, 3'—in a homogenous field for electrons with emission angles ψ_0 worth 40°, 30°, 20° respectively, 1, 2, 3,—in a field with compensated spherical aberration and the same emission angles. The pointers show the width of the annular focus in a homogeneous field.

1. Calculations of a Focusing Field with Compensated Spherical Aberration

On fig. 1a the relative position of the basic homogeneous magnetic field and the transversal field superimposed upon it is shown in a plane containing the symmetry axis of the instrument;

[10]) S. Frankel, Phys. Rev. **73** (1948) 804.

[11]) D. J. Mayer and F. H. Schmidt, Phys. Rev. **94** (1954) 927.

[12]) B. S. Dželepov, No Sen Chan and P. A. Tishkin, Izvest. Akad. Nauk SSSR Ser Fiz. **20** (1956) 947.

[13]) V. M. Kelman and I. V. Rodnikova, JETP **21** (1951) 1364;
V. M. Kelman and S. Ya. Yavor, JETP **24** (1954) 1329.

on fig. 1b in a plane perpendicular to the symmetry axis. The origin, shown on this figure, of the cylindrical system of coordinates r, φ, z, which we will further use, is matched with the point source of electrons and the z-axis is directed along the symmetry axis of the instrument. The transversal field is created by a coil, the turns of which are arranged symmetrically with respect to the axis. If we presume, that the turns of the coil are at a sufficiently short distance from each other, the intensity of such a field will be $H = H_1/r$. The lines 1, 2, 3 and 1′, 3′ on fig. 1a do not represent the real paths of the electrons, since the rotation of the electrons around the axis of symmetry is not taken into account on this figure. They only represent the relation between the radial distances of the electrons and axis z. Thanks to the symmetry of the problem it is evidently quite sufficient to know the relation $r(z)$ to be able to find the annular focus. The lines on fig. 1b represent the real projections of the trajectories on a plane, perpendicular to axis z.

When there is no compensating field, the trajectories of the electrons, the last parts of which are represented by the dotted lines 1′ and 3′ and the end of trajectory 2 form a rather wide annular focus. It is necessary to choose such a form of the boundary of the compensating field, which will reduce the width of the annular focus to zero. In this case the relations $r(z)$, when the spherical aberration is compensated, are represented by the continuous lines 1, 2, 3.

In the zone from the source to the compensating field the electrons move in a homogeneous magnetic field along spirals:

$$r = -\frac{1}{K_0}\sin\psi_0 \cdot \sin\varphi\,, \qquad \varphi = -\frac{K_0 z}{\cos\psi_0}\,. \tag{1}$$

Here $K_0 = eH_0/2pc$ where e is the electron charge, H_0 the intensity of the homogeneous magnetic field, c-light velocity, p-momentum of the electron. For electrons K_0 is negative. ψ_0—the angle between the initial direction of the velocity and axis z. The angle φ is read from the plane containing axis z and the initial direction of the electrons velocity†.

In the region where a field with the intensity $H = H_1/r$ is superimposed on the homogeneous magnetic field, the differential equations for the movement of electrons reduces to quadratures, which can be written as follows

$$\frac{z - z_0}{r_0} = \int_1^\rho \frac{(\cos\psi_0 + K\ln\rho)\,d\rho}{\sqrt{1 - (\sin\psi_0 \sin\varphi_0\rho)^2 - (\cos\psi_0 + K\ln\rho)^2}}$$

$$\varphi - \varphi_0 = \int_1^\rho \frac{\sin\psi_0 \sin\varphi_0\, d\rho}{\sqrt{1 - (\sin\psi_0 \sin\varphi_0\rho)^2 - (\cos\psi_0 + K\ln\rho)^2}} \tag{2}$$

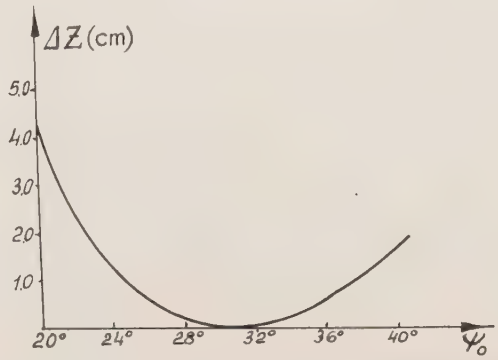

Fig. 2. The relation between Δz and the emission angles ψ_0 when $r = 4.6$ vm.

Here $\rho = r/r_0$; r_0, φ_ρ, z_0 are the coordinates of the point, where the electron enters into the heterogeneous field; $K = -H_1/H\rho$ where $H\rho$ is a quantity which characterizes the momentum of the electron. Since the compensating field was placed near to the summit of the trajectory; one could consider that ρ in the expressions (2) little changes and put $\rho = 1 + x$ where $x \ll 1$ and $\ln\rho = x - \frac{1}{2}x^2$. Thus the expressions can be integrated:

$$\frac{z - z_0}{r_0} = -\frac{1}{\sqrt{c}}\left[\cos\psi_0 - \frac{bK}{2c} - \frac{K}{4c}\left(\frac{3b^2}{4c} - a\right)\right] \cdot$$
$$\cdot\left[\arcsin\frac{2cx + b}{\sqrt{-\Delta}} - \arcsin\frac{b}{\sqrt{-\Delta}}\right] +$$
$$+\frac{K}{c}\left[1 - \tfrac{1}{4}\left(x - \frac{3b}{2c}\right)\right]\sqrt{a + bx + cx^2} -$$
$$-\frac{K}{c}\left(1 + \frac{3b}{8c}\right)\sqrt{a}\,, \tag{3}$$

$$\varphi - \varphi_0 = -\frac{1}{\sqrt{-c}}\sin\psi_0 \sin\varphi_0 \cdot$$
$$\cdot\left[\arcsin\frac{2cx + b}{\sqrt{-\Delta}} - \arcsin\frac{b}{\sqrt{-\Delta}}\right].$$

† The coordinate φ is connected with the coordinate ϑ introduced in the paper[13]) by the relation $\varphi = \pi - \vartheta$.

Here: $a = 1 - \sin^2\psi_0 \sin^2\varphi_0 - \cos^2\psi_0$,

$b = -2\sin^2\psi_0 \sin^2\varphi_0 - 2K\cos\psi_0$,

$c = -\sin^2\psi_0 \sin^2\varphi_0 - K^2 + K\cos\psi_0$,

$\Delta = 4ac - b^2$.

The additional field was so chosen, that trajectories of electrons with emission angles 30° were in a homogeneous field the whole time. The paths of electrons emitted at other angles must be displaced by the additional field so as to pass through the point r_i, z_i in the plane $r(z)$ lying on the annular focus of the infinitely narrow beam of electrons with emission near to 30° ($r_i = 4.6$ cm, $z_i = 30.2$ cm). A plot of the relation between the necessary displacement Δz (viz. fig. 1a) and the emission angles is given on fig. 2. The magnitude of the displacement will depend on the boundary of the additional field and on its intensity. At the summit of the path $(dx/dz)_m = (dx/d\varphi)_m = 0$. It follows from (2) that the value $x = x_m$ corresponding to the summit of the path, can be determined out of the equation $a + bx + cx^2 = 0$. From eq. (3) one can find the values of the coordinates φ_m, z_m at the summit of the path, if the coordinates of the point of intersection of the electrons path and the boundary of the additional field are chosen in some definite way.

$$\frac{z_m - z_0}{r_0} = \frac{1}{\sqrt{-c}}\left[\cos\psi_0 - \frac{bK}{2c} - \frac{K}{4c}\left(\frac{3b^2}{4c} - a\right)\right] \cdot \left(\tfrac{1}{2}\pi + \arcsin\frac{b}{\sqrt{-\Delta}}\right) - \frac{K}{c}\left(1 + \frac{3b}{8c}\right)\sqrt{a},$$

$$\varphi_m - \varphi_0 = \frac{1}{\sqrt{-c}}\sin\psi_0 \sin\varphi_0 \left(\tfrac{1}{2}\pi + \arcsin\frac{b}{\sqrt{-\Delta}}\right)$$

$$r_m = r_0(1 + x).$$

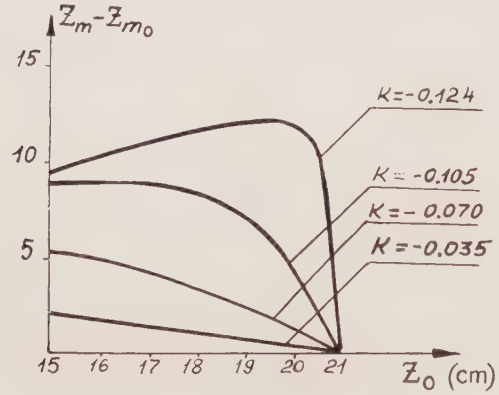

Fig. 3a

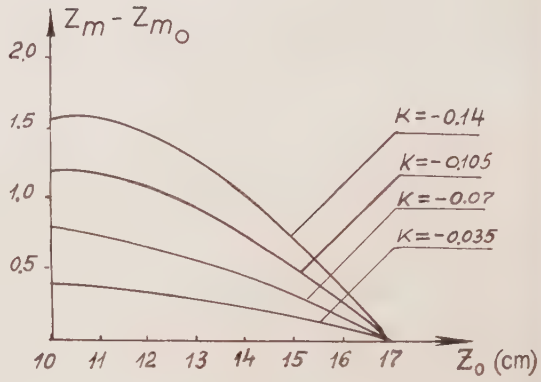

Fig. 3b

Fig. 3. The relation between the value of the displacement of the paths summit and the position of the beginning of the additional field at different values of the intensity of the additional field (a) $\psi_0 = 20°$, (b) $\psi_0 = 40°$.

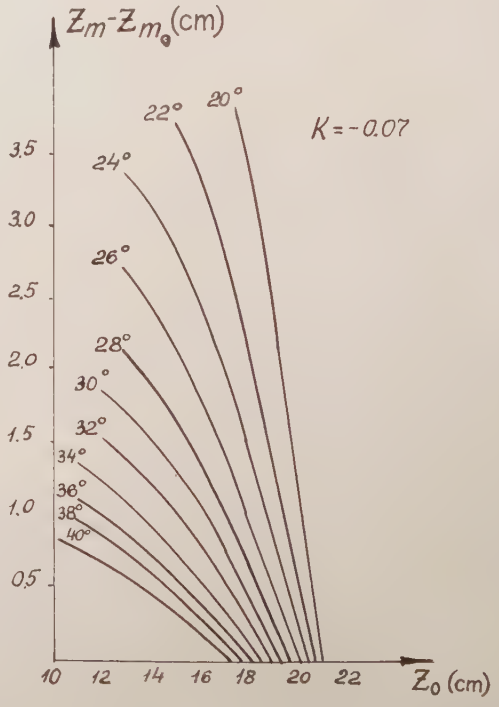

Fig. 4. The relation between the value of the displacement of the path's summit and the point where the additional field is applied for emission angles of electrons between 20° and 40°; $K_0 = -0.07$, $K = -0.07$.

Here a, b, c, and Δ have the same meaning as before. Taking different initial conditions r_0, $\varphi_0 z_0$ and values of the intensity K one can find the displacement of the summit of the paths of electrons passing through a region of heterogeneous field, with respect to its position in a homogeneous field $\Delta z_m = z_m - z_{m0}$ where z_{m0} is the coordinate of the path's summit in the absence of an additional field. If the paths are symmetrical with respect to their summit and the focus lies in a homogeneous field, spherical aberration will be compensated if $\Delta z_m = \frac{1}{2}\Delta z$.

Calculations of Δz_m where made for emission angles $\psi_0 = 20°$ and $40°$ and for different values of K. The results are presented on fig. 3a and 3b. One sees, that the displacement grows with the growth of the intensity of the additional field. The value $K = -0.07$, which can ensure the necessary displacement Δz, was chosen from here. For this value of K and for the value $K_0 = -0.07$, characterizing the homogeneous longitudinal magnetic field, the relation between the displacement Δz_m for different emission angles and the position of the beginning of the additional field was calculated. The result of these calculations is presented on fig. 4. Using this plot and fig. 2, one can find such a form of the boundary of the additional field, which ensures an annular focus without aberration. The results received in this way are presented on table 1. The form of the boundary of the additional field and the paths of electrons in the rotating plane (r,z) are shown on fig. 5.

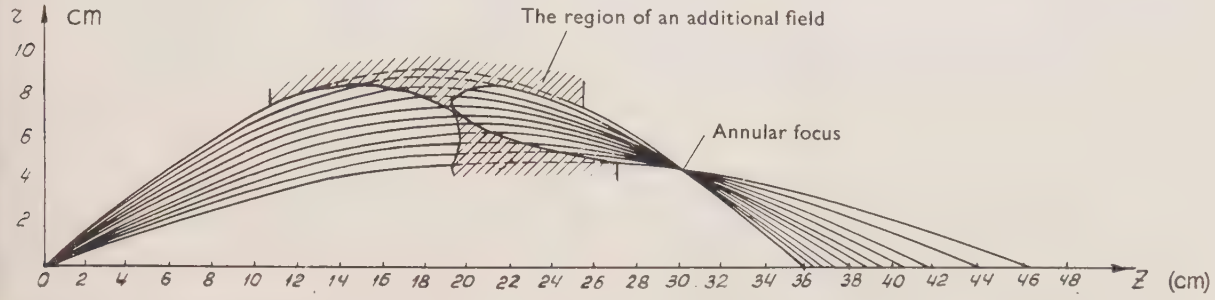

Fig. 5. The relation $r = r(z)$ in a field with compensated spherical aberration for emission angles ψ_0 between 20° and 40°.

The paths of electrons with different energies were calculated, so as to determine the dispersion in a field with compensated spherical aberration (fig. 6). In a homogeneous field the paths of electrons emitted by a point source with different energies, form annular focuses, which lie on a straight line containing the source, in the plane (r,z). Since the position of the annular focus in a field with compensated spherical aberration is determined by the path of the electrons, emitted by the source at an

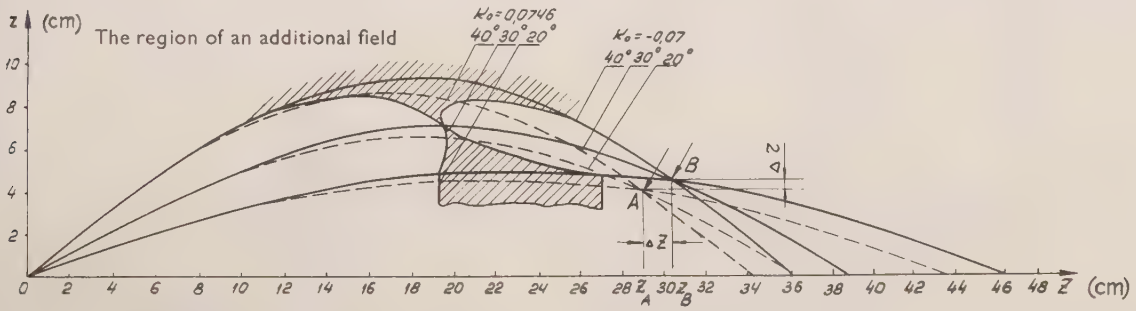

Fig. 6. The relation $r = r(z)$ in a field with compensated spherical aberration. $\psi_0 = 20°$, $30°$, $40°$. $K_0 = -0.07$, $K = -0.07$–full lines. $K_0 = -0.0746$, $K = -0.0746$–dotted lines.
A and B annular focuses. Δz–longitudinal dispersion, Δr–transversal dispersion.

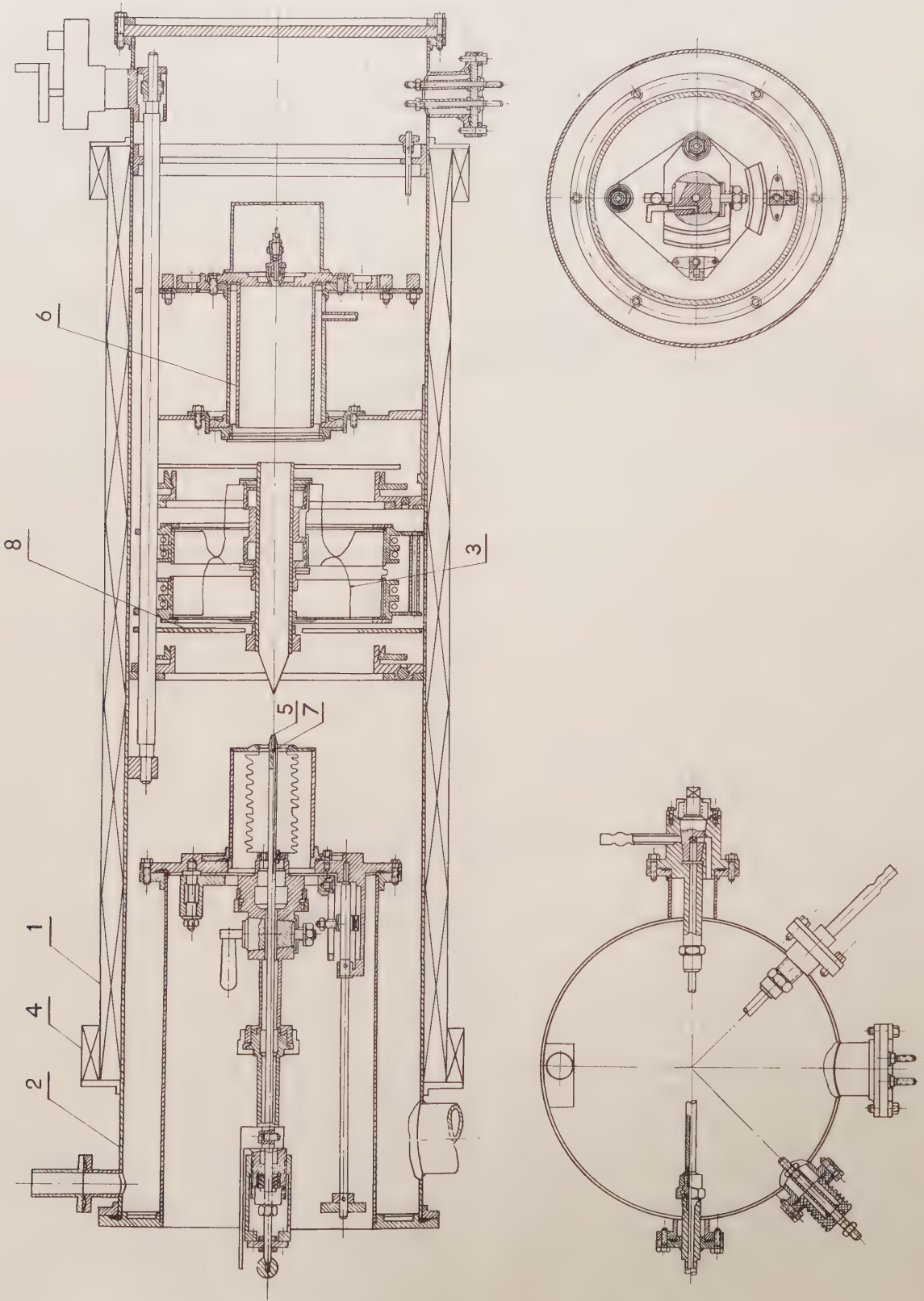

Fig. 7. Scheme of the spectrometer

Table 1

φ_0	Δz	$z_m - z_{m0}$	z_0	r_0	z_{m0}	z_m	r_m
20°	4.58	2.29	19.3	4.84	21.09	23.28	4.94
22°	2.32	1.16	19.40	5.33	20.81	21.81	5.38
24°	1.14	0.57	19.55	5.80	20.50	21.97	5.82
26°	0.46	0.23	19.67	6.26	20.17	20.41	6.27
28°	0.12	0.05	19.70	6.71	19.81	19.87	6.71
30°	0	0	19.43	7.14	19.43	19.43	7.14
32°	0.02	0.01	19.0	7.57	19.03	19.04	7.60
34°	0.26	0.13	18.0	7.98	18.60	18.73	7.99
36°	0.59	0.30	16.5	8.32	18.17	18.46	8.41
38°	1.03	0.52	14.4	8.42	17.78	18.20	8.86
40°	1.56	0.78	10.6	7.57	17.19	17.97	9.43

angle of 30°, which lies wholly in the homogeneous field, the dispersion in this case will be the same as in a homogenous field.

Construction of the device

To create the longitudinal magnetic field H_0 we used the solenoid 1 (fig. 7), wound on a copper tube 2, which served as the chamber of the spectrometer. There were additional correcting coils 4 wound upon the solenoid, so that the field would be homogeneous in the operating region. By means of these coils it was possible to reduce the heterogenity of the field in the operating region from 3% to 0.5%.

The form of the turns of the coil coincided with the calculated form of the field's boundary everywhere, except those regions, where the paths of those electrons lie, which are emitted at the angles 20° and 40° (fig. 8). The coil consisted of 30 turns of wine with a diameter 1 mm (fig. 9). Using such a coil, one lost 15% of the radiation. According to the calculations the currents in the solenoid creating the homogeneous field and in the inner correcting coil must be the same. The solenoid and the coil were parallely connected and were supplied from storage batteries. The chamber of the spectrometer consists of a copper tube with an inner diameter 32 cm,

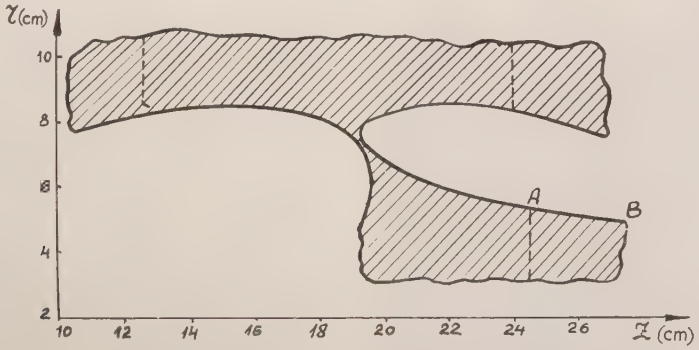

Fig. 8. Form of the boundary of the additional field which ensures the compensation of the spherical aberration of the annular focus in a homogeneous longitudinal magnetic field. The dotted line shows the shape of the turn, creating the compensating field, which in the other parts coincides with the form of the field's boundary.

The field compensating the spherical aberration, the intensity of which changes according to the law $1/r$ was created by the inner coil 3, the turns of which lay symmetrically with regards to the axis.

length 142 cm and of a number of flanges. On one side of the chamber the radioactive source 5 (fig. 7) is placed, on the other side the counter 6. The source was stuck to the holder 7, which is fixed to a stem. The stem was brought into the

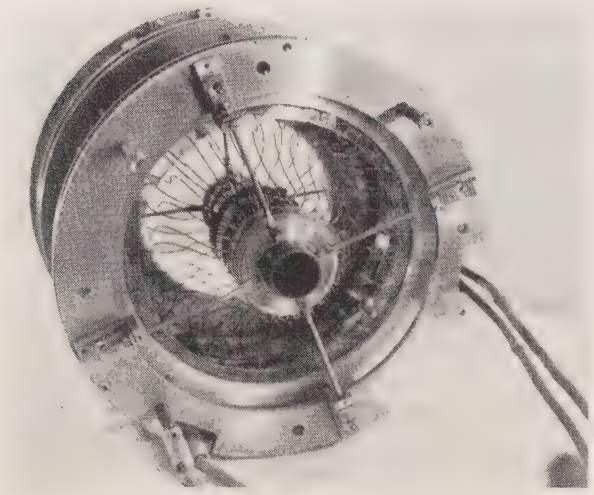

Fig. 9. A photography of the inner coil.

chamber through a Wilson joint and a vacuum cock, so that one could change the source without disturbing the vacuum. Using a special mechanism, one can move the source in a plane, perpendicular to the axis of the instrument. Such a freedom of movement was necessary for the adjustment of the instrument. The duralumin input diaphragm 8 made it possible to separate electrons with angles between 20° and 40° or 25° and 40°. The chamber was evacuated by vacuum pumps to the pressure 5×10^{-5} mm Hg.

Investigation of the Qualities of the β-Spectrometer

A. INVESTIGATIONS WITH AN ELECTRON GUN

The qualities of the spectrometer were preliminarily investigated with the help of an electron gun, which was connected by flanges to the chamber of the spectrometer. The cathode of the electron gun was a tungsten filament, bent to an angle, so as to create a point source of electrons. The vertex was in the point which corresponded to the calculated position of the source. The image of the electron beam with energy 8–10 keV was observed by means of a fluorescent screen, covered with willemit. The screen was moved along the axis of the tube and its position could be fixed accurately within 1 mm.

The primary investigations with an electron gun showed, that the width of the annular image decreases 2.5–3 times in comparison with the width of the annular image in a homogeneous field, when the current in the inner coil is twice as big as in the basic solenoid. Results of the investigation are presented on fig. 10. The deviation of the experiment-data from the calculated can be explained as follows. Outside the region of the calculated field the additional transversal field is not equal zero, as it should be according to the calculations, because of border effects, and in the region it only approximately follows the law $1/r$. Besides this the additional field is so calculated that the paths of electrons with emission angles near to 20° and 40° in a certain region go along the turns of the correcting coil. In this region the fields of separate turns influence the electron paths and thereby distort the expected effect of decreasing the spherical

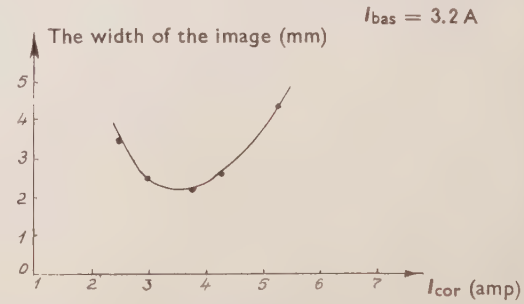

Fig. 10. The relation between the width of the annular focus and the current in the additional coil I_{cor}. The current in the windings of the solenoid I_{bas} = 3.2A.

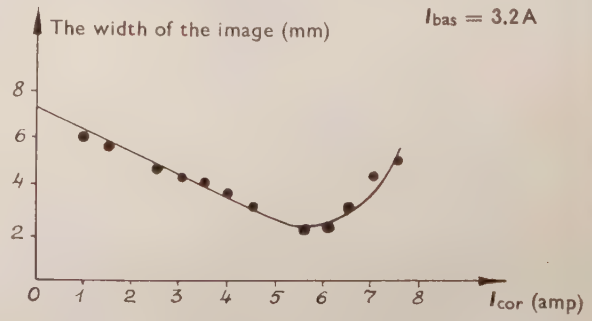

Fig. 11. The relation between the width of the annular focus and the current in the additonal coil with a corrected shape of the oils.

aberration. To decrease the influence of these fields, those parts of the turns, along which the electron paths lie, were removed. The form of

the turns, which was thus obtained is shown on fig. 8 by the dotted line.

With the corrected coil the width of the annular image was determined once more. The results of the investigations showed, that the width of the annular focus diminishes 2.5–3 times, with the same current in the correcting coil as in the coil, creating the homogeneous longitudinal magnetic field (fig. 11).

PHOTOGRAPHING THE ANNULAR IMAGE

Before one could start to investigate spectra or conversion lines it was necessary to determine the position of the annular focus and its dimensions, so as to choose the dimensions and position of the annular diaphragm correctly. For this reason a Roentgen film, on which an image of the electron beam was to be obtained, was put into the path of the electrons from the source. An active sediment of thorium was used as the radioactive source and the F-line with energy 148 keV was measured. So as to define the position of the annular focus, the Roentgen film was first placed slopingly, approximately at the angle 70° to the axis of the instrument. A photography of the electron image obtained upon the film is presented on fig. 12. Those parts of the film, on which the annular image was smeared out least of all were evidently in the right position. The dimensions of the annular focus were determined with the help of a film, which was put perpendicularly to the axis of the instrument, in the place where the annular focus was according to the previous photography (fig. 13).

On fig. 14 are presented the microphotograms of the annular image of the beam of electrons with emission angles between 20° and 40° (solid angle 8.7% of 4π), for a field with compensated spherical aberration and for a homogeneous field. On the X-axis are the distances along the radius from the outer edge of the annular image, on the Y-axis—the intensity of the electrons in arbitrary units. In the field with compensated spherical aberration the extrapolated width of the line at the base is 5 mm, but the main intensity (88%) is concentrated

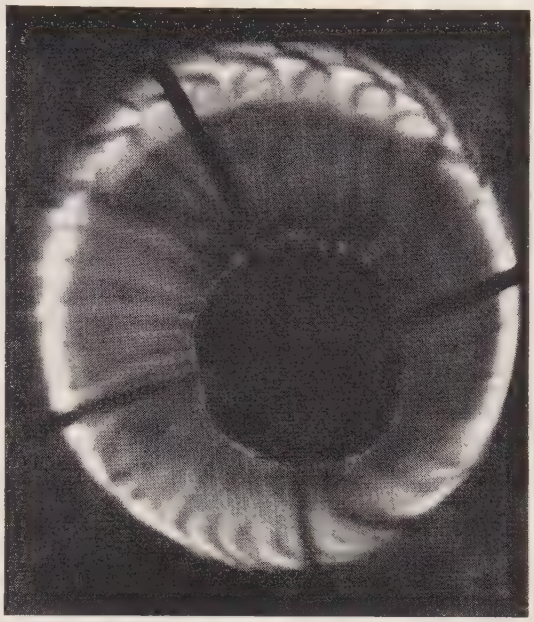

Fig. 12. A photography of the electron image in a field with compensated spherical aberration. The film is set at an angle of 70° to the axis of the spectrometer.

at the width 3 mm. The outer diameter of the annular image is 108 mm. On the grounds of these results an annular diaphragm was chosen with an outer diameter 108 mm and an inner diameter 102 mm. Such a diaphragm should

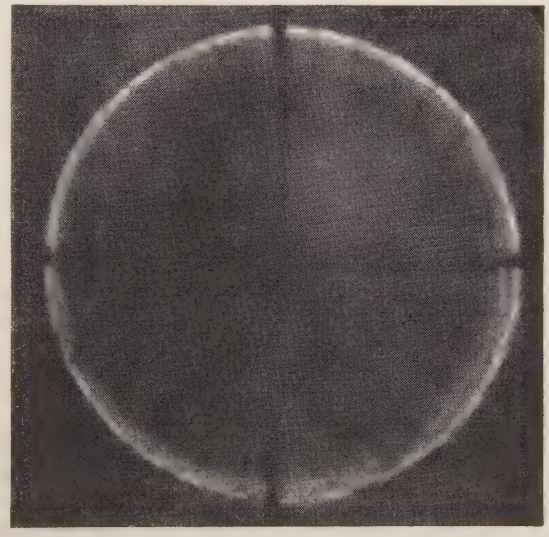

Fig. 13. A photography of the annular image in a field with compensated spherical aberration. The emission angles of the electrons φ_0 lie between 20° and 40°. The film was perpendicular to the axis of the instrument.

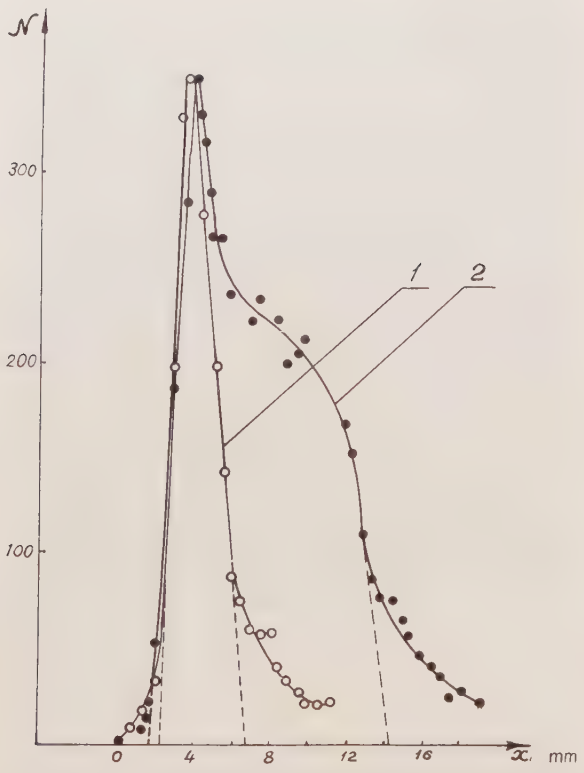

Fig. 14. A microphotogram of the annular focus, taken along the radius. 1. Field with compensated spherical aberration. 2. Homogeneous field.

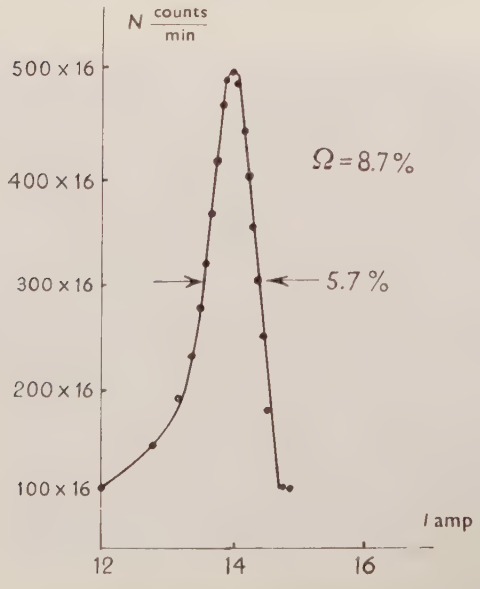

Fig. 15. The relation between the intensity of the counting and the magnitude of the current in the coils. On the X-axis are the values of the current in amperes, on the Y-axis the number of pulses per minute. $\Omega = 8.7\%$ of 4π.

pass 88% of the radiation. Electron images for a beam of electrons with emission angles between 25° and 40° (solid angle 70% of 4π), were obtained in the same way. With the help of a microphotogram it was possible to determine the dimensions and position of the annular focus for this case. They showed to be approximately the same as in the case of the solid angle 8.7% of 4π.

It follows from the microphotogram of the annular focus, made in a homogeneous field, when the inner coil was switched off, which is presented on fig. 14 for comparison, that in this case the width of the line at its base is 12 mm, but the main intensity (87%) is concentrated at the width 9 mm. The outer diameter of the annular image is 188 mm. Thus the photographing of the annular image proved the data, obtained by the investigations with an electron gun, i.e. that if one switches on the inner correcting coil, the width of the annular image decreases about three times in comparison with its width in a homogeneous longitudinal magnetic field.

C. EXPERIMENTAL INVESTIGATION OF THE QUALITIES OF THE INSTRUMENT BY MEANS OF A COUNTER

To determine the resolving power of the instrument the conversion F-line ThB was measured, using an end type counter GM-6 (fig. 7), with a diameter of the window 90 mm. The results are presented on fig. 15. On the X-axis are the values of the current in the coils in amperes, on the Y-axis the intensity in impulses par minute.

The line half-width for the solid angle 7% of 4π proved to be 1.4%, when the dimension of the source was 1×1 mm^2. As was mentioned above, not all the radiation liberated in the given solid angle will hit the counter. Part of it will be lost because of the inner coil, which is in the path of the beam (15%) and because the diaphragm passes only 88% of the radiation. Because of this the transmission of the instruments is only 5.2%.

When the transmission is 6.5% (Ω worth

8.7% of 4π) the line half-width is 1.9% (fig. 16) with the same dimensions of the source 1×1 mm^2. For a source with the ⌀ 5 mm and other conditions the same a line half-width 3% was obtained.

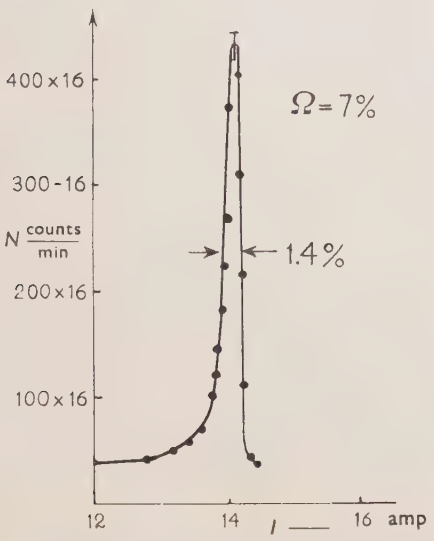

Fig. 16. The relation between the intensity of the counting and the magnitude of the current on the coil for a homogeneous field. $\Omega = 8.7\%$ of 4π.

In a homogeneous field when the solid angle was 8.7% and the dimensions of the source 1×1 mm^2 the line half-width showed to be 5.7% (fig. 17), and this coincided with theoretical calculations.

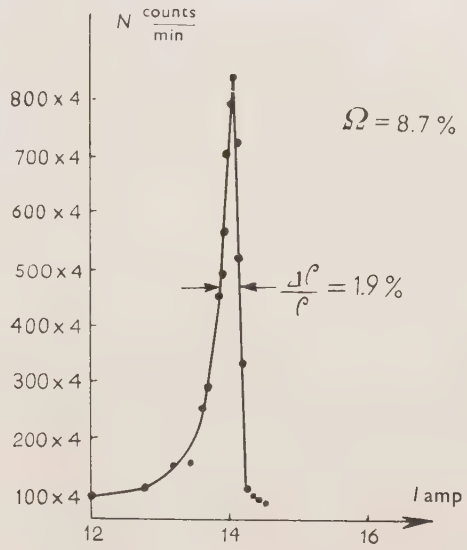

Fig. 17. The relation between the intensity of the counting and the magnitude of the current on the coil for a homogeneous field. $\Omega = 8.7\%$ of 4π.

NUCLEAR INSTRUMENTS AND METHODS 5 (1959) 280–291; NORTH-HOLLAND PUBLISHING CO.

THE TUNINGFORK FREQUENCY MODULATOR OF THE CERN SYNCHRO-CYCLOTRON

PART I. GENERAL DESIGN

FRANK KRIENEN

CERN, *Geneva*

Received 19 May 1959

This report deals with the design of the tuning fork modulator for the 600 MeV Synchro-Cyclotron, which accelerator has come into operation for the first time in August 1957. The intricated position of the modulator in the accelerator as a whole, required the development of the principle of scaling. Basic design considerations have been put forward. These considerations have initiated an experimental program, which in its turn verified and corrected the starting point. Suitable mechanical and electrical analogues have been derived, which in many respects clarify the nature of the problem. The control and initial operation of the system have been described and possible improvements are mentioned. The report as such is drawn up from author's unpublished divisional reports, engineering notes and communications with contractors.

1. Introduction

1.1.

One of the leading concepts for the design of the 600 MeV Synchro-Cyclotron was the scaling up of a known Synchro-Cyclotron of lower energy. We compute this scale factor and show how the factor reflects on the high frequency requirements. The starting relation is:

$$\omega = \frac{eB}{m} = \frac{v}{r} \tag{1}$$

in which ω is the angular frequency of the high frequency field, v is the velocity, r rhe radius, e the charge, m the relativistic mass of the particle and B the magnetic flux density at radius r. The second identity of (1) $eBr = mv = p$ gives with $p^2c^2 = E^2 - E_0^2$ in which E is the total energy and E_0 is the rest energy:

$$E^2 - E_0^2 = (ecBr)^2 . \tag{2}$$

Now multiplication with a factor g of all parts of a magnetic circuit including the number of ampere turns, leaves unaltered the field configuration, whatever the amount of magnetic saturation may be. From this we conclude that the critical radius at which the n-value of the machine

$$n = -\frac{r}{B}\frac{\mathrm{d}B}{\mathrm{d}r} = 0.2 \tag{3}$$

also increases with the factor g. Consequently the scale factor between two similar machines with total energy E_1 and E_2 respectively is given by:

$$g^2 = \frac{E_1^2 - E_0^2}{E_2^2 - E_0^2} . \tag{4}$$

The first identity of (1) $\omega = 2\pi f = eB/m$ gives with $E = mc^2$

$$f = \frac{eBc^2}{2\pi E} . \tag{5}$$

From this we conclude that the upper frequency limit for both machines is the same, whereas the lower frequency limit is inversily proportional with the total energy.

Now the electrode system which accelerates the protons is part of a transmission line, the total length of which is closely related to the upper frequency limit.

$$L \simeq \tfrac{1}{2}\lambda_{\min} . \tag{6}$$

This relation becomes plausible if one agrees that the system should work in the lowest possible mode. The standing wave associated with the upper frequency limit has necessarily a voltage node at a radius about equal to the pole radius, hence the lowest mode for this frequency could be a half wave, open line section,

and the frequency variation could be obtained by shunting a variable capacitance at the open end.

Apparently the construction of bigger machines becomes increasingly difficult. Not only the frequency interval to be covered by the modulator increases, but the high frequency system as a whole tends to get squeezed between the magnet poles and coils.

Mostly by trial and error improvement of a preliminary design is obtained by shifting the variable capacitance along the line and changing the characteristic impedance of some line sections to suit special requirements with respect to the voltage distribution, the capacitance variation and loading, and the oscillator tube behaviour. It appeared always essential to keep the total length as short as possible and to minimize the total stored electro-magnetic energy. As a result of the above considerations a suitable place for the variable capacitance could be found in the region where the stray field of the magnet goes through zero. The problem has also been approached by considering Foster's reactance theorem in connection with some properties of the energy function[1]), leading to essentially the same results.

1.2.

A variable capacitance is not the only way to modulate the frequency. Serious attempts have been made to use ferrite loaded tuning elements. The results were not encouraging. The heat dissipation in the ferrite slabs were estimated to be about half a megawatt high frequency, and 100 kW low frequency for a machine of this size. However for smaller machines ferrites are very well possible[2]).

1.3.

For the variable capacitance two possible designs were considered. One is the conventional rotating capacitor, the other a tuning fork type of capacitor.

In designing a rotating capacitor one has to face, in addition to a formidable engineering on machining and balancing, such problems as rotating vacuum seals, high frequency bypassing of the bearings, heavy duty stand off insulators and the suppression of parasitic modes along the rotor. A tuning fork design also requires formidable engineering on machining and balancing but the other requirements are less stringent. We therefore concentrated on the latter design, although it is now clear that a rotating capacitor for a high energy Synchro-Cyclotron can be made to work[3]).

2. Design Considerations

2.1. ELECTRICAL SYSTEM

Many investigations were needed before the design of the modulator could be frozen and the manufacturing could be started. Experiments to that end were undertaken at the Philips Physical Laboratory, Eindhoven (Netherlands) by Mr. B. Bollée, who under the supervision of Mr. G. de Vries carried out high frequency tests on a $\frac{1}{10}$ scale model working in the U.H.F. range of 150–300 MHz with the Philips tubes EC 56 and EC 55. The results were in fair agreement with preliminary calculations. Thus the various line sections and the capacitance range were determined. In fig. 1 are given the most important high frequency parameters:

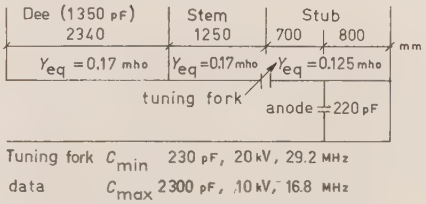

Fig. 1. Transmission line analogue.

Although in principle the electrical system was herewith determined some further experiments were done at the manufacturing department of Philips by Mr. S. Kortleven, under the supervision of Mr. L. van Mechelen. Work was done on a model in vacuum, operating at true

[1]) M. Morpurgo, Some considerations on Synchro-Cyclotron high frequency systems. 1955 CERN/SC 136.

[2]) F. Krienen, Application of Ferrites in R. F. systems for Synchro-Cyclotron. 1952 CERN/SC 26.

[3]) A. L. Mints *et al.*, R. F. System for the 680 MeV proton Synchro-Cyclotron. Institute for Nuclear Problems U.S.S.R. In proceedings CERN Symposium 1956. Vol. 1, p. 419.

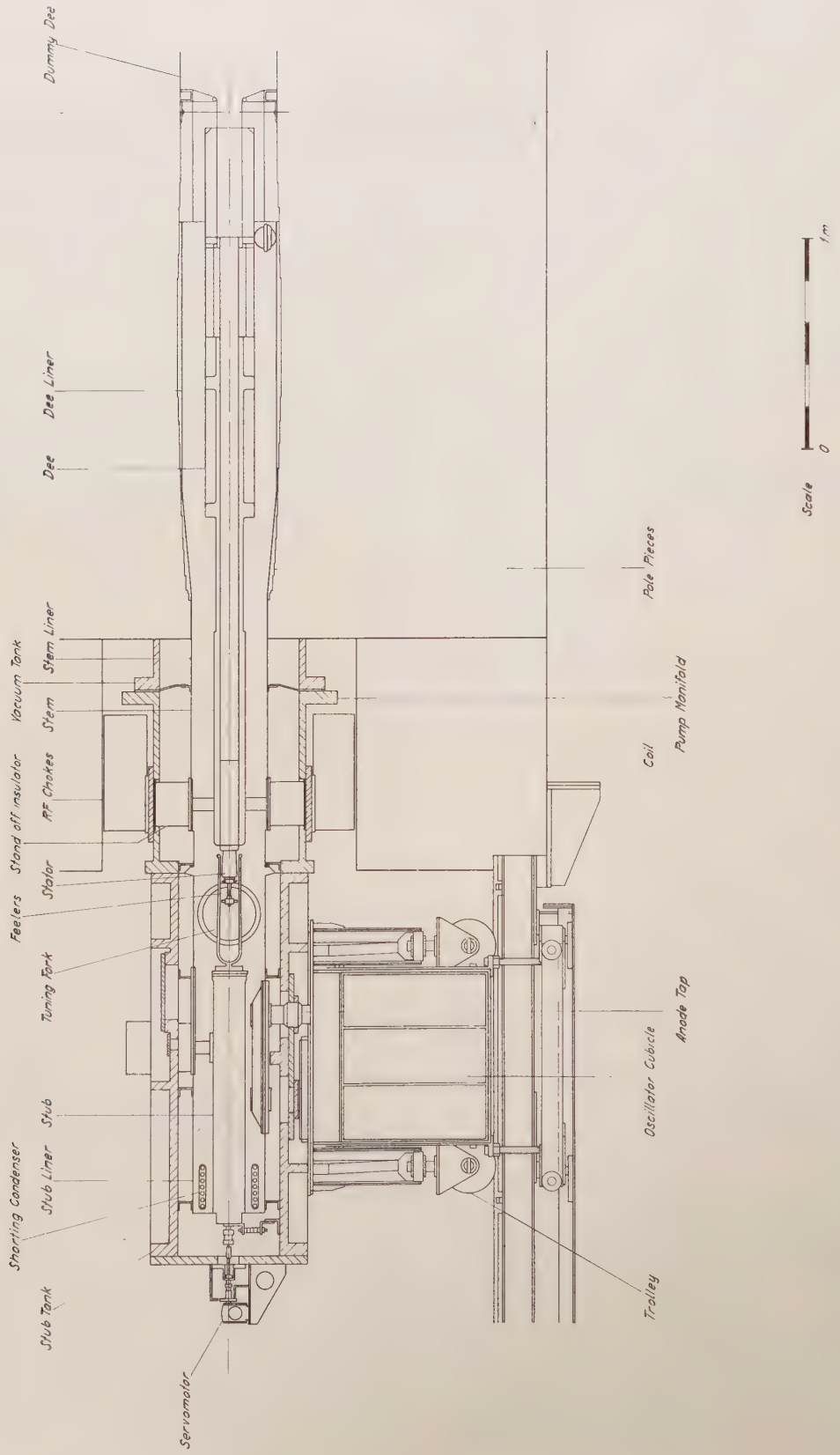
Dummy Dee
Dee Liner
Dee
Stem Liner
Vacuum Tank
Stem
Stand off insulator
RF Chokes
Stator
Feelers
Tuning Fork
Stub
Stub Liner
Shorting Condenser
Stub Tank
Servomotor
Pole Pieces
Coil
Pump Manifold
Anode Top
Oscillator Cubicle
Trolley
Scale
0
1m

Fig. 2

frequencies but scaled up in the impedancies. A slice of a true size tuning fork was used to modulate. Also a life size model was constructed in wood. It worked in air with the true oscillator tube at slightly reduced voltage and was modulated by a flap capacitor, considered in electrical respect equivalent to a tuning fork.

Both series of experiments indicated that throughout the desired frequency range the conditions for stable oscillations could be met. but the adjustments were very critical. Considerable improvement could be obtained if the conventional anode and cathode coupling of the oscillator tube was abandoned. Instead the grid driving power is derived from the anode directly through phasing elements, the transmission line acting now as an electrical flywheel[4]). Fig. 2 shows a radial section through the system.

2.2. TUNING FORK CAPACITOR

The tuning fork capacitor ressembles in cross section a normal tuning fork with two prongs and a handle which is transformed into a baseplate. The variable capacitance is formed between the stator and the tips of the tuning fork, as is shown in fig. 3. In order to obtain sufficient capacitance the tuning fork has to be rather wide. The above requirements were met with an overlap of 100 mm and a width of 2 meters. The minimum gap is 1.5 mm and the maximum gap is 25 mm.

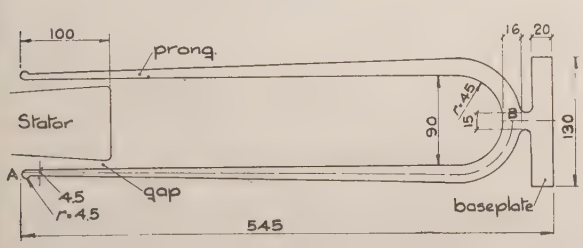

Fig. 3

The stator is tapered so as to have the minimum gap constant. Therefore, in the position of minimum capacitance the gap is not constant. This effect added to the stray capacitance accounts for the fact not withstanding the gap ratio of $\frac{1}{16}$ the minimum capacitance is about one tenth of the maximum capacitance. The width of 2 meters of the tuning fork is a convenient size to connect up to the Dee structure and leaves enough space for accomodating the two vacuum diffusion pumps. The machining of the tuning fork out of a solid block, although difficult was considered to be better than to clamp two flat blades on a common beam. (See fig. 4.) Since the stresses in the material are proportional to the frequency of free vibration, a safe figure for the latter was found to be 55 Hz. The high frequency voltage requirements associated with this modulator frequency could be met also. In Part II[5]) the mechanics of the tuning fork is discussed.

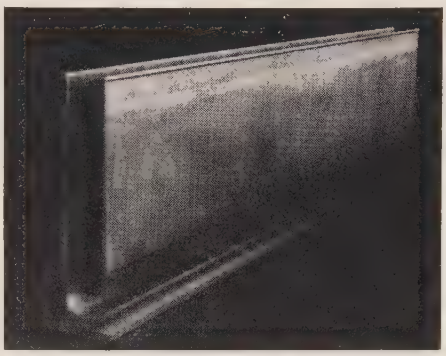

Fig. 4

2.3. TUNING FORK DRIVE

The tuning fork is driven in free vibration by means of an electro-mechanical transducer attached to the baseplate. This underlies a reversal of the principle of a tuning fork: when in motion and resting on a soundboard, it will transmit energy to the latter and so produce sound. Thus if energy is fed in the reverse direction and in the proper frequency the prongs will be set in vibration. (For a discussion of the mechanics see section 3.) The proper frequency is maintained by means of a feedback loop which in the final execution took shape as an optical device.

As a result of the low losses in the tuning fork proper, very little power is required to obtain

[4]) K. H. Schmitter, In publication.

[5]) F. Krienen, Mechanics of Tuningfork, (part II), Nuclear Instruments 5 (1959) 292.

the full amplitude. This makes the system very sensitive to additional losses, among which the eddy currents caused by the stray field of the magnet appeared to be of importance. The tuning fork is located symmetrical with respect to the median plane of the magnet, the motion is therefore nearly parallel with the magnetic flux. Indeed no losses were measured on a quarter scale model placed in 800 gauss but the conditions were not quite reproducible and special measures had to be taken in the actual machine. (See under 5.) The electrostatic force of attraction between tuning fork tip and stator, due to the high frequency voltage between them, contributes in the case of pulsed operation some driving power to the tuning fork. Since the voltage is only on during the time that the gap decreases the force has the same direction as the velocity and work is done on the moving system (of the order of 2 watt).

The heating up of various parts of the electrode system and the vacuum tank may cause some deformation and reflect in a twist or a translation of the tuning fork with respect to the stator. Also the switching on of the magnetic field or the vacuum pumps may cause similar non reproducible effects. From the above it will be clear that elaborate measures have to be taken to ensure the proper amplitude and position of the tuning fork. This will be discussed in section 4.

2.4. TUNING FORK COOLING

The high frequency currents in the tuning fork blades cause heat dissipation. To this may be added the deformation heat developed with the vibration. The high frequency current flows on the outside of the blades. Since the path is short compared with the wavelength the (surface) current density can be assumed constant, and likewise the specific heat dissipation, except at the tip where also current flows on the inside.

The current in an open transmission line is proportional to the Dee voltage, the line admittance and the sine of the electrical length. If one averages these quantities, a representative current is found to be 1600 A, and thus a surface current density $K = 400$ A/m. The corresponding heat dissipation is found with:

$$S = \sqrt{\frac{\omega\mu}{8\sigma}}\, K^2 . \tag{7}$$

This turns out to be 160 W/m² for aluminium, if the representative frequency is chosen to be 20 MHz and $\sigma = 2 \times 10^7$ mho/m. This figure has still to be multiplied with the duty cycle $\approx \frac{1}{2}$ since the h.f. current only flows when the high frequency decreases. If this heat should be reradiated the temperature would be probably too high. Therefore watercooling is provided for at the base plate of the tuning fork. The temperature is now highest at the tip and lowest at the base plate. Neglecting the effect of reradiation the equation for the temperature gradient becomes:

$$\int_0^x S_x \,\mathrm{d}x + \tau h_x \frac{\mathrm{d}T}{\mathrm{d}x} = 0 \tag{8}$$

in which x is the distance from the tip, τ the coefficient for heat conduction ≈ 140 watt/m°C, and h_x is the thickness of the blade.

In first approximation the temperature gradient is constant because the blade is tapered linearly from tip to base; substitute only

$$\int S_x \,\mathrm{d}x = Sx \quad \text{and} \quad h_x = ax .$$

This is very fortunate, because under these conditions the temperature dilatation would be stress free and the much feared buckling of the blade would not occur. The actual situation reveals a total temperature drop of 13° C and both tip and base about 2 degrees lower than constant temperature gradient would prescribe[6]).

2.5. EXPERIMENTAL WORK AND MANUFACTURING

Considering the desired life time of the tuning fork in the order of 10^9 vibrations and the high stresses in the aluminium, selection of a metal with a high fatigue limit is indicated. In addition the metal should be homogeneous in large slabs

[6]) B. Bollée, Cooling and temperature progress of the modulator for the 600 MeV Synchro-Cyclotron. (1955) Philips Nat. Lab. No. 3121 (In Dutch).

of 2000 × 550 × 130 mm and should not require special treatment after machining. The emphasis is herewith put on rather simple alloys among which type 57 S was selected. The supplier was the Netherlands Aluminium Company (N.A.M.), Utrecht, who delivered blocks of the above size ready for machining. Supersonic tests were carried out on each block, and X-ray test on samples. The machining was entrusted to the Rotterdam Drydock Company (R.D.M.), Rotterdam (Netherlands), who used the method of successive approximation to obtain the desired profile. Special care was taken on the finish of the interior curved part, since maximum stresses occur in that region. Thickness deviations measured on lines parallel to the long side could be kept below 0.1 mm. Straightness of the blades was within 0.2 mm. Tests on two quarter scale models in vacuum were undertaken[7]). They provided data on the life time, drive power, constancy of frequency and amplitude and undesired modes of vibration. Since tests on full size tuning forks could only be performed on the completely assembled Synchro-Cyclotron, preliminary tests were done in a hydrogen atmosphere. The damping compared with air atmosphere is an order less and next best to vacuum. Data were obtained on undesired modes, temperature dilatation and the suspension of the tuning fork. The final tests in which the vibrating tuning fork carries the full high frequency current, could only be done in situ and is discussed in section 5.

3. Driving System

3.1. PRINCIPLE

Various principles have been considered, among which we may mention magneto striction, working on a higher harmonic of the base plate motion; magnetized rotating disks pushing and pulling the base plate, and moving coil arrangements, enabling to apply purely sinusoidal forces. The forces on the base plate are fairly high, supposing they are in phase with the velocity:

$$P = \tfrac{1}{2}\omega \mid x \mid F \qquad (9)$$

in which P is the net power to be supplied to the tuning fork, say 16 watt, $\mid x \mid$ is the amplitude of the base plate, 0.1 mm, ω is angular frequency of about 330. Consequently the amplitude of the force amounts to 1000 newton. In virtue of this an electro-mechanical transducer had to be designed in which the magnetic forces could be reduced by a factor of 10. It was also advisable to suspend tuning fork plus driving system as a whole, so as to prevent forces being transmitted to the framework. The transducer is schematically arranged as follows (see fig. 5).

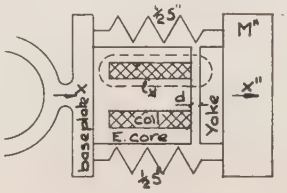

Fig. 5

E core plus coil are fixed to the base plate. The yoke plus the attached mass can move relatively to the base plate through a set of springs. The coil carries a current of suitable periodicity and shape. The current may be harmonic with half the frequency of vibration, or DC biased or pulsed, each method works and has advantages; essential is that the magnetic force sets the yoke plus attached mass into vibration relatively to the base plate. Mass and spring are tuned approximately to the tuning fork frequency:

$$M''S'' + MS'' - \omega_0^2 MM'' = 0\,. \qquad (10)$$

Apparently the amplitude of the yoke is 10 times the base plate amplitude (in order to reduce the magnetic force a factor of 10). This determines the minimum stiffness of the spring: $S'' = 1000$ newton/mm and consequently the minimum mass in found to be $M'' = 10$ kg ($\omega^2 = 10^5$). The above arrangement with the forces everywhere in phase with the velocity is however far too critical for practical use and we have to choose considerably higher mass and stiffness (approx. 2 times).

[7]) W. Luiten and B. Bollée, Investigation on failure of quarter scale model tuning fork. (1953) Philips Nat. Lab. No. 78153 (In Dutch).

3.2. TUNING FORK ANALOGUE

It is useful to have an expression for the driving point admittance of the tuning fork. The driving point here is obviously the base plate. Although the tuning fork is a continuous system, it can be represented in the neighbourhood of the resonance frequency at the ground mode by two masses connected through a spring (see fig. 6).

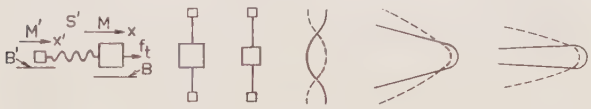

Fig. 6

The idea is this: the tuning fork originates from a flat plate swinging in two nodes. Upon concentrating the mass in the centre and at the ends we get a workable analogue, but the displacements may be incorrect. Increase of the mass in the centre at the expense of the mass at the ends brings probably the proper displacements and finally to replace the transverse vibrations of the two springs by a longitudinal vibration of one spring is a matter of convenience. Indeed with the available parameters M', S' and M we may equate the total energy W, the amplitude $|x|$ at the driving point (M) and the frequency of free vibration ω_0. Losses are brought into the picture as frictions B acting on the masses. If x is the displacement of M, x' the displacement of M' and f_t is the driving force, the equations of motion are given by:

$$\begin{aligned} M\ddot{x} + B\dot{x} + S'(x - x') &= f_t \\ M'\ddot{x}' + B'\dot{x}' + S'(x' - x) &= 0 . \end{aligned} \tag{11}$$

From this one finds easily that in the case of a harmonic force, by splitting off the time factor $\exp(-i\omega t)$, the driving point admittance is given by

$$Y_t = \frac{\omega^2 M' - S' + i\omega B'}{B'(\omega^2 M - S') + B(\omega^2 M' - S') + i\omega(M'S' + MS' - \omega^2 MM' + BB')} \tag{12}$$

where Y_t is the complex ratio of velocity and driving force

$$\dot{X} = Y_t F \tag{13}$$

obviously the power fed into the system is given by:

$$P = \tfrac{1}{2}|F|^2 \operatorname{Re}(Y_t) . \tag{14}$$

We may associate B' with the deformation loss of the material and eventually eddy current losses as they occur in the tuning fork due to the stray field of the magnet. B may represent the suspension losses which in first approximation can be neglected.

$$\operatorname{Re}(Y_t) = \frac{B'S'^2}{B'^2(\omega^2 M - S')^2 + \omega^2(M'S' + MS' - \omega^2 MM')^2} . \tag{15}$$

We are now in the position to express M, M', S' and B' in terms of measurable quantities. The resonance condition is determined by the maxima in $\operatorname{Re}(Y)$. With sufficient accuracy, anticipating $S' \ll \omega_0^2 M$, we find:

$$M'S' + MS' - \omega_0^2 MM' = 0 . \tag{16}$$

Half the power absorption occurs at:

$$\pm\omega(M'S' + MS' - \omega^2 MM') = B'(\omega^2 M - S') . \tag{17}$$

This equation is connected with the quality factor Q by introducing the detuning $\Delta\omega$. Approximately one obtains:

$$Q = \frac{\omega_0}{2\Delta\omega} \simeq \omega_0 M'/B' \simeq S'/\omega_0 B' . \tag{18}$$

At off-resonance one finds:

$$1/Y_t \simeq -i\omega M . \tag{19}$$

In this case we expect the tuning fork to behave as its true mass so that M of the analogue equals the true mass of the tuning fork (this includes of course dead weight as well).

The power absorption at resonance may be expressed in the amplitude $|x|$ of the base plate. One finds using (16) and (18):

$$P_{\text{res}} = \frac{\tfrac{1}{2}\omega_0^2 |x|^2 B'}{\left|\frac{M'}{M}\right|^2 + \frac{1}{Q^2}} \tag{20}$$

By measuring P_{res} or deducting this value from

$$Q = \frac{\omega W}{P} \tag{21}$$

in which W is the total stored energy, known from Part II[8]), the equations (16), (18) and (20) may be solved for M', S' and B'.

[8]) Part II, loc cit. p. 294.

3.3.

Having thus established the characteristics of the tuning fork proper, we may now consider its behaviour in combination with the spring loaded mass of the iron yoke (S'', M'') and eventually refine the approximate expression (10). Let fig. 7 represent the analogue of the

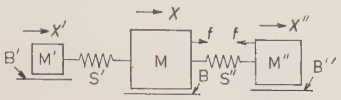

Fig. 7. T.F. analogue including driving system.

combination. We assume equal and opposite forces f between M and M'', they are of course magnetic forces. The resulting force f_t acting on the tuning fork will then be:

$$f_t = f + S''(x'' - x) = -M''\ddot{x}'' - B''\dot{x}''. \qquad (22)$$

We may associate B'' with deformation loss in the spring S'' and the hysterisis and eddy current losses in the magnetic circuit.

The complex equivalent of (22) works out as:

$$\dot{X} - \dot{X}'' = YF \qquad (23)$$

in which the driving point admittance for the magnetic force is given by:

$$Y = \cfrac{1}{\cfrac{S''}{-i\omega} + \cfrac{1}{Y_t + \cfrac{1}{B'' - i\omega M''}}}. \qquad (24)$$

Y is presented here in a form to emphasize the analogy with electrical circuits. We may do the same for Y_t in (12) and find the circuit presented in figure 8 (Y_t is the upper branch).

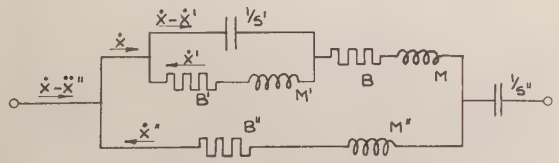

Fig. 8. Electrical analogue.

The resonance condition is found upon maximizing Re(Y). One finds in due course that the figures quoted in section 3.1 are minimum values. One may try to realize an electrical network according to (24). However, the quality is, even with the damping due to eddy currents, higher than say a thousand. Equivalent qualities are found in quartz crystals. Indeed if one draws up the dual network, the branch representing the tuning fork proper is in this case exactly the electrical analogue of a quartz crystal, and numerical equivalence can be obtained easily.

3.4.

Assuming the flux density B homogeneous in all parts of the magnetic circuit shown in fig. 5, the force is given by:

$$F = \tfrac{1}{2}B^2a/\mu_0 \qquad (25)$$

in which a is the area crossed by the magnetic flux. B is related to the current I and the voltage V in a somewhat complicated manner since the path of integration for $\int H\,\mathrm{d}l$ is not constant. Assuming no saturation in the iron we find readily:

$$\begin{aligned} nI &= B(h - 2(x - x''))/\mu_0 \\ h &= l_y/\mu_r + 2d \\ V &= IR + \tfrac{1}{2}na\,\mathrm{d}B/\mathrm{d}t \end{aligned} \qquad (26)$$

in which n is the number of turns of the coil and h is a constant, and R is the resistance of the coil. Apparently f, B, I and $x - x''$ cannot be simple harmonic functions, even if one of them is so, but they will be in any case periodic functions and can be expressed adequately as a Fourier series, for instance the force:

$$f = \tfrac{1}{2}\sum_{-\infty}^{+\infty} F_n \exp(-in\omega t) \qquad (27)$$

with the restriction that F_{-n} is the conjugate of F_n and F_0 is real. The equations of motion (11) and (22) are linear, according to them we may add solutions associated with each force component and obtain:

$$\dot{x} - \dot{x}'' = \tfrac{1}{2}\sum_{-\infty}^{+\infty} Y_nF_n \exp(-in\omega t) \qquad (28)$$

in which Y_n is the driving point admittance associated with the frequency $n\omega$ and Y_{-n} is the complex conjugate of Y_n. As may be verified $Y_0 = 0$.

The velocity (28) may be integrated to provide the displacement in (26). Only a given series in B allows a straight forward computation for I and V.

The arrows in fig. 9 give the sequence in which the quantities have to be computed. With a few components in B the general trend in the system becomes clear and optimum design parameters may be fond. The introduction of the driving point admittance on the basis of current and voltage is less suitable in this case. However, a moving coil system in a constant magnetic field lends itself to such a treatment very well.

Fig. 9. Possible system for computing electro-mechanical quantities.

4. Control

4.1. SUSPENSION

The tuning fork suspension is entirely built inside the stub and is therefore in a region free from high frequency (see fig. 10). The high frequency current passes from the outside of the tuning fork through thin phosphor bronze strips S to the stub liner. The system is hung from two steel straps attached at the bottom corners of the base plate. The effective length of the steel straps is about 10 cm. The section is 20×0.2 mm. Corner pieces enable to adjust each strap independently. This adjustment is motor driven (M).

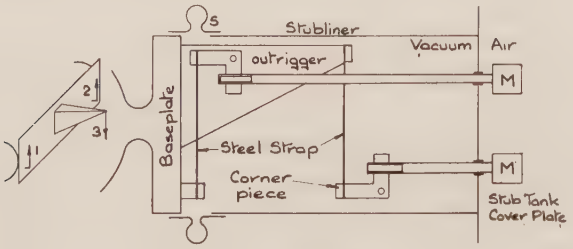

Fig. 10. Suspension.

4.2. FEELERS

In view of the minimum gap of 1.5 mm, section 2.1, the relative position of stator and tuning fork tip has to be kept with an accuracy of 0.1 mm. This relative position is measured mechanically by means of teflon feelers shown schematically in fig. 11. If they are touched by the moving tuning fork, a built-in microswitch opens, giving a signal to the control system. The rest position of the feeler is equivalent to a minimum gap of 1.4 mm. From time to time the feeler is brought up in two successive steps of 0.1 mm each, to indicate minimum gaps of 1.5

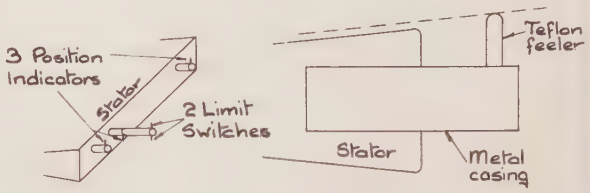

Fig. 11

and 1.6 mm respectively. The signals received from the microswitches are translated in the control system to give the required commands to the servomotors M and the amplitude control motor. Assuming the tuning fork motion at all times to perform reproducible, full position indication can be achieved with four feelers, requiring the translation of 3^4 possible positions. The problem becomes much easier if for instance the information on the inclination is omitted. One requires in this case three feelers all at the same distance from the stator, as shown in fig. 11. The information on the inclination is secured by two limit switches which act independently as safety switches.

The principles of signalling, control and faultfinding are indentical with the standards adopted elswhere in the machine[9]).

4.3. FEEDBACK LOOP

Another part of the control system is the signal derived from the tuning fork motion and fed into the amplifier which supplies energy for the driving system. Several methods have been tried. One of them consisted of a barium titanate crystal glued on the inside of the tuning fork. The voltage conditions were found to be quite good but the gluing was delicate, high frequency filtering is required and also separation from the

[9]) P. Debraine *et al.*, The design of the CERN Synchro-Cyclotron control system. 1956 CERN 56–1.

bias voltage. Another method consisted of a capacitive sonde mounted in the stator, the capacitance variations providing a frequency modulated signal. Also this system and variants thereof had some merits except for flashovers. The system now in use is an optical device. Light is projected on the edge of the tuning fork, the reflected light passes through a collimator onto a phototransistor. The system works quite well, is easily accessible as it is outside the vacuum tank. Light passes through a perspex window.

Whatever pick-up system is used, a phasing element has to be introduced to fulfill the conditions for self-oscillation. A flywheel circuit allows the system to miss a beat and a filter helps to suppress spurious modes of vibration. In the block diagram (12) also frequency halving is required in conjucntion with the magnetic circuit which operates in unbiased condition.

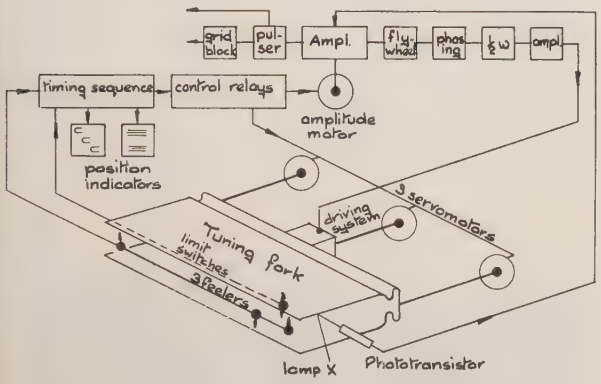

Fig. 12. Block diagram control + feed back system.

4.4.

From the tuning fork motion are derived various timing pulses required to operate the machine. One of them serves to gate the high frequency oscillator. Others may be used to time physical apparatus. The primary pulse is obtained from the preamplifier stage of the feedback loop which proved to perform highly reproducible.

5. Initial Operation

The relative position of stator and tuning fork suffers a random shift of about 0.5 mm, as a result of repeated switching on and off of magnet field and vacuum pumps. This is quite favourable in view of the much larger deflections occuring elsewhere. The starting of the machine requires adjustment before the high frequency generator can be turned on. This adjustment is effected automatically and displayed on the position indicators. Once the machine is set for continuous operation the drift due to heating up appears to be very small, and the system can work for hours before the automatic position control has to adjust. The amplitude control is more often in action. The reason for this is under investigation. The ultimate goal in this matter is of course to reduce the automatic control system to a safety device.

As mentioned in section 2.3, the stray field of the magnet caused more damping than originally anticipated. Measurements revealed several cm shift of the median plane with respect to mid plane of the stator. This was corrected locally by an auxilliary coil of 10 turns carrying 400 amperes. The eddy current losses in the tuning fork tips reduced by this procedure from 20 watt to 6 watt. Nevertheless the existing springs S″ of the driving system, (see section 3.3) ares loaded to peak value. They will be replaced in due course by heavier springs. The effective total power delivered by the amplifier is about 30 watt but voltage and current are not at all in phase $\cos \phi \approx 0.1$. Possible improvements are in study.

The cooling circuit requires constancy of in- and outlet temperature; the setting is not very critical. The cooling pipe of square section is clamped on the base plate of the tuning fork. Flexible junctions of a corrugated type connect up to the cooling conduit on the stub. The vibrations transmitted to the latter had to be tuned away. This was done by adding some 60 kg mass to the aluminium frame of the stub. Otherwise no noticeable penetration of vibration has been found on the vacuum tank.

We may calculate the influence of this by considering the analogue of cooling pipe and phosphor bronze strips S, fig. 10. It is like a spring S‴ attached between base plate and an

infinite mass (surrounding). Obviously one has to make S‴ sufficiently small compared with S″. The extra damping (cooling pipe junction) is incorporated in the friction B, fig. 7.

The voltage conditions between tuning fork and stator seem to be favourable. No excessive flashover or pitting of the aluminium occur. The stator dc bias voltage is — 2200 volt; the tuning fork dc bias voltage is — 800 volt. The h.f. peakvoltage at maximum gap ist estimated to be 20 kV; the h.f. peakvoltage at minimum gap is about 10 kV.

Fig. 13 shows a picture of the mounted tuning fork taken through the porthole on the left of the stubtank. Fig. 14 shows on the right coils plus part of the magnetic circuit screwed on the base plate of the tuning fork; and on the left yoke plus brass slabs to form M″ and the two springs to form S″. Fig. 15 shows the latest version of the teflon feeler.

Fig. 13

The tuning fork has by now operated for 6000 hours, which is equivalent to somewhat more than 10^9 vibrations. We may assume therefore that the probability of fatigue setting in is very remote. In addition we have checked from time to time the frequency of vibration. Consistent with the calculations this frequency drops one part in 300 during the warming up period, but the level remains constant within the error of measurement. We consider this also significant that fatigue has not set in since the development of miniature cracks in the material lowers the stiffness, so that with the masses

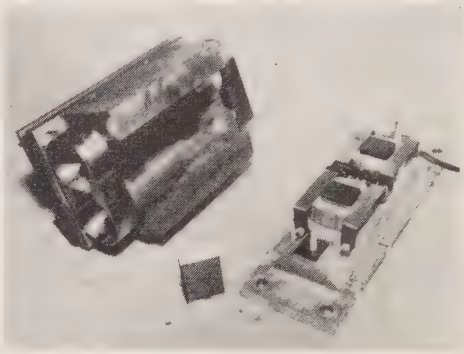

Fig. 14

remaining the same, the frequency of vibration has to lower also. In fact checking on the frequency is the only test one could perform to anticipate a possible failure, without interfering with the machine operation. As such the measurement is valuable, since it is estimated that one could gain several weeks machine time if the spare tuning fork has to be put into operation.

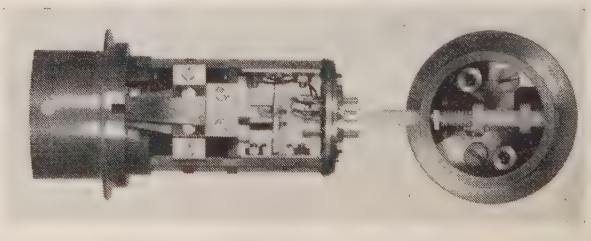

Fig. 15

Acknowledgements

The present report contains the work for which—as member of the CERN Synchro-Cyclotron Division—the author was mainly responsible. It covers the period July 1952–August 1957. The work was discussed at several meetings of the Division during this period.

The members and the consultants of the Division, who were participating in the design,

the construction and the testing of the machine are mentioned below:

C. J. Bakker (Director General), W. Gentner (Division Director), F. Blythe, F. Bonaudi, G. Boyadjian, E. Braunersreuther, D. H. Broadbent, J. M. Cassels, P. Debraine, B. Hedin, O. Frederiksson, M. Georgijević. M, van Gulik, F. Krienen, M. Lažanski, M. J. Moore, M. Morpurgo, W. Paul, T. G. Pickavance, K. H. Schmitter, H. W. B. Skinner, Th. Svedberg, J. H. Vermeulen, F. J. Woodcock.

NUCLEAR INSTRUMENTS AND METHODS 5 (1959) 292–299; NORTH-HOLLAND PUBLISHING CO.

THE TUNINGFORK FREQUENCY MODULATOR OF THE CERN SYNCHRO-CYCLOTRON

PART II MECHANICS OF TUNINGFORK

FRANK KRIENEN

CERN, *Geneva*

Received 19 May 1959

An analysis is given of the motion of a tuningfork, whose prongs are tapered. A suitable expression for the resonance frequency and the stresses in the material has been obtained, in fair agreement with experiment. The application of aluminium has been shown to be not inferior to steel. An expression for the longitudinal motion, important for the driving system, has been obtained. The higher modes of vibration are discussed qualitatively together with the possible effects on the performance.

1. Introduction

The calculation of the motion of the tuning fork and the stresses in the material has to be done in steps. It is plausible to consider as a first approximation the vibration of flat rectangular blades, which are clamped rigidly along one side and tapered towards the tip. This is done in para. 2, 3 and 4. We then proceed in para. 5 to consider the motion of two such blades which at the thicker part are curved along a quarter of a circle and so joined together. Finally in para. 6 the higher modes of vibration are discussed.

Already Kirchhoff[1]) considered the vibration of sharp wedges and sharp cones. Compared with the vibrations of cylindrical bars of rectangular or circular cross-section respectively he found considerably lower stresses in the tapered bars, provided the material, the mode of vibration, the frequency and the displacement of the free end is the same.

This is of some importance for our CERN-machine if we adopt the tuning fork capacitor for varying the frequency. Unfortunately we cannot have the blades tapered to zero thickness for constructional and electrical reasons. We therefore have to analyse the problem anew and to look what can be gained with a tapering to finite thickness. We shall see that the general solution is the same as in Kirchhoff's case.

2. Equation of motion

Let Q be Young's modulus, ρ the density, S the area of the cross-section and I the moment of inertia of the cross-section about an axis through its centre of gravity perpendicular to the plane of bending. I and S being a function of the independent variable u which is thought along the axis of the bar. If t is the time variable then the displacement x is considered to be a function of u and t only.

$$x = x\,(u,t)\,. \tag{1}$$

The slope at a point of the neutral zone is given by:

$$g = \frac{\partial x}{\partial u}. \tag{2}$$

[1]) G. Kirchhoff, Über die Transversal Schwingungen eines Stabes von veränderlichem Querschnitt. Annalen der Physik und Chemie **10**, (1880) pp. 501–512.

The bending moment we find from:

$$M = -QI\frac{\partial^2 x}{\partial u^2}. \tag{3}$$

The shearing force as:

$$F = \frac{\partial M}{\partial u} = -Q\frac{\partial}{\partial u}\left(I\frac{\partial^2 x}{\partial u^2}\right). \tag{4}$$

The resultant force acting on a length $\mathrm{d}u$ of the bar is given by:

$$\frac{\partial F}{\partial u}\mathrm{d}u = -Q\frac{\partial^2}{\partial u^2}\left(I\frac{\partial^2 x}{\partial u^2}\right)\mathrm{d}u \tag{5}$$

which must be equal to the mass in question ($\rho S\,\mathrm{d}u$) multiplied with the acceleration ($\partial^2 x/\partial t^2$).

So the equation of motion is given by:

$$\frac{\partial^2 x}{\partial t^2} = -\frac{Q}{\rho S}\frac{\partial^2}{\partial u^2}\left(I\frac{\partial x^2}{\partial u^2}\right). \tag{6}$$

Splitting off the harmonic time variable with $\dot{x} = y\exp(-i\omega t)$ we get:

$$\omega^2 y = \frac{Q}{\rho S}\frac{\mathrm{d}^2}{\mathrm{d}u^2}\left(I\frac{\mathrm{d}^2 y}{\mathrm{d}u^2}\right). \tag{7}$$

Confining ourselves to a linear taper as mentioned:

$$S = S_0 u \qquad \text{and} \qquad I = I_0 u^3 \tag{8}$$

we then have to solve:

$$\omega^2 y = \frac{QI_0}{\rho S_0 u}\frac{\mathrm{d}^2}{\mathrm{d}u^2}\left(u^3\frac{\mathrm{d}^2 y}{\mathrm{d}u^2}\right). \tag{9}$$

Changing the independent variable u into v with:

$$\omega u\,(S_0\rho)^{\frac{1}{2}} = v\,(I_0 Q)^{\frac{1}{2}} \tag{10}$$

we get:

$$vy = \frac{\mathrm{d}^2}{\mathrm{d}v^2}\left(v^3\frac{\mathrm{d}^2 y}{\mathrm{d}v^2}\right). \tag{11}$$

Now a general solution of both equations:

$$v\frac{\mathrm{d}^2 y}{\mathrm{d}v^2} + 2\frac{\mathrm{d}y}{\mathrm{d}v} = \pm y \tag{12}$$

is also a solution of the former equation. The general solution of this equation is therefore a linear combination of these two. They are respectively:

$$\begin{aligned} y &= \tfrac{1}{2}v^{-\frac{1}{2}}Z_1\,(2v^{\frac{1}{2}}) \\ y &= \tfrac{1}{2}v^{-\frac{1}{2}}Z_1\,(2iv^{\frac{1}{2}}) \end{aligned} \tag{13}$$

in which Z_1 stands for a linear combination of Bessel functions of the first order. For the real argument we chose:

$$Z_1\,(2v^{\frac{1}{2}}) = AJ_1\,(2v^{\frac{1}{2}}) + BN_1\,(2v^{\frac{1}{2}}) \tag{14}$$

and for the imaginary argument:

$$Z_1\,(2iv^{\frac{1}{2}}) = -iCJ_1\,(2iv^{\frac{1}{2}}) - DH_1^{(1)}\,(2iv^{\frac{1}{2}}). \tag{15}$$

Upon changing the independent variable v into w by $2v^{\frac{1}{2}} = w$ our displacement is given by:

$$y = (1/w)\,[Z_1\,(w) + Z_1\,(iw)] \tag{16}$$

or written in full:

$$y = (1/w)\,[AJ_1\,(w) + BN_1\,(w) - iCJ_1\,(iw) - DH_1^{(1)}\,(iw)]. \tag{17}$$

For obtaining g, M and F we note that:

$$\frac{\mathrm{d}}{\mathrm{d}u} = \omega \left(\frac{S_0\rho}{I_0Q}\right)^{\frac{1}{2}} \frac{\mathrm{d}}{\mathrm{d}v} = \omega \left(\frac{S_0\rho}{I_0Q}\right)^{\frac{1}{2}} \frac{2}{w} \frac{\mathrm{d}}{\mathrm{d}w}$$

$$S = \frac{S_0}{\omega}\left(\frac{I_0Q}{S_0\rho}\right)^{\frac{1}{2}} v = \frac{S_0}{\omega}\left(\frac{I_0Q}{S_0\rho}\right)^{\frac{1}{2}} \frac{w^2}{4}$$

$$I = \frac{I_0}{\omega^3}\left(\frac{I_0Q}{S_0\rho}\right)^{\frac{1}{2}} \frac{w^6}{64} \tag{18}$$

$$\frac{\mathrm{d}}{\mathrm{d}w}\left[w^p Z_p\,(aw)\right] = aw^p Z_{p-1}(aw)$$

$$\frac{\mathrm{d}}{\mathrm{d}w}\left[w^{-p} Z_p\,(aw)\right] = -\,aw^{-p} Z_{p+1}(aw)\,.$$

With the time factor $\exp(-i\omega t)$ omitted we find successively:

$$\begin{aligned} g &= -\,(g_0/w^2)\,[Z_2(w) + iZ_2(iw)] \\ M &= -\,M_0 w^3\ [Z_3(w) - Z_3(iw)] \\ F &= -\,F_0 w^2\ \ [Z_2(w) - iZ_2(iw)] \end{aligned} \tag{19}$$

in which:

$$\begin{aligned} g_0 &= 2\omega\left(\frac{S_0\rho}{I_0Q}\right)^{\frac{1}{2}} \\ M_0 &= \frac{QI_0}{16\omega}\left(\frac{I_0Q}{S_0\rho}\right)^{\frac{1}{2}} \\ F_0 &= \tfrac{1}{8}QI_0 \end{aligned} \tag{20}$$

Three other quantities are of interest, namely the bending stress σ, the shearing stress τ, the total stored energy W. From $M = 2I\sigma/h$ in which h, the thickness of the bar, expressed in I and S is given by:

$$h = 2\,(3I/S)^{\frac{1}{2}} \tag{21}$$

we find:

$$\sigma = -\,(3Q\rho)^{\frac{1}{2}}\,(\omega/w)\,[Z_3(w) - Z_3(iw)] \tag{22}$$

and from $F = S\tau$ we find:

$$\tau = -\,\tfrac{1}{2}\omega\,(\rho Q)^{\frac{1}{2}}\left(\frac{I_0}{S_0}\right)^{\frac{1}{2}}[Z_2(w) - iZ_2(iw)]\,. \tag{23}$$

Assuming y to be the amplitude of the displacement, the amplitude of the velocity is given by ωy. The elementary mass having this velocity is given by $\mathrm{d}M = \rho S\,\mathrm{d}u$ so the total stored energy is given by:

$$W = \tfrac{1}{2}\int_{u''}^{u'} \rho S\omega^2 y^2\,\mathrm{d}u \tag{24}$$

written with w as independent variable, we get:

$$\begin{aligned} W = \frac{I_0Q}{16}\int_{w''}^{w'} w\,[Z_1(w) + Z_1(iw)]^2\,\mathrm{d}w = \frac{I_0Q}{16}\Bigg|\frac{w^2}{2}\,[Z_1(w)\,Z_1(w) - Z_0(w)\,Z_2(w) \\ + Z_1(iw)\,Z_1(iw) - Z_0(iw)\,Z_2(iw)] + iwZ_1(w)\,Z_0(iw) - wZ_0(w)\,Z_1(iw)\Bigg|_{w''}^{w'}\,. \end{aligned} \tag{25}$$

3. Boundary conditions

If the bar is clamped at $u = u'$, equivalent to $w = w'$, then we have

$$y = y' = 0 \qquad \text{so} \qquad Z_1(w') + Z_1(iw') = 0$$

we also have

$$g = g' = 0 \qquad \text{or} \qquad Z_2(w') + iZ_2(iw') = 0\,.$$

This condition however reduces to:

$$Z_0(w') + iZ_0(iw') = 0$$

as

$$Z_2(w') + iZ_2(iw') = \frac{2}{w}[Z_1(w') + Z_1(iw')] - [Z_0(w') + iZ_0(iw')] .$$

At the free end $u = u''$ or alternatively $w = w''$ we have

$$M = M'' = 0 \qquad \text{or} \qquad Z_3(w'') - Z_3(iw'') = 0$$

also

$$F = F'' = 0 \qquad \text{or} \qquad Z_2(w'') - iZ_2(iw'') = 0$$

written in full:

$$\begin{aligned} &AJ_0(w') + BN_0(w') + CJ_0(iw') - iDH_0^{(1)}(iw') = 0 \\ &AJ_1(w') + BN_1(w'') - iCJ_1(iw') - DH_2^{(1)}(iw') = 0 \\ &AJ_2(w'') + BN_2(w'') - CJ_2(iw'') + iDH_2^{(1)}(iw'') = 0 \\ &AJ_3(w'') + BN_3(w'') + iCJ_3(iw'') + DH_3^{(1)}(iw'') = 0 . \end{aligned} \tag{26}$$

These conditions admit a solution if the determinant formed by the Bessel functions is zero, giving at the same time a functional relation between w' and w''.

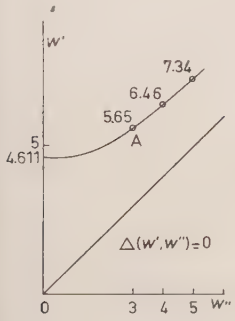

Fig. 1

$$\Delta(w',w'') = \begin{vmatrix} J_0(w') & N_0(w') & J_0(iw') & -iH_0^{(1)}(iw') \\ J_1(w') & N_1(w') & -iJ_1(iw') & -H_1^{(1)}(iw') \\ J_2(w'') & N_2(w'') & -J_2(iw'') & iH_2^{(1)}(iw'') \\ J_3(w'') & N_3(w'') & iJ_3(iw'') & H_3^{(1)}(iw'') \end{vmatrix} (= 0) \tag{27}$$

In fig. 1 is plotted the relation between w' and w'' for the fundamental mode of vibration. As it is important to obtain accurate values of w' and w'' we consider also the determinant $\Delta(w' + \delta w', w'' + \delta w'')$ in which $\delta w'$ and $\delta w''$ are arbitrary small increments of w' and w'' respectively. Omitting this operation, which is straightforward, we get:

$$\Delta(w' + \delta w', w'' + \delta w'') = \left(1 - \frac{\delta w'}{w'} - \frac{\delta w''}{w''}\right)\Delta(w', w'') + \tag{28}$$

$$+ 2\delta w' \begin{vmatrix} 0 & 0 & -iJ_1(iw') & -H_1^{(1)}(iw') \\ J_1(w') & N_1(w') & 0 & 0 \\ J_2(w'') & N_2(w'') & -J_2(iw'') & iH_2^{(1)}(iw'') \\ J_3(w'') & N_3(w'') & iJ_3(iw'') & H_3^{(1)}(iw'') \end{vmatrix} + 2\delta w'' \begin{vmatrix} J_0(w') & N_0(w') & J_0(iw') & -iH_0^{(1)}(iw') \\ J_1(w') & N_1(w') & -iJ_0(iw') & -H_1^{(1)}(iw') \\ 0 & 0 & iJ_3(iw'') & H_3^{(1)}(iw'') \\ J_3(w'') & N_3(w'') & 0 & 0 \end{vmatrix} +$$

$$+ \cdots \text{ higher powers of } \delta w' \text{ and } \delta w'' .$$

With a given pair of w' and w'' we find the coefficients A, B, C and D as the minors of the elements of a certain row of $\Delta(w',w'')$, that is to say in proportion.

The bending stress at the clamped end reduces to a simple form:

$$\sigma' = -(3Q\rho)^{\frac{1}{2}}(\omega/w'')[Z_3(w') - Z_3(iw')] = (3Q\rho)^{\frac{1}{2}}(2\omega/w')Z_1(w') \tag{29}$$

as

$$Z_3(w') - Z_3(iw') = (4/w')[Z_2(w') + iZ_2(iw')] - [Z_1(w') - Z_1(iw')]$$

in which the first term is zero on behalf of $g' = 0$ and the second term reduces to $-2Z_1(w')$ on behalf of $y' = 0$.

The displacement of the free end can also be written in a simpler form:

$$y'' = (1/w'')[Z_1(w'') + Z_1(iw'')] = -(2/w'')Z_3(w'') \tag{30}$$

as

$$Z_1(w'') + Z_1(iw'') = (4/w'')[Z_2(w'') - iZ_2(iw'')] - [Z_3(w'') + Z_3(iw'')]$$

in which the first term is zero on behalf of $F'' = 0$ and the second term reduces to $-2Z_3(w'')$ on behalf of $M'' = 0$.

Now σ' expressed in terms of ω and y'' yields:

$$\sigma' = \sigma_0 \omega y'' = -(3Q\rho)^{\frac{1}{2}} \frac{w''}{w'} \frac{Z_1(w')}{Z_3(w'')} \omega y'' \tag{31}$$

in which σ_0 can be regarded as a mode-shape factor. The slope at the free end expressed in terms of ω and y'' results in:

$$g'' = \left(\frac{S_0\rho}{I_0 Q}\right)^{\frac{1}{2}} \frac{2}{w''} \frac{Z_2(w'')}{Z_3(w'')} \omega y'' . \tag{32}$$

The total stored energy can be reduced to:

$$W = \frac{I_0 Q}{16} [\{w' Z_1(w')\}^2 - \{w'' Z_3(w'')\}^2] \tag{33}$$

or expressed in the displacement y'' squared:

$$W = \frac{I_0 Q}{64} w'^4 \left[\frac{w'' Z_1(w')^2}{w' Z_3(w'')} - \frac{w''^4}{w'}\right] y''^2 . \tag{34}$$

4. Example

A suitable pair is formed by $w'' = 3.00$ and $w' = 5.65$. From this we find: $A = 1.472$; $B = 2.280$; $C = 0.0144$; $D = 9.77$ also: $Z_1(w') = -0.6516$; $Z_2(w'') = 0.3495$; $Z_3(w'') = -0.773$ consequently:

$$\begin{aligned} \sigma' &= -0.447\ (3Q\rho)^{\frac{1}{2}}\ \omega y'' \\ g'' &= -0.301 \left(\frac{S_0\rho}{I_0 Q}\right)^{\frac{1}{2}} \omega y'' \\ W &= \quad 1.94\ \ I_0 Q y''^2 . \end{aligned} \tag{35}$$

With the practical values: $(Q/\rho)^{\frac{1}{2}} = 5000$ m/sec; $\omega = 314$; $y'' = 0.0125$ m; $g'' = -0.04$ we find $(I_0/S_0)^{\frac{1}{2}} = h_4/12^{\frac{1}{2}}$ in which h_0 is the thickness of the bar at unity distance from the origin. In our case $h_0 = 0.0205$ (dimensionless) with

$$u = \left(\frac{I_0 Q}{S_0 \rho}\right)^{\frac{1}{2}} \frac{w^2}{4\omega} = 0.0236\ w^2$$

we find the coordinate of the free end $u'' = 0.212$ m; and of the clamped end $u' = 0.755$ m.

With $(Q\rho)^{\frac{1}{2}} = 4.06 \times 10^7$ kg/m² sec (steel) we find:

$\sigma' = 123 \times 10^6\ N/m^2$ (= 12.5 kg/mm²),

with $(Q\rho)^{\frac{1}{2}} = 1.4 \times 10^7$ kg/m² sec (aluminium) we find:

$\sigma' = 42.5 \times 10^6\ N/m^2$ (= 4.3 kg/mm²).

We note that both in steel and aluminium the velocity of elastic waves is about the same $(Q/\rho)^{\frac{1}{2}} = 5000$ m/s. From this we conclude that the resonance frequency for equal bars made of either material is the same. The stresses are proportional to $(Q\rho)^{\frac{1}{2}}$. They are thus for steel a factor of 3 higher. Since the fatigue limits are quoted also a factor of 3 higher for steel, one may conclude that both materials are equivalent in performance. Per meter width of the bar the total stored energy is found to be:

$W = 46$ J (for steel) and $W = 16$ J (for aluminium).

In fig. 2 is shown the dimensions of the bar, provided:

$(Q/\rho)^{\frac{1}{2}} = 5000$ m/sec (steel or aluminium)

$\omega = 314$

$g'' = 0.04$ at $y'' = 0.0125$ m.

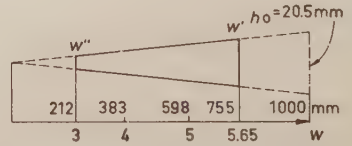

Fig. 2. $w'' = 3.00$; $w' = 5.65$; (point A of figure 1) $(Q/\rho)^{\frac{1}{2}} = 5000$ m sec; $\hat{y}'' = 0.0125$ m; $g'' = 0.04$; $\omega = 314$.

Without going into detail we found for a sharp wedge, $w'' = 0$, $w' = 4.611$:

$$\sigma'' = -0.222\,(3Q\rho)^{\frac{1}{2}}\,\omega y'' \tag{36}$$

and without taper, i.e. beam of constant section:

$$\sigma' = -(3Q\rho)^{\frac{1}{2}}\,\omega y'' . \tag{37}$$

The chosen taper seems to be a good compromise between a reduction of the bending stress and the possibility of making the bar.

One can ask for still better (non linear) tapers, solutions of which can be found if $S = S_0 u^m$ and $I = I_0 u^n$, m and n being integers, see also Nicholson[2]). However, the machining of curved surfaces seems to be a tedious task.

5. Actual Case

In the preceding paragraphs fairly exact solutions could be obtained, for which a simple indication is the measured resonance frequency. In the actual case of a tuning fork no such exact solutions could be found. However, of practical interest is to answer the question whether the stresses in the tuning fork at given frequency and amplitude are much higher than in corresponding straight bars. The experimental evidence is now that the resonance frequency of a tapered straight bar does not change much if the bar were bent to form one half of the tuning fork. Furthermore stroboscopic measurements reveal practically identical amplitude distribution. We conclude then that in both cases the kinetic energy is the same and likewise the potential energy which is here deformation energy. We easily calculate that the bulk of the deformation energy is found in the thick part of the bar. If we now assume that the neutral zone of the curved bar remains in the half way position, then we could be confident that the stress distribution in both cases are identical. However, some studies on the motion of rings reveal that the position of the neutral zone is not fixed and as a result we have to include a safety margin of some 20%. In the course of the experimental programme we were able to apply strain gauges with sufficient accuracy. The measured maximum stress was found on the inside at the bend and amounts to 6.5 kg/mm² for the actual tuning fork at full amplitude.

Even in the ground mode the motion is not purely sinusoidal. The one-dimensional treatment for slender straight bars is accurate enough and holds also for the tuning fork in sofar the stresses and the transversal motion are concerned. But with the help of a stroboscope one sees that the tuning fork moves also perpendicular to the base plate. The pattern of that motion is very much dependent on the suspension and the driving force. Since in actual fact the driving force does work against this longitudinal motion and so transmits energy to the tuning fork, it is of interest to find a suitable expression. For this we consider the free vibration of the freely suspended tuning fork. The centre of gravity remains then at rest and we obtain as working quantity the displacement of the base plate (see fig. 3).

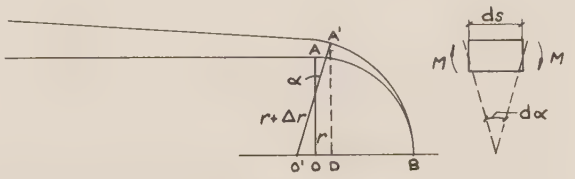

Fig. 3

The rotation of one section with respect to another spaced ds is given by

$$\frac{d\alpha}{ds} = \frac{M}{QI} \tag{38}$$

and happens to be practically constant over the quarter circle AB and thus A'B stays part of a circle. In our case $\alpha = 6 \times 10^{-3}$ radians at full amplitude. The projection OD of AA' is easily found to be:

$$OD = \left(1 - \frac{2}{\pi}\right) r\alpha \simeq 0.14 \text{ mm} . \tag{39}$$

[2]) J. W. Nicholson, The lateral vibrations of bars of variable section, Proc. Roy. Soc. **93** A (1917) pp. 506–519.

For symmetry reasons we neglect the effect of straight parts of the tuning fork. At the most they contribute to the second harmonic of the longitudinal motion. If now the curved part of the tuning fork, the base plate and the dead weight attached to the base plate had no mass, the amplitude of the base plate with respect to the centre of gravity would be the above calculated 0.14 mm. Upon bringing the above masses also into consideration the amplitude is somewhat less ≈ 0.1 mm.

6. Higher Modes Vibration

In the course of the experiments many higher modes of vibration were discovered with the help of the stroboscope or by means of a sand pattern[3]). In analogy with the discussion of section 5 we may identify one class of these modes with the vibration of thin rectangular plates clamped along one edge. In this class opposite points on the prongs of the tuning fork always move in opposite direction. We may designate these modes by the number of node lines and require two indices, but the index associated with solutions of the one-dimensional case of section 3 may be discarded as the frequencies involved are many times the ground frequency (as a matter of fact the pureness of tone of a tuning fork is based on this). A second class exists which has about the same node lines but lacks the symmetry, opposite points on the prongs move always the same way.

There are two reasons why one should be concerned with these modes. If the frequency of one of these is very nearly equal to the ground mode frequency there is a risk that the self consistent oscillating system locks into wrong vibration. Secondly the harmonics of the driving force may coincide with one of the higher modes of vibration, the effect of it being a superposition of this mode on the ground mode.

We can only deal qualitatively with the problem. Suppose we plot the frequency vs the number of lateral nodes and connect the discrete points for each class separately. Then we may consider the ground mode as the starting point for the symmetrical class. The frequency of the next point (one node) must be necessarily higher because there is an additional deformation energy due to the lateral bending, and so on. The lateral deformation energy decreases with increasing width of the tuning fork, which sets a limit to the width in view of

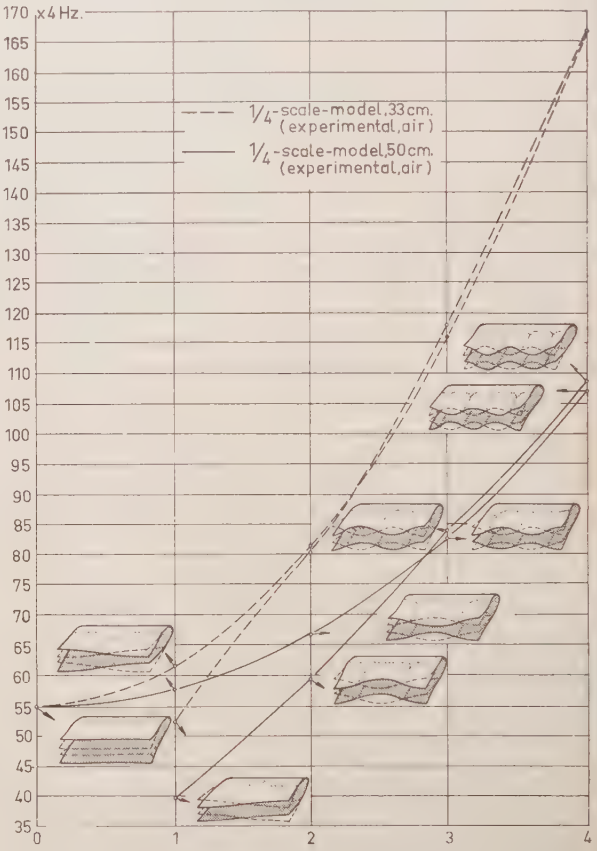

Fig. 4. Frequencies of the symmetric- and asymmetric modes of the first as a kind a function of the number of nodes at the edges.

the possibility of interference. The a-symmetrical class starts obviously with one node, which frequency may be lower than the ground mode. This is not surprising because a considerable amount of the deformation energy results from a twist, which is an entirely different mechanism. So any of the modes belonging to the a-symmetrical vibration may be dangerously close to the ground mode. With respect to

[3]) B. Bollée, Chladni's figures on the vibrating capacitor of a synchro-cyclotron. Philips Technical Review, Vol. 19 (1957/58) p. 84.

harmonics of the driving force the second provides a dangerous zone. In fig. 4 are shown the two classes experimentally measured by Philips-Eindhoven.

In the course of the experiments such a dangerous zone was successfully shifted by increasing the lateral stiffness. To this end a L-shaped aluminium rib was screwed on the tuning fork (see fig. 5). The mechanical requirements are fortunately not high: as the rib is there to prevent the occurence of lateral modes, shearing forces on the screws do not exist.

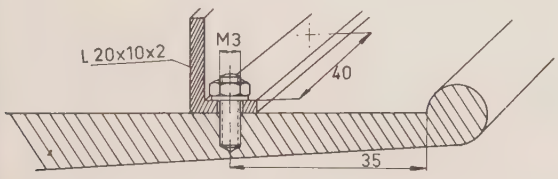

Fig. 5

At first sight it seems accidental that an harmonic of the driving force lies within the natural bandwidth of an unwanted mode. The explanation must be sought in the so called crossing of modes[4]). The frequency of free vibration depends on the temperature through dilatation, density variation and change of the modulus of elasticity. There is also evidence, at least for aluminium, that the frequency is depending on the amplitude. The effects are not the same for every mode of vibration and consequently their relative position on the frequency scale shifts. If we subject the tuning fork to all conceivable regimes of temperature and excitation, the shift is measured to be many natural bandwidths of the system. So for instance under conditions of complete operation of the synchro-cyclotron, the frequency lowers one part in 300 during a warming-up period. Since the qualities involved are of the order of several thousand, one sees that the shift measured in bandwidths is appreciable[5]).

[4]) R. L. Thornton, Frequency modulation and radio frequency system for the modified Berkeley Cyclotron. In proc. CERN Symposium 1956. Vol. **1**, p. 413.

[5]) Part I. General Design (same author) Nuclear Instruments **5** (1959) 280.

NUCLEAR INSTRUMENTS AND METHODS 5 (1959) 300–311; NORTH-HOLLAND PUBLISHING CO.

SELECTEUR 1000 CANAUX TEMPS DE VOL

J. APTER, J. ROUSSEL, J. M. TISSIER

Ingénieurs

et

R. WAHL

Directeur de la Division Nucléaire

Société Intertechnique, Versailles

Reçu le 25 juin 1959

The one thousand channels time-of-flight analyzer is an Argonne type analyzer[1]) with magnetic cores memory used for data storage.

This analyzer is a time analyzer used for spectrum measurements of neutrons by time-of-flight analysis.

The apparatus is able to count statistically the number of neutrons corresponding to a determined energy and to store the data in a memory. The spectrum can be seen in a cathode ray tube and then traduced channel by channel, printed or recorded. This apparatus has three separate inputs corresponding each to one particular group of channels, permitting to use it simultaneously with three detectors.

A very simple commutation allows:

(1) to change the region of interest setting the group of 1000 channels on a scale of 10 000 T (T being the channel width) by steps of 100 T;

(2) to obtain an address correction, directly correcting the number of channels lost during the time of memory cycle;

(3) to choose the channel width.

1. Principe de Fonctionnement

1.1. MESURE DU TEMPS DE VOL

Considérons une source de neutrons et un obturateur à disque tournant muni de N trous. Le disque, en tournant, libère un faisceau de neutrons chaque fois qu'un trou se trouve en regard de la source. Un faisceau lumineux tombant sur une cellule photoélectrique est coupé à chaque passage du disque; il lui correspond une impulsion appelée "impulsion d'obturateur" qui sert à définir le temps 0 de la mesure.

L'arrivée d'un neutron à une distance choisie du disque est détectée après un temps compris entre MT et $(M + 1)\,T$ (T étant la largeur du canal et M son numéro d'ordre).

Le temps T sera défini avec précision par le circuit HORLOGE.

Le classement des neutrons par canal se fera coup par coup en classant chaque fois le neutron dans le canal correspondant à son énergie.

[1]) R. W. Schuman et J. P. McMahon, Argonne 256, Channel pulse height analyser, Rev. sci. Instr. **27**, No. 9 (1956) 675–685.

1.2. APPLICATION AU SELECTEUR DE TEMPS DE VOL

La sélection des neutrons suivant leur temps de vol se fait de la façon suivante: l'horloge étant déclenchée par le signal d'obturateur (temps zéro), un train d'impulsions est émis et compté par des circuits compteurs; le train d'impulsion est bloqué, mais non l'oscillateur, lors de l'arrivée de la première impulsion du détecteur de neutron. Le nombre d'impulsions d'horloge libérées représente le rang d'énergie du neutron et constitue l'information d'adresse.

L'intervalle de temps compris entre l'ouverture du faisceau et la fin de la région de temps utilisée ou région d'intérêt constitue le cycle principal.

Un circuit programmeur commandé par la première impulsion d'horloge sélectionnée permet de définir dans le temps les opérations de mémoire comprenant le stockage des informations et l'inscription du nouveau coup fourni par l'impulsion du détecteur.

Un signal de correction de l'adresse précède la

remise à zéro des circuits. Pendant tout le temps du cycle de mémoire, c'est-à-dire le temps de stockage d'un coup dans la mémoire, les circuits d'entrée sont bloqués.

L'impulsion de fin de cycle ouvre à nouveau les voies de mesure et la porte qui bloquait les impulsions d'horloge.

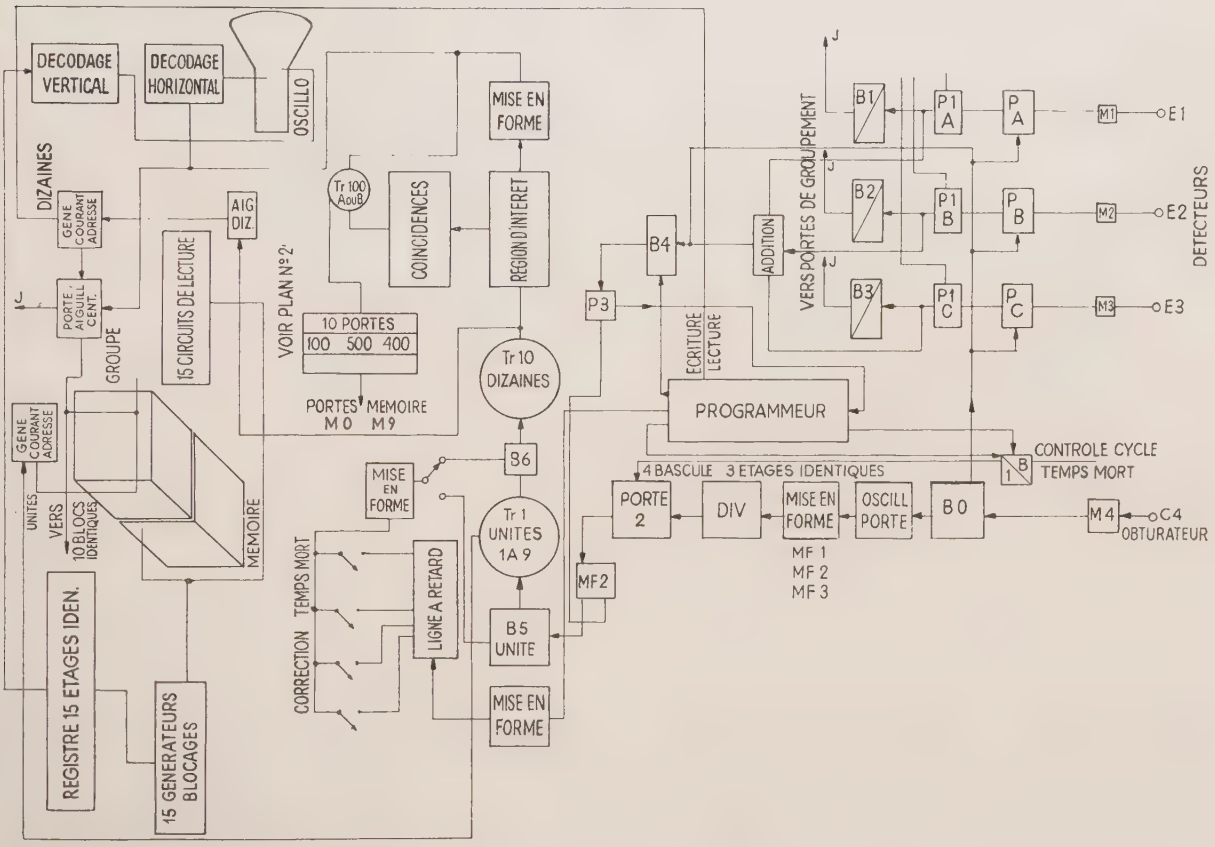

Fig. 1. Schéma synoptique. Ensemble selecteur.

2. Description des différents circuits

Les trois châssis principaux sont:

le châssis horloge-programme et contrôle des cycles,

le châssis d'adresse et contrôle des opérations de mesure,

le panneau mémoire.

2.1. CHASSIS HORLOGE-PROGRAMME

Considérons le schéma de principe (fig. 1). Nous distinguons:

(a) les trois entrées de mesure E_1, E_2, E_3 avec leurs circuits de mise en forme M_1, M_2, M_3 ainsi que les portes de blocage et déblocage P_A, P_B, P_C, P_{1A}, P_{1B}, P_{1C}, qui sont utilisées pour le groupement des canaux;

(b) le circuit d'addition;

(c) la bascule B_4;

(d) la porte P_3;

(e) le programmeur;

(f) l'entrée du signal d'obturateur C_4;

(g) l'horloge proprement dite comprenant:

(1) l'oscillateur porte;

(2) le circuit de mise en forme des signaux fournis par l'oscillateur;

(3) les circuits de division DIV;

(4) la porte 2 qui permet le blocage des impulsions d'horloge.

Fonctionnement

Le signal d'obturateur débloque un oscillateur-porte qui fournit un train d'impulsions que l'on divise (DIV) et qui constitue, après la porte 2,

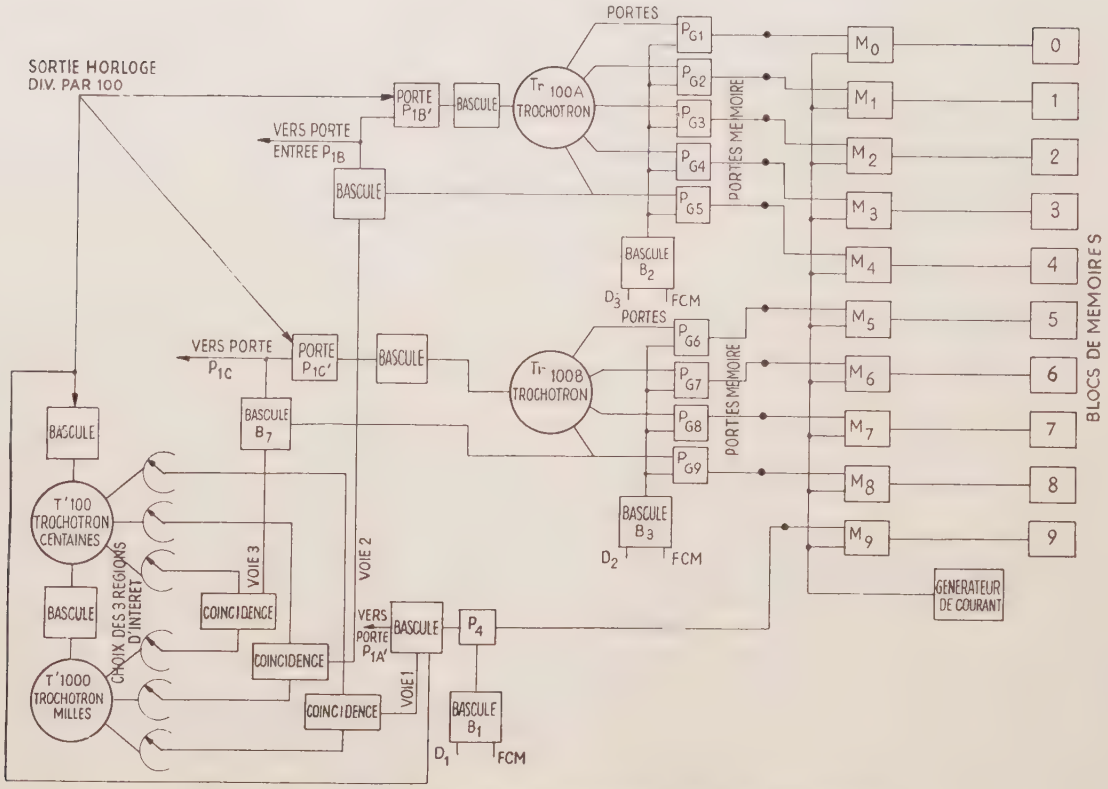

Fig. 2. Aiguillage des centaines et groupement des blocs de mémoire.

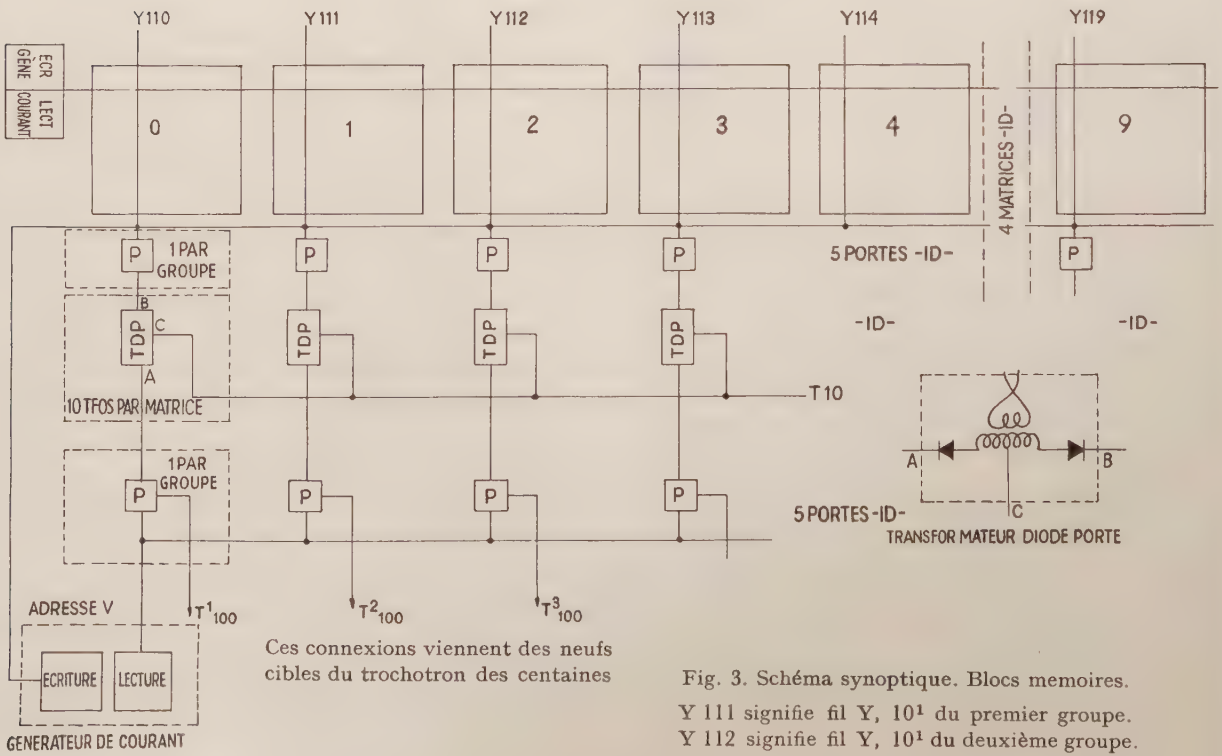

Ces connexions viennent des neufs cibles du trochotron des centaines

Fig. 3. Schéma synoptique. Blocs memoires.

Y 111 signifie fil Y, 10^1 du premier groupe.
Y 112 signifie fil Y, 10^1 du deuxième groupe.

les impulsions d'horloge. Celles-ci sont envoyées au châssis d'adresse qui les compte. Lors de l'arrivée d'un neutron sur l'une quelconque des trois voies de mesure, un signal est fourni après le circuit d'addition. Les portes P_A, P_B, P_C sont ouvertes par la bascule B_4 à l'état de repos, la porte P_2 étant bloquée par B_1 pendant le cycle de mémoire (voir fig. 4).

Il y a commande à ce moment du cycle de mémoire; le programme est alors en état de fournir les impulsions d'ordre des opérations de mémoire: lecture, addition d'un coup, écriture, correction de l'adresse, fin de cycle. Pendant le cycle de mémoire les portes P_A, P_B, et P_C sont fermées et à la fin du cycle, l'impulsion fin de cycle les rouvre. Tous les coups arrivés pendant le cycle de mémoire sont perdus. Un certain nombre d'impulsions d'horloge est perdu également; aussi est-il nécessaire de corriger l'adresse Cette correction s'effectue toujours pendant le même temps fixe appelé temps de correction de l'adresse.

Gamme de largeur des canaux

Les largeurs de canaux sont obtenues en disposant de trois oscillateurs portes dont les sorties commandent la chaîne de diviseurs.

La commutation se fait en coupant la tension d'alimentation des deux tubes non utilisés.

Les valeurs de T se répartissent alors comme suit:

Gamme 1 (μs)	Gamme 2 (μs)	Gamme 3 (μs)
0.5	2.5	3
1	5	6
2	10	12
4	20	24
8	40	48

Programmeur

On entend par là le groupe de circuits qui permet d'obtenir les divers signaux qui commandent les opérations de mémoire. Ces signaux sont au nombre de cinq; ils se suivent à 4 μs environ l'un de l'autre dans le temps et ont des largeurs de 2 à 4 μs. L'écart de temps entre deux signaux devant être fixé, on a choisi de l'obtenir par une ligne de retard.

Les impulsions de commande sont obtenues en déclenchant des monostables et en sortant les signaux sur des étages à charge cathodique pour avoir des signaux sous basse impédance.

L'attaque de la ligne se fait par l'intermédiaire d'un circuit de mise en forme (voir fig. 5).

La première impulsion d'horloge entrant dans le programmeur ferme l'interrupteur bascule B_1 qui ne s'ouvre de nouveau qu'à la fin du cycle de mémoire.

Un signal spécial de correction d'adresse est fourni par le programmeur pour déclencher les circuits de correction de l'adresse (contenus dans le châssis d'adresse).

2.2. CHASSIS ADRESSE ET CONTROLE DES OPERATIONS DE MESURE

Considérons la fig. 1. Nous distinguons:

l'échelle d'adresse proprement dite ou chaîne de comptage;

les circuits de région d'intérêt et de coïncidence (fig. 2);

les circuits de groupement des canaux (fig. 2);

les circuits de correction de l'adresse.

Chaîne de comptage

C'est une échelle de 1000 constituée par deux trochotrons[2,3]) Tr_1 et Tr_{10} et un étage compteur des centaines qui est, suivant les régions d'intérêt, constitué par un trochotron Tr_{100} A ou B ou une bascule B_7. B_5 et B_6 sont des bascules de commande de Tr_1 et Tr_{10}.

Déplacement de la région d'intérêt

(a) Problème du déplacement. Le déplacement du groupe de 1000 T (1000 canaux) doit se faire par bonds de 100 T sur une échelle d'étendue maximum de 10 000 T. Pour cela, il suffit de déplacer l'échelle d'adresse et de la fixer à la valeur choisie comme nouveau zéro;

[2]) S. P. Fan, The magnetron beam switching tube; its operation and circuit design criteria, J. Brit. IRE **15** (1955) 335–354.

[3]) H. Alfvén et L. Lindberg *et al.*, Theory and applications of trochotrons; Transact. of the Royal Institution of Technology, Stockholm (1948), No. 22.

le comptage de l'adresse proprement dite ne commence qu'à partir de cette valeur.

Toutefois le chiffre du canal de départ sera toujours de la forme: $c = a_3\ 10^3 + a_2\ 10^2 + a_1 10^1 + a_0 10^0$ avec $a_1 = a_0 = 0$; les bonds étant de 100 T.

Donc, on pourra se contenter d'afficher les valeurs a_3 et a_2 sur deux nouveaux trochotrons centaines et milles: Tr'_{100} et Tr'_{1000}.

(b) Réalisation du déplacement. Afin de ne pas perturber la véritable indication d'adresse, la nouvelle position de l'échelle est obtenue en déconnectant le trochotron des centaines Tr_{100} par une bascule, au début du cycle principal et en ouvrant en même temps une porte d'accès aux deux trochotrons supplémentaires: Tr'_{100} et Tr'_{1000}.

On remet l'échelle en état de compter normalement par un signal de coïncidence entre le chiffre fourni par Tr'_{100} et celui fourni par Tr'_{1000}.

Groupement des canaux

(a) Problème du groupement des canaux Afin de pouvoir faire trois mesures distinctes, il est possible dans cet appareil de scinder le bloc mémoire en trois groupes, ce qui permet d'utiliser les trois voies de mesures E_1, E_2, E_3.

L'opérateur peut à son gré choisir l'emplacement de ces trois groupes de canaux sur l'échelle de 1000 T.

(b) Réalisation du groupement. Pour réaliser le groupement, trois circuits de région d'intérêt sont utilisés et trois étages de comptage des centaines (2 trochotrons Tr_{100A}, Tr_{100B} et une bascule B_8).

Chacun des circuits de coïncidence relatif aux trois régions d'intérêt ouvrent des bascules B_1, B_2, B_3 qui commandent des portes (P_{G1}, P_{G2}, P_{G3}, P_{G4}, P_{G5}, P_{G6}, P_{G7}, P_{G8}, P_{G9}) groupées suivant le nombre de canaux voulus par voie de mesure et commandant les portes d'aiguillage des centaines dans le panneau mémoire (fig. 2). Ces portes M_0, $M_1 \cdots M_9$ sont ouvertes par les signaux venant des sorties des étages compteurs des centaines correspondants. Les trois portes P_{1A}, P_{1B}, P_{1C}, placées dans les trois voies E_1, E_2, E_3 ne sont ouvertes que pendant les régions d'intérêt correspondantes.

Pour obtenir un fonctionnement correct du sélecteur dans le cas où deux neutrons se présenteraient simultanément sur deux voies différentes, on utilise pour l'aiguillage sur les groupes un circuit à 3 voies dont une seule est ouverte à la fois.

Circuits de correction de l'adresse

(a) Principe de la correction. Le cycle de mémoire dure L μs.

On peut dire alors qu'il y a N impulsions d'horloge perdues pendant le stockage si $N = L/T$.

Autrement dit, l'échelle d'adresse se trouve avoir commis une erreur de N après chaque cycle de mémoire.

On corrigera alors l'affichage d'adresse en faisant compter les trochotrons du nombre supplémentaire N.

Toutefois, les impulsions d'horloge ayant une récurrence maxima de 0.5 μs, on devra corriger pour cette échelle de temps de $N = 20/0.5 = 40$ impulsions. Le temps nécessaire pour effectuer cette correction serait alors de 20 μs. Pour diminuer ce temps, on remarque que le nombre d'impulsions à corriger suivant les valeurs de T est:

μs	Nombre impulsions	μs	Nombre impulsions	μs	Nombre impulsions
0.5	40	2.5	8	3	7
1	20	5	4	6	3
2	10	10	2	12	2
4	5	20	1	24	
8	2	40	0	48	

On voit ainsi que N est de la forme $a_1 \times 10^1$ avec $a_1 = 1, 2, 4$ ou de la forme $a_0 \times 10^0$ avec $a_0 = 1, 2, 3, 4, 5, 7$.

Dès lors, on remarque que le nombre d'impulsions de correction à fournir va être compris entre 1 et 7. Lorsque le nombre d'impulsions de correction est un facteur de 10, on aiguillera le nombre correspondant à ce facteur sur le trochotron des dizaines et, lorsque le nombre

d'impulsions de correction sera inférieur à 10, on aiguillera le nombre correspondant sur le trochotron des unités.

Les impulsions de correction sont choisies à une récurrence de 0.5 μs, ce qui fait que le temps nécessaire à ce comptage sera au maximum de:

$$7 \times 0.5 = 3.5\ \mu s$$

Une impulsion spéciale dite de correction d'adresse est fournie par le programmeur pour inclure ce temps dans le cycle de mémoire. Les opérations de mémoire proprement dites dureront 16 μs.

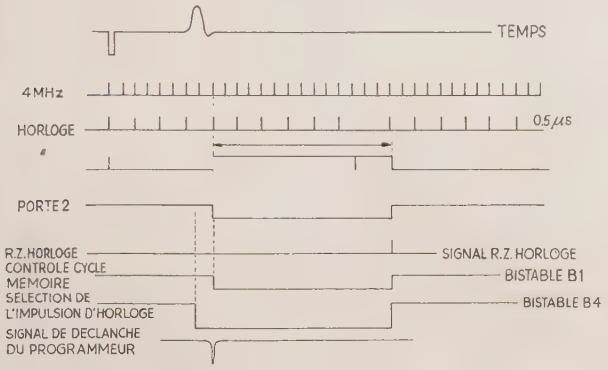

Fig. 4. Cycles de temps.

on distingue les étages compteurs rapides avec des trochotrons Burroughs type M0 10 R fréquence 2 MHz, et les étages compteurs lents avec des trochotrons Burroughs type 6700 fréquence 500 kHz.

(a) Etage compteur rapide. Il est constitué par une bascule rapide et un trochotron. L'attaque du trochotron se fait en continu et ce tube est alimenté en négatif de façon à avoir des impulsions de sortie dont le point de départ est à une tension négative. La tension négative appliquée à la cathode est fournie par un tube régulateur. La bascule rapide est constituée par deux tubes pentodes faiblement chargés, dont le couplage anode de l'une à grille de l'autre se fait par l'intermédiaire de cathodes suiveuses; ce montage permet de réduire l'influence des capacités parasites sur la charge d'anode et par là même de pouvoir augmenter celle-ci en conservant des formes d'onde correctes à la sortie de la bascule.

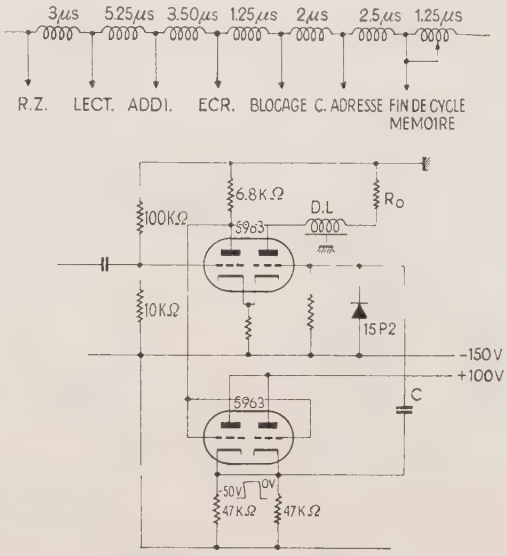

Fig. 5. Programmeur.

(b) Circuits de correction. Les impulsions de correction sont fournies par une ligne à retard utilisée dans les deux sens, c'est-à-dire avec réflexion; elle est munie de prises allant à un contacteur manuel couplé avec le sélecteur de gamme de temps.

Une fois ce réglage effectué, la correction d'adresse est automatique, l'aiguillage se faisant soit sur le circuit unités, soit sur le circuit dizaines.

Etude détaillée des circuits d'adresse

L'échelle d'adresse est essentiellement constituée par des circuits de comptage à trochotrons.

Dans les conditions où ils sont utilisés dans l'appareil, il faut remarquer que:

ce sont des tubes compteurs décimaux;

leur commande se fait par l'intermédiaire des bascules;

les 10 cibles sont sorties et permettent des commutations externes;

Un potentiomètre réglant la tension des écrans permet de trouver le seuil de déclenchement correct de la bascule.

(b) Etages compteurs lents. Les étages compteurs lents diffèrent un peu des étages rapides en ce sens que les trochotrons sont du type 6700 et que les bascules de commande

sont des bascules classiques. L'attaque du trochotron se fait toujours en continu avec des circuits alimentés en négatif.

(c) Circuits de région d'intérêt. Ils sont constitués par deux trochotrons dont les 10 cibles respectives sont reliées chacune aux plots de deux fois trois commutateurs dix positions. Les sorties de ces groupes de trois commutateurs sont connectées chacune aux grilles d'un étage de coïncidence qui ne fournit un signal que si l'une et l'autre des grilles sont excitées. Le positionnement de ces six commutateurs permet la détermination de la région d'intérêt sur les 3 voies de mesure.

2.3. MEMOIRE

Principe

Le fonctionnement de la mémoire magnétique est analogue à celui des circuits décrits par Forrester[4]), Papian[5,7]) et Rajchmann[6]).

Cette mémoire est dite à coïncidence de courant. Elle utilise des petits noyaux magnétiques en ferrite de 2 mm de diamètre qui sont montés en basculeurs magnétiques.

Remarquons qu'il faut des courants de l'ordre de 800 mA pour que les tores changent d'état, cette valeur de courant n'étant pas tout à fait la même suivant les qualités des ferrites. Comme nous voulons utiliser un comptage décimal pour l'adresse, 1000 n'étant pas un carré parfait, on ne peut concevoir une mémoire carrée, c'est-à-dire ayant autant de fils unités que de fils dizaines. On utilise donc 10 blocs de $10 \times 10 \times 15$ (la capacité de la mémoire allant jusqu'à 2^{15} coups).

Chacun de ces blocs représente 100 canaux maximum et le choix du quantième des centaines se fait par la sélection du bloc matrices relatif à ce quantième.

Réalisation pratique (fig. 3)

Afin de réaliser la sélection des centaines, tous les fils "colonne" sont couplés en parallèle en respectant leur numéro d'ordre par matrice. Ainsi, le fil sortant du transformateur commandant la première colonne de la matrice 0 est en parallèle avec les fils sortant des colonnes 1 des matrices allant de 100 à 900. Les jonctions de tous les fils colonnes seront par la suite désignées sous le nom de groupes.

Inscription dans la mémoire et lecture

Nous avons plus haut que le courant nécessaire pour faire basculer un tore est de 800 mA. On a choisi de faire la sélection unité-dizaine par une coïncidence de courants; ces deux courants de coïncidence seront donc de 400 mA chacun.

Ils sont fournis par un générateur de courant donnant environ 70 mA attaquant un transformateur diode.

(a) Transformateur diode (fig. 3). C'est un transformateur de rapport 6 environ dont les enroulements primaires sont terminés par deux diodes avant d'être connectés aux plaques du générateur de courant qui fonctionne en symétrique.

Ces diodes CR_1 et CR_2 servent à permettre l'utilisation du même transformateur pour les opérations symétriques: lecture-écriture. L'impulsion fournie par le trochotron des dizaines attaque le transformateur-diode en son point milieu. Cette impulsion, lorsqu'elle arrive, débloque CR_1 ou CR_2; le générateur de courant peut alors débiter.

Les extrémités A et B des transformateurs-diodes sont reliées ensemble par matrice et connectées à travers une porte constituée par une pentode à faible résistance interne EL 81, commandée sur sa grille par le signal venant du trochotron des centaines.

(b) Fonctionnement du générateur de courant (fig. 6). Les tubes V_1 et V_3 sont des amplificateurs qui élèvent le niveau des

[4]) J. W. Forrester, Digital information storage in 3 dimensions using magnetic cores, J. Appl. Phys. **22** (1951) 44–48.

[5]) W. N. Papian, A coincident-current magnetic memory cell for the storage of digital information, Proceed. IRE **40** (1952) 475–478.

[6]) J. A. Rajchmann, (a) Static magnetic matrix memory and switching circuits, R.C.A. Review **13** (1952) 183–201; (b) A Myriabit magnetic core matrix Memory, Proceed. IRE **41** (1953) 1407–1421.

[7]) W. N. Papian, New ferrite core Memory, Electronics **28** (1955) 194–197.

impulsions lecture-écriture. Les tubes V_2 et V_4 sont débloqués pendant un temps très court par l'impulsion amplifiée et fournissent un courant impulsionnel de valeur suffisante pour que les ampères-tours nécessaires à l'inscription soient obtenus au secondaire du transformateur. La diodes en opposition évitent de coupler par ce circuit de régulation les voies: lecture, écriture.

Registre-Circuits arithmétiques

Les circuits étudiés ci-dessus ont réalisé l'opération de stockage. Nous allons voir

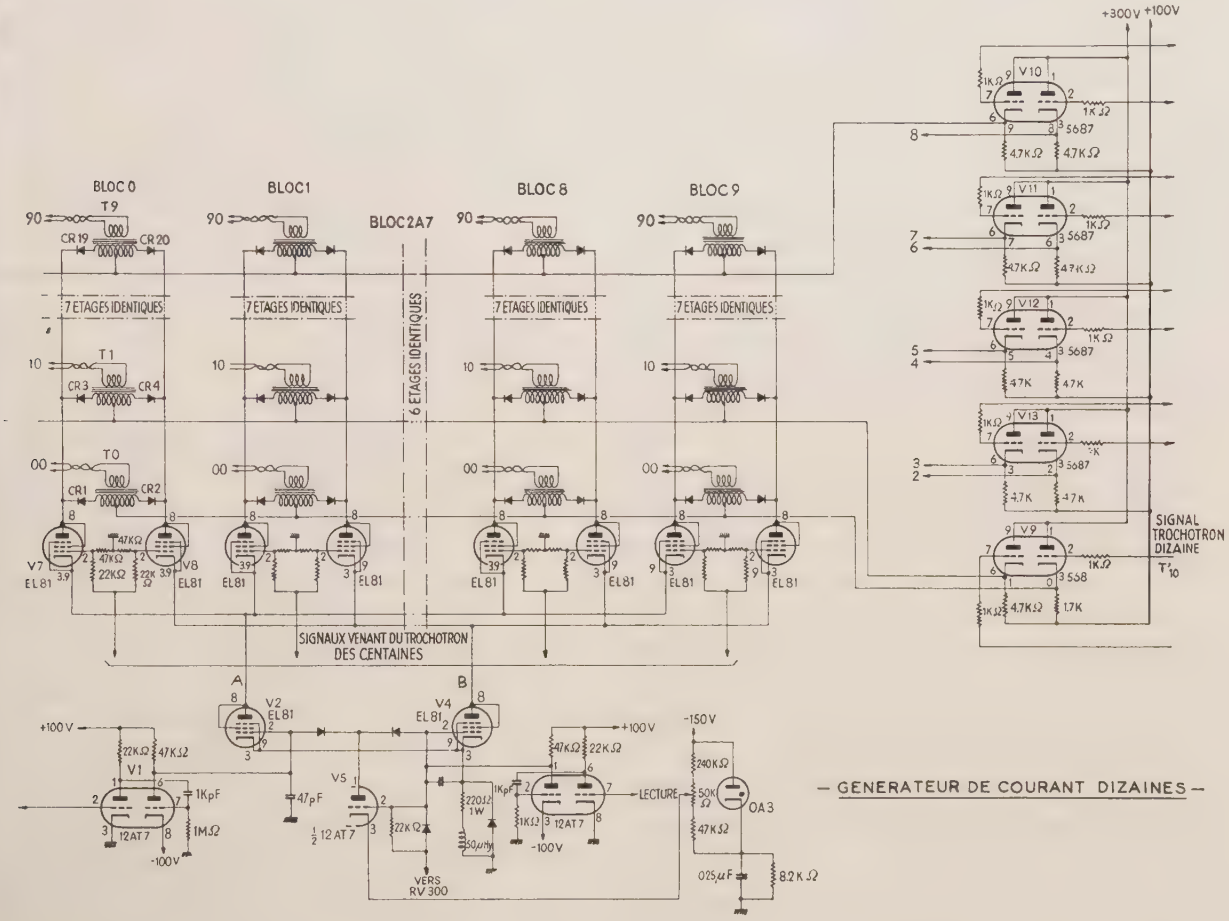

Fig. 6

particularité de ce générateur de courant par rapport à ceux décrits par Schumann et Mc Mahon[1]) réside dans l'adjonction en A et B d'une porte supplémentaire.

Les tubes V_7 et V_8 sont des portes qui sont débloquées par le signal venant des sorties de l'étage compteur des centaines. Il y a deux générateurs de courant, dizaines et unités, et 10 portes d'aiguillage des centaines branchées sur les plaques de sortie du générateur des dizaines. Les tubes V_5 et le régulateur néon constituent une chaîne de régulation du courant. Deux diodes en opposition évitent de coupler par ce circuit de régulation les voies: lecture, écriture.

Registre-Circuits arithmétiques

Les circuits étudiés ci-dessus ont réalisé l'opération de stockage. Nous allons voir maintenant comment l'on sort les résultats de la mémoire. Le principe en est le suivant:

analyse des tores qui ont basculé;

envoi de cette information sur une échelle;

addition d'un coup aux bascules de l'échelle par l'impulsion "addition d'un coup" du programmeur, le nombre présent dans la mémoire étant toujours celui du nombre de coups précédents;

réinscription dans la mémoire.

C'est le rôle de l'impulsion écriture qui suit celle de lecture à 4 μs dans le temps.

(a) Principe de l'analyse des tores ayant basculé. Chaque matrice de 10×10 ou planche, possède un fil traversant tous les tores, les sorties de ce fil sont connectées à des transformateurs d'impulsions afin d'amplifier l'impulsion et cette impulsion amplifiée est appliquée à l'étage correspondant du registres. Ce sont les voies appelées "circuits de lecture".

En vue de la réinscription dans la mémoire, on envoie des courants d'adresse dans les deux mêmes fils, mais négativement. Cette opération remettra tous les noyaux de la colonne sélectionnée dans l'état 1, mais un quatrième fil appelé fil de blocage passe dans tous les noyaux d'une planche et ce fil peut recevoir en même temps un courant positif, ce qui annule l'effet du courant d'écriture négatif. Si le courant de blocage est envoyé pendant le signal d'écriture, le noyau reste dans l'état zéro. Dans le cas contraire, il est remis dans l'état 1.

Le signal de blocage est fourni par des circuits appelés "générateur de courant de blocage".

(b) Générateur de courant de blocage (fig. 7). On désire appliquer le courant de blocage à une planche pendant l'opération d'écriture seulement et, en aucun cas, pendant l'impulsion de lecture.

Ce signal est appliqué seulement si on veut écrire un zéro à une adresse donnée.

Si l'étage du registre est dans l'état 0, une impulsion sera produite par le tube V_2 fournissant le courant de blocage. Le transformateur situé dans la plaque de ce circuit a un rapport de 12. Le tube V_2 doit donc débiter environ 30 mA pendant l'impulsion, soit un courant moyen assez faible. Le but de la diode CR_1 située au secondaire est de restituer le niveau moyen après chaque impulsion de courant.

S'il n'y avait pas cette diode, il y aurait une variation importante du niveau moyen, car les impulsions de courant sont d'une seule polarité. Cette diode permet d'avoir une constante de temps rapide pour la restitution. Sans cette précaution, non seulement le courant dans les noyaux gênerait l'opération pendant l'impulsion de lecture suivante, mais encore l'amplitude de la prochaine impulsion de blocage serait plus petite.

Il est nécessaire d'utiliser une diode ayant une résistance directe faible, car cette résistance tend à diminuer la constante de temps du secondaire. Or, il est obligatoire d'avoir une grande constante de temps au secondaire pour que le courant de blocage n'ait pas un sommet descendant de plus de quelques pour cent pendant la durée de l'impulsion. On doit avoir environ 100 Ω pour 10 mA. La diode HD 2151 nous a donné de bons résultats.

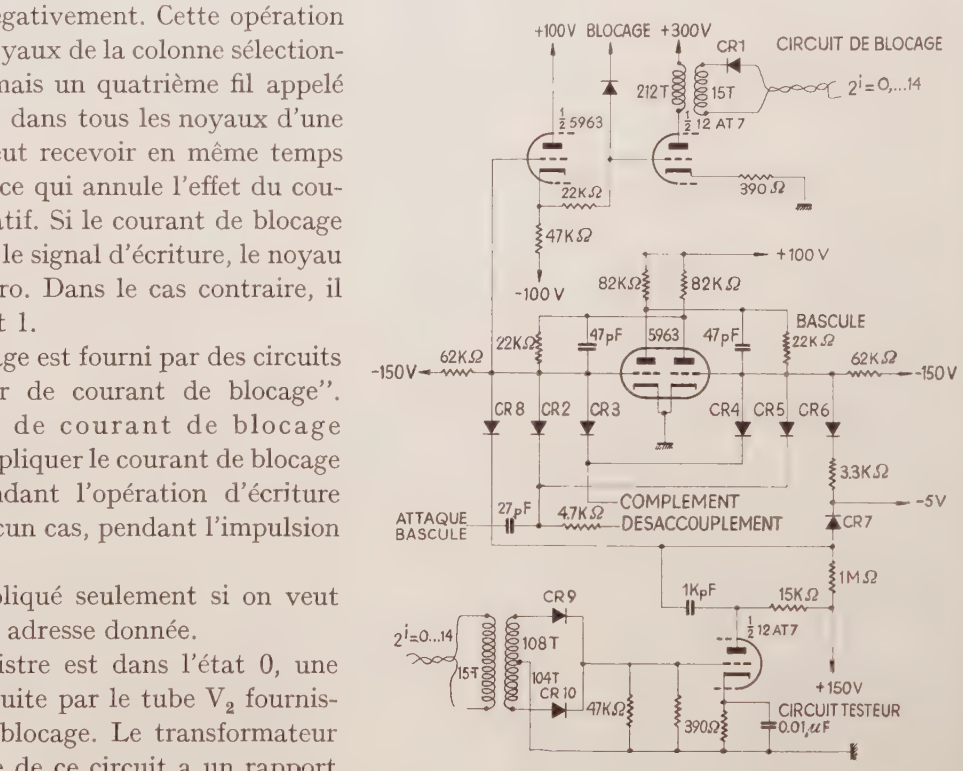

Fig. 7. Registre—étage type.

(c) Le registre (fig. 7). Le registre proprement dit est constitué par une série de 15 bascules, terminées par un circuit d'amplification.

Pour les opérations de décodage, on fait compter ce registre jusqu'à saturation en lui envoyant un nombre d'impulsions de "saturation" que l'on compte dans une autre échelle. Toutefois, cette opération ne peut se faire qu'après avoir affiché sur le registre le nombre $\overline{N}$, complèment de N, chiffre affiché précédemment.

Pour afficher $\overline{N}$, tout revient à inverser la

position de chaque bascule, opération appelée "complément".

Pour réaliser cette opération, on déconnecte les bascules par une ligne spéciale dite "ligne de désaccouplement" qui bloque les portes à diodes placées entre chaque bascule.

2.4. SORTIE DES RESULTATES

Circuits de décodage

Il est nécessaire d'avoir deux groupes de circuits de décodage, l'un horizontal, l'autre vertical. Le décodage horizontal est chargé de fournir des tensions proportionnelles par leur amplitude aux nombres représentatifs de l'adresse. Ces circuits de décodage sont utilisés, entre autres, pour donner une représentation du spectre dans son ensemble sur un tube cathodique.

(a) Décodage vertical. Le décodage vertical procède par une transformation binaire analogique, afin de traduire le nombre de coups stockés par canal. Les 15 matrices représentant les nombres binaires allant de 2^0 à 2^{15} sont envoyées sur un commutateur de 9 galettes, 11 positions, le plot variable de ce commutateur étant relié à un groupe de diodes de décodage. Ces diodes sont réparties en deux groupes de 4 fois 2, séparés par une résistance de 1.5 kΩ. La tension qui est appliquée aux deux diodes est proportionnelle au rapport des résistances R_1/R donné par la tension de base 2^0 multipliée par 2^1, 2^2, 2^3, 2^4, 2^5, 2^6, 2^7, 2^8. En effet on a à décoder les nombres:

64	128	256	512	1 024
2 048	4 016	8 192	16 384	32 768

La tension la plus faible est proportionnelle à 64 et les résistances servant à calibrer les courants se déduisent l'une de l'autre par une facteur de 2. La tension de base est doublée pour les chiffres supérieurs par l'adjonction d'une résistance en série de 1.5 kΩ dans la ligne de sortie décodée et on peut ainsi réutiliser le même groupement de résistances 50 kΩ, 100 kΩ, 200 kΩ, 400 kΩ. Le courant le plus faible est calculé pour que la charge des diodes soit négligeable vis-à-vis de lui. La précision du décodage avec un tel système est de l'ordre de 0.1%.

Le commutateur produit un changement d'échelle d'un facteur 2 par position. Le circuit de décodage vertical est inclus dans le châssis oscilloscope.

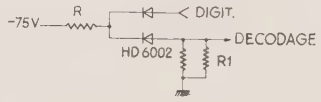

Fig. 8. Cellule de décodage vertical.

(b) Décodage horizontal. Le décodage horizontal se fait par l'intermédiaire d'un codage 1, 2, 2, 4. Les sorties des diodes sont groupées en 4 voies attaquant des cathodes suiveuses. Des résistances de précision placées aux bornes d'un groupement symétrique de diodes permettent d'obtenir des courants calibrés suivant le code 1, 2, 2, 4. Grâce à un pont diviseur précis, on peut ainsi obtenir des tensions exactement calibrées pour envoyer sur l'oscilloscope. Les signaux à décoder sont pris directement sur les cathodes suiveuses recevant les signaux des trochotrons de l'adresse.

(c) Décodage pour l'enregistrement. Un moteur tournant à 1 tour/seconde permet de faire avancer l'échelle d'adresse canal par canal ce qui donne ainsi un décodage de la courbe point par point; le spot suit le tracé de la courbe et on peut lire chaque fois le nombre de coups par canal.

Echelle arithmétique et contrôle imprimeur

L'échelle arithmétique est composée de 5 décades normalisées en éléments standard enfichables. Les sorties de ces décades sont connectées aux entrées du système sélecteur pas à pas, décrit plus haut.

Un circuit monostable et un circuit de mise en forme permettent l'attaque correcte de ce réseau de comptage.

On trouvera également sur ce châssis des cathodes suiveuses servant à fournir les signaux d'adresse à basse impédance au convertisseur de puissance pour l'imprimeur, ces signaux attaquant également le sélecteur pas à pas. Ces

circuits sont classiques; ils reçoivent le nombre codé en 1, 2, 2, 4.

L'échelle arithmétique sert à compter le nombre de coups contenus dans le registre.

Pour analyser celui-ci on fait un "complément" et on fait compter le registre à 100 kHz jusqu'à saturation.

Le nombre N' d'impulsions nécessaires pour saturer le registre est compté par l'échelle arithmétique décrite ci-dessus, N' étant égal à $N + 1$ coups, N étant le nombre vrai. On corrige le nombre obtenu en ne comptant finalement pas la première impulsion à 100 kHz.

Commande enregistreur-imprimeur

Les circuits imprimeurs sont constitués par:

(1) un châssis convertisseur de puissance comprenant une alimentation et permettant l'attaque des électroaimants de l'imprimante;

(2) un système de marquage des canaux sur l'enregistreur, disposé sur le panneau mémoire.

(1) Fonctionnement du convertisseur de puissance pour l'attaque des électroaimants. Un multivibrateur commande un moteur pas à pas qui explore successivement les informations contenues dans l'adresse et dans le registre après transcodage en 1, 2, 2, 4. Ces informations sont appliquées à des grilles de tubes ayant pour charge des relais couplés de façon à réaliser le réseau de commutation conforme au décodage cherché. Ces relais commutent des circuits qui aiguillent une tension de 160 V pour l'envoyer sur les électroaimants.

(2) Système de marquage des canaux sur l'enregistreur. L'impulsion du trochotron des dizaines Tr_{10} et celle de l'étage compteur des centaines sont envoyées sur un amplificateur qu'elles débloquent, et qui actionne un relais placé dans le potentiomètre enregistreur.

Sortie des résultats

Les résultats sont sortis en clair sur une imprimante et transformée dans un code télégraphique à 5 trous dans la même imprimante afin de pouvoir attaquer un ordinateur IBM 650.

Un châssis de commutation spécial (matrice de traduction) permet de commander l'imprimante par les signaux provenant du sélecteur proprement dit.

L'imprimante utilisée est un télétype Olivetti TCL 2 dont les touches sont actionnées au moyen d'électro-aimants.

La durée totale d'inscription des 1000 canaux est d'environ une demi-heure.

Tout autre type d'imprimantes plus rapides, peut être adapté au sélecteur.

Le spectre peut être obtenu sous forme analogique au moyen d'un potentiomètre enregistreur.

3. Caractéristiques d'ensemble du sélecteur IT 1000 canaux de temps de vol

Mesure des temps de vol allant de 0.5 μs à 48×10^4 μs en 3 échelles de 5 positions.

Capacité maximum de la mémoire: 32 767 coups

Nombre de canaux: 1000

Sensibilité sur le signal obturateur: 10 à 20 V

Sensibilité sur signal détecteur seuil régable de: 1 à 10 V

Région maximum d'investigation par bonds de 100 T: 0 à 10 000 T

Précision de l'horloge: (a) Jitter de l'impulsion à la sortie T donnée à $\pm \frac{1}{4}T$ près, (b) Précision du quartz: 10^{-5}

Cycle de mémoire: 16 μs

Durée de la correction de l'adresse: 4 μs

Durée totale du programme: 20 μs

Efficacité de la correction d'adresse valable jusqu'à: $T = 20$ μs

Erreur possible: $\leqslant$ 1 canal, 3 voies de détection avec possibilité d'affecter à chacune de ces voies respectivement 100, 400 et 500 canaux.

Possibilité de fixer le spectre pendant la mesure par simple manipulation d'un contacteur (Position "oscillo" et position "lecture").

Décodage des informations sur machine à imprimer et bandes perforées.

Enregistrement possible sur potentiomètre enregistreur.

Temps de décodage sur imprimeur: 30 minutes avec imprimante Olivetti.

4. Conclusion

La réalisation du sélecteur 1000 canaux temps de vol a été effectuée pour le compte du Commissariat à l'Energie Atomique.

Nous tenons à remercier ici les physiciens et les techniciens du C.E.A. qui nous ont aidé à la définition technique de ce sélecteur et aux essais physiques de son fonctionnement.

D'autres améliorations sont en cours de réalisation sur une nouvelle série de 3 de ces appareils, portant en particulier la largeur minimum du canal à 0.25 μs.

Le sélecteur réalisé pour le compte du Centre de HARWELL comportera un codage MERCURY-FERRANTI des informations du registre prévélées directement sous forme binaire avec transcription sur bande perforée.

Différentes publications sont prévues sur les expériences physiques réalisées avec cet appareil.

NUCLEAR INSTRUMENTS AND METHODS 5 (1959) 312–322; NORTH-HOLLAND PUBLISHING CO.

ACTIVATION ANALYSIS IN PETROLEUM EXPLORATION RESEARCH

RICHARD L. CALDWELL and WILLIAM R. MILLS, Jr.

Socony-Mobil Oil Company, Inc., Field Research Laboratory, Dallas, Texas

Received 17 August 1959

In many geological studies detection of the principal and minor elements in rocks is of interest. Neutron activation techniques are described for the rapid, quantitative determination of silicon, aluminium and magnesium, three of the most common elements in the rocks of the earth's crust. The accuracy and reproducibility of the analyses and interferences from other elements in sedimentary rocks are given.

Neutrons for activation were produced with Van de Graaff positive-ion accelerators using the reaction deuterium-tritium to give 14-MeV neutrons and the reaction deuterium-beryllium (plus a water moderator) to give slow neutrons. The activation techniques were checked against standard samples previously analyzed by other methods and against known mixtures of pure elements. Typical results obtained in the activation analysis of approximately four hundred core samples are given. The core analyses are described in connection with correlation studies in a limestone formation, identification of dolomite in carbonate rocks, measurement of the shale content of carbonate rocks and aluminum and silicon content of siliceous rocks.

1. Introduction

Petroleum research using a positive-ion accelerator as a controlled source of neutrons has resulted in new methods of nuclear logging of oil wells[1,2,3]). Accelerator sources of neutrons are also useful for laboratory analysis of samples of rocks taken from wells. This paper describes neutron activation analyses with Van de Graaff accelerators as sources of fast and slow neutrons and gives typical results obtained in geologic studies.

2. Activation Analysis

2.1. GENERAL CONSIDERATIONS AND BASIC PRINCIPLES

"Activation" by some type of nuclear reaction is used to produce a radioisotope from the element to be determined. Since the radioisotope formed decays with its own characteristic radiations and half-life, it is feasible to make activation analysis very specific. Of all the possible nuclear reactions, the neutron reactions have been most often used in activation analysis. The advent of nuclear reactors provided high fluxes of slow neutrons and successful application of activation analysis to the determination of microgram and submicrogram quantities of many elements. Its prime importance has been in determining certain trace elements which present difficulties for other analytical techniques.

In many geological studies detection of the principal and minor, but not trace, elements is of interest. Table 1 gives a list of the common elements found in sedimentary rocks. In studies of the occurrence of these elements it is frequently desirable to analyze hundreds of samples. Analyses by conventional techniques (wet chemical, X-ray diffraction, emission spectrograph) at the concentration levels encountered in geology samples is both time-consuming and costly. We have developed neutron activation techniques for the determination of several elements of interest which occur in common sedimentary rocks at levels from less than one percent to twenty or more percent. Both slow and fast (14 MeV) neutron bombardments are used. Activation analysis of core

[1]) R. L. Caldwell and R. F. Sippel, New developments in radioactive well-logging research; Bull. American Asso. Petroleum Geologists 42, No. 1 (1958).

[2]) R. L. Caldwell, Using nuclear methods in oil-well logging; Nucleonics, 16, No. 12 (1958) 58–65.

[3]) J. Tittman and W. B. Nelligan, Laboratory studies of a pulsed neutron source technique in well logging; Society Petroleum Engineers, AIME, Rocky Mountain Regional Meeting, Casper, Wyoming (April 2–3, 1959) Paper No. 1227-G.

TABLE 1

Common elements in sedimentary rocks†

	Shale (%)	Sandstone (%)	Limestone (%)	Dolomite (%)	Calcite (%)	Kaolinite (%)
SiO_2	58.90	78.64	5.20			46.5
Al_2O_3	15.63	4.77	0.81			39.5
Fe_2O_3	4.07	1.08				
FeO	2.48	1.30				
MgO	2.47	1.17	7.92	21.9		
CaO	3.15	5.51	42.74	30.4	56.04	
Na_2O	1.32	0.45	0.05			
K_2O	3.28	1.32	0.33			
H_2O_+	3.72	1.33	0.56			14.0
TiO	0.66	0.25	0.06			
P_2O_5	0.17	0.08	0.04			
CO_2	2.67	5.03	41.70	47.7	43.95	
Misc.	1.47	0.07	0.05			

† Handbook of Rocks, J. F. Kemp, p. 193.

samples has the advantage over other analytical methods of being non-destructive and of giving an average value for the entire core.

The activation method depends upon the production of radioactive isotopes by neutron reactions and the subsequent counting of the beta and/or gamma rays emitted by the radioisotope. By selection of neutron energy and irradiation time, the energies of radiation detected and the time of measurement of induced activity, interpretations of the results can often be made in terms of specific chemical elements. Activation analysis cannot be expected to determine a number of elements simultaneously with high sensitivity or accuracy.

When an element is bombarded, the resulting initial intensity of activity, I_0, is given by:

$$I_0 = \frac{W}{A} N f \sigma E m \, (1 - \exp(-\lambda t)) \qquad (1)$$

where

W = weight of element in grams
N = Avogadro's number
A = atomic weight
f = flux of neutrons (neutrons/cm²/second)
σ = elemental cross-section
E = efficiency of counter for the radiation detected
m = percentage isotopic abundance
λ = decay constant

$(1 - \exp(-\lambda t))$ is the saturation factor which may also be expressed as

$$1 - \exp\left(-\frac{0.693\, t}{T_{\frac{1}{2}}}\right).$$

The saturation factor depends upon the length of bombardment time, t, compared to the half-life, $T_{\frac{1}{2}}$, of the isotope formed.

From this equation it can be seen that the number of grams of material that give a specified activity is inversely proportional to the neutron flux. Thus the higher the neutron flux, the higher the sensitivity for detection of a given isotope.

In activation analysis, as in many other analytical methods, the results for unknowns are compared with standards, since relatively large errors may arise in the absolute determination of neutron flux, counting efficiency, geometry, etc. Also, neutron cross-sections are not generally accurate to better than 10, 20 or even 40 percent. The standards and unknowns are bombarded and counted under the same conditions.

For comparison of expected activities from a given weight of each of many different elements it is convenient to combine A, N, σ, λ and m into a single constant, F, characteristic of each element and independent of the bombardment time[4]). Eq. (1) then becomes:

$$I_0 = WfEF \frac{(1 - \exp(-\lambda t))}{\lambda}. \qquad (2)$$

TABLE 2

Computed relative sensitivity of the 14 MeV neutron activation analysis method for common elements in sedimentary rocks

Element	Half-life	Isotope produced	Gamma-ray energy (MeV)	F Relative activity †
Oxygen	7.4 sec	N–16	6.1, 7.1	1.05×10^{-2}
Silicon	2.3 min	Al–28	1.8	1.31×10^{-3}
Phosphorus	2.3 min	Al–28	1.8	8.5×10^{-4}
Aluminium	9.5 min	Mg–27	0.84, 1.0	8.56×10^{-5}
Magnesium	1.0 min	Na–25	0.4, 0.6, 1.0	7.54×10^{-5}
Silicon	6.6 min	Al–29	1.3, 2.4	1.02×10^{-5}
Iron	2.6 h	Mn–56	0.8, 1.8, 2.1, 3	4.58×10^{-6}
Magnesium	15.0 h	Na–24	1.4, 2.8	3.02×10^{-6}
Silicon	9.5 min	Mg–27	0.84, 1.0	2.09×10^{-6}
Aluminium	15.0 h	Na–24	1.4, 2.8	1.41×10^{-6}
Chlorine	32 min	Cl–34	1.1, 2.1	9.5×10^{-7}
Potassium	37 min	Cl–38	1.6, 2.1	6.15×10^{-7}
Potassium	1.8 h	A–41	1.3	5.25×10^{-7}

† For bombardment times which are short compared to the half-life of the activity.

The quantity F, called the "figure of merit", is

$$F = \frac{N\lambda\sigma m}{A} .$$

Because for short bombardment time, the quantity $(1 - \exp(-\lambda t))$ may be approximated by λt, eq. (2) becomes

$$I_0 = W\phi EFt .$$

F is a measure of the relative sensitivity of the method for bombardment times which are short compared to the half-life of the activity. Table 2 gives the values of F for 14 MeV neutron bombardment of a number of elements found in sedimentary rocks.

The neutron activation cross-section graphs of Meinke and Maddock are useful for comparing expected activities from slow neutron bombardment[5]). From these graphs and table 1, it can be concluded that a few minutes bombardment of most sedimentary rocks with slow neutrons should yield principally aluminium-28 activity from the $Al^{27}(n,\gamma)$ reaction. Some activity is also expected from chlorine-37, magnesium-26, calcium-48 and silicon-30.

2.2. ANALYSIS OF SILICON, ALUMINIUM AND MAGNESIUM

Silicon, aluminium and magnesium are of interest in petroleum geology in studies of carbonate rocks and shaly sands and are particularly amenable to activation analysis using the neutron outputs available from a 2 MeV accelerator. The X-ray spectrograph has been used by Chodos and others for major element analyses within limited rock types[6]). The samples analyzed by Chodos contained 45–52% SiO_2, 13–19% Al_2O_3 and 4–8% MgO. The accuracy for the direct determination of elements was 2–3% for silicon; aluminium and magnesium yielded erratic results. By a combination of the direct and tungstic acid techniques it was possible to attain accuracies of 2–3% for aluminium and 2–6% for magnesium with analysis time of two hours. The emission spectrograph has been used by Kvalheim for analysis of silicate rocks[7]). His results show a relative average error of 10% for a wide range of concentrations of silicon, sodium, potassium, aluminium, calcium, magnesium, iron and

[4]) S. E. Turner, Fast neutron activation analysis; Anal. Chem. 28 (1956) 1457.

[5]) W. W. Meinke and R. S. Maddock, Neutron activation cross-section graphs, Anal. Chem. 29 (1957) 1171.

[6]) A. A. Chodos, J. J. R. Branco and C. G. Engel, Rock analysis by X-ray fluorescence spectroscopy, Proc. Conf. Ind. Appl. X-Ray Analy., 6th, Denver (1957) 315–327.

[7]) Aslak Kvalheim, Spectrochemical determination of the major constituents of minerals and rocks; J. Opt. Soc. Am. 37, No. 7 (1947) 585.

TABLE 3

Nuclear constants of some common earth elements

Element	Isotope	Abundance (%)	Nuclear reaction		Q (MeV)	Cross-section		Half-life	Energy	
						Neutron energy	σ (mb)		γ	β_{max}
Silicon	28	92.17	n,p	Al^{28}	— 3.868	14 MeV	220	2.3 min	1.78	2.87
	29	4.71	n,p	Al^{29}	— 3.0	14 MeV	101	6.6 min	1.28	1.4
									2.03	2.5
	30	3.12	n,γ	Si^{31}	+ 6.594	thermal	130	2.6 h	1.26	1.48
	30	3.12	n,α	Mg^{27}	— 4.219	14 MeV	46	9.5 min	0.18	
									0.84	1.75
									1.02	
Aluminium	27	100	n,p	Mg^{27}	— 1.829	14 MeV	79	9.5 min	0.18	1.57
									0.84	1.75
									1.02	
	27	100	n,γ	Al^{28}	+ 7.723	thermal	230	2.3 min	1.78	2.87
	27	100	n,α	Na^{24}	— 3.155	14 MeV	135	15 h	1.38	1.39
									2.75	
Magnesium	24	78.8	n,p	Na^{24}	— 4.749	14 MeV	191	15 h	1.38	1.39
									2.75	
	25	10.1	n,p	Na^{25}	— 3.0	14 MeV	45	60 sec	0.38	2.6
									0.58	3.4
									0.98	4.0
									1.60	
	26	11.1	n,γ	Mg^{27}	+ 6.439	thermal	60	9.5 min	0.18	1.57
									0.84	1.75
									1.02	
	26	11.1	n,α	Ne^{23}	— 5.454	14 MeV		40 sec	0.44	3.8
									1.65	4.2
Calcium	44	2.1	n,p	K^{44}	— 5.3	14 MeV		22 min	1.1	1.5
									2.1	4.9
									2.5	
	48	0.185	n,γ	Ca^{49}	+ 5.12	thermal	1.1b	8.8 min	3.1	2.0
									4.0	
									4.7	
Iron	56	91.6	n,p	Mn^{56}		14 MeV	124	2.58 h	0.85	0.7
									1.8	1.0
									2.1–3	2.8
	57	2.2	n,p	Mn^{57}		14 MeV		1.7 min	0.12	2.6
									0.134	
									0.69	
Sodium	23	100	n,p	Ne^{23}	— 3.606	14 MeV	34	40 sec	0.44	3.8
									1.65	4.2
	23	100	n,γ	Na^{24}	+ 6.956	thermal	0.5b	15 h	1.38	1.39
									2.75	
	23	100	n,α	F^{20}	— 3.898	14 MeV		11 sec	1.63	5.42
Potassium	41	6.8	n,γ	K^{42}	+ 7.526	thermal	1.19b	12.5 h	0.32	2.0
									1.5	3.5
	41	6.8	n,p	A^{41}	— 1.742	14 MeV	81	1.82 h	0.129	1.2
										2.5
	41	6.8	n,α	Cl^{38}	— 0.125	14 MeV	31	37.3 min	1.6	1.1
									2.1	2.7
										4.8
	39	93.2	n,2n	K^{38}		14 MeV		7.7 min	2.1	2.7
Phosphorus	31	100	n,α	Al^{28}	— 1.957	14 MeV	146	2.3 min	1.78	2.87
	31	100	n,p	Si^{31}		14 MeV		2.6 h	1.26	1.58
	31	100	n,2n	P^{30}	— 12.4	19.3MeV	14.4	2.5 min	none	3.3β^+
Titanium	50	5.3	n,p	Sc^{50}		14 MeV		1.7 min	1.2	3 .5
									1.6	
	50	5.3	n,γ	Ti^{51}		thermal	200	5.8 min	0.32	1.5
									0.61	2.1
									0 93	
	49	5.5	n,p	Sc^{49}		14 MeV		57 min	none	2.0

Table 4
Analysis of silica samples

Sample	SiO_2 (grams)	Specific activity, counts/min/gm SiO_2			Ave.
NBS 97	1.40	67 400	67 400	66 800	67 200
Sand	3.82	67 700	65 000		66 350
Quartz	2.72	68 250	(ave. of 14 detns.)		68 250
Si metal	5.75	68 800			68 300
	0.90	67 400	68 600		68 000
	0.60	68 800	68 300		68 550
	0.394	67 500			67 500
			ave. 67 500 ± 890 or ± 1.3%		

manganese in various rocks and minerals. No information was given for the time required for an analysis.

Rosenfeld and Fitch[8]) have developed routines for the rapid chemical analysis of sedimentary rocks. The chemical procedures used are colorimetric for SiO_2, Al_2O_3, Fe_2O_3 and TiO_2, titrimetric for CaO and MgO, and gasometric for CO_2. Analysis for nine components in each sample requires about three hours.

2.2.1. Silicon

Silicon, bombarded with 14 MeV neutrons, yields the 2.3 minute half-life aluminium-28 activity with a gamma decay energy of 1.78 MeV. In our initial work on silicon analysis we bombarded one unknown and one monitor sample at the same time for 30 seconds at a target current of about 30 microamperes[4]). After a one-minute delay (to allow for 7.3-second nitrogen-16 decay), the sample was counted for a period of 2.5 minutes. Thirty seconds after the end of the sample count, the monitor was counted for two minutes. Table 4 gives the results of this method for the analysis of 7 samples, the silicon content of which ranged from 0.4 to 5.75 grams (reported as SiO_2). The observed standard deviation of the values is 1.3% with a maximum deviation from average of 3.1%.

To speed up the analysis of core samples, the procedure was modified to bombard four core samples and a silicon standard at one time by rotating them in an aluminium holder at 56 rpm in front of the 14 MeV neutron source for one minute. Starting one minute after the end of bombardment, the samples were placed in succession in a well-type sodium iodide scintillation crystal counter for a 30-second count. The silicon standard was counted last, starting at 4 minutes after the end of bombardment. Table 5 gives the results for twelve runs on identical samples of pure SiO_2. The standard deviation is 2.6% and the maximum deviation from the average is 6.0%.

Table 5
Reproducibility of silicon analysis

Weight of silicon in sample (grams)	Silicon weight determined by activation analysis		
	Run 1	Run 2	Run 3
2.0	1.93	1.93	1.98
2.0	1.92	1.88	2.01
2.0	1.90	2.06	2.02
2.0	2.03	2.01	2.03
	Average deviation = 2.6%		
	Maximum deviation = 6.0%		

For the silicon analysis the integral-type discriminator was set at 1.4 MeV to count the 1.78 MeV gamma-rays from the $Si^{28}(n,p)Al^{28}$ reaction. As can be seen from table 3, this energy selection eliminates most of the activities that might be produced from other common elements in sedimentary rock samples. Interference from phosphorus, chlorine and iron is

[8]) Rosenfeld and Fitch, unpublished work at the Field Research Laboratory, Socony-Mobil Oil Company, Dallas, Texas.

TABLE 6
Interfering elements in silicon analysis

Sample	Observed CPM/gm	Calculated relative activity from elements in the amounts found in rocks			
		Shale	Sandstone	Limestone	Dolomite
Si	32 737	100	100	100	100
Al	276	0.25	0.056	0.15	0.15
Fe	241	0.13	0.035		
Mg	751	0.12	0.044	4.5	12.5
Ca	59	0.015	2.3	1.6	
Na	802	0.081	0.022	0.036	0.036
K	514	0.16	0.047	0.18	0.18
Ti	213	0.012	0.0033	0.012	0.012
P	12 049	0.10	0.035	0.27	0.27
Cl	1 059	0.029	0.021		

possible. To check possible interference each of the common elements found in sedimentary rocks was bombarded together with a silicon standard. Table 6 shows the results for aluminium, iron, magnesium, calcium, sodium, potassium, titanium, phosphorus and chlorine. The activity from the amounts of these elements normally found in a sandstone or shale is less than 1 percent of the activity from the silicon. In a limestone or dolomite where the silicon content is low and the magnesium content may be appreciable, the interference in silicon analysis may be as much as 14 percent.

Silicon analyses were made of 3 National Bureau of Standards rock samples and 2 core samples previously analyzed in this laboratory by wet chemical and X-ray diffraction methods. The results are given in table 7.

TABLE 7
Silicon and aluminium analysis of "known" rocks

Sample	Actual	% SiO_2 found by activation analysis			% error
		run 1	run 2	ave.	
NBS 98–Plastic clay	59.11	54.9	55.9	55.4	6.3
NBS 97–Flint clay	42.87	42.1	41.0	41.55	3.1
NBS 1A–Argillaceous limestone	14.11	13.3	13.0	13.15	6.8
Woodbine sandstone	84.1†		81.3		3.3
Core No. 26	53††		51.9		2.1

Sample	Actual	% Al_2O_3 found by activation analysis	% error
NBS 98–Plastic clay	25.54	26.43	3.5
NBS 97–Flint clay	38.77	39.74	2.5
NBS 1A–Argillaceous limestone	4.16	4.25	2.3
Woodbine sandstone	3.3	3.2	2.0
Core No. 26	23.0	22	4.4

† X-ray analysis. †† Wet chemical analysis.

2.2.2. Aluminium

Fast neutron bombardment produces sodium-24 from aluminium by the (n,α) reaction and from magnesium by the (n,p) reaction. Manganese-56 produced by the (n,p) reaction on iron-56 can also cause some interference, but in most sedimentary rocks of interest to petroleum geologists the interference from iron is not serious. Results obtained with this method can be interpreted in terms of "apparent" aluminium content. If the magnesium (and iron) content is known to be low, the apparent values are close to actual aluminium concentrations. On the other hand, an independent method for aluminium analysis enables one to interpret the results in terms of magnesium content. Aluminium analysis by slow neutron bombardment was therefore investigated to develop a rapid method for use on hundreds of core samples. †

Slow neutron capture by aluminium gives 2.3-minute aluminium-28 activity. Neutrons from the deuterium-on-beryllium reaction were slowed down by water moderation. The beryllium target was in the center of a barrel 2 feet in diameter by 4 feet long. A fast neutron flux near the target in the water was evidenced by the production of aluminium-28 from phosphorus-31 and silicon-28. Therefore, the neutron flux along the axis of the target extension tube was measured at various distances from the target using activation of silicon standards. Samples were counted in a well-type sodium-iodide scintillation crystal with integral bias set at 0.9 MeV. Each sample was counted twice, first within a few minutes after the end of bombardment to count the 2.3-minute activity from fast neutron activation and again 75 minutes later to count the 2.6-hour activity after the short-lived activity had decayed. The results of these measurements are given in fig. 1. Silicon activation is about the same from 5 to 7 inches and is higher at closer positions to the target. A distance of 5 inches was selected for aluminium activation. The measured flux of indium resonance neutrons at this position with about 20 microamperes deuteron beam current on the beryllium target was 5.5×10^7 neutrons/cm²/second.

For routine analyses, an integral bias setting of 1.4 MeV was selected. This eliminates the radiation from slow neutron induced activities in magnesium and silicon, and no measurable activity is expected from slow neutron bombardment of calcium. However, at the 5-inch position in the barrel moderator there is still some fast neutron flux which produces activity in silicon, magnesium, calcium, iron and other less abundant elements. Interference can also come from slow neutron capture by the small amounts of chlorine and sodium present in sedimentary rocks. All of the common elements in sedimentary rocks were therefore bombarded at the 5-inch position and the activities measured one minute after the end of bombardment. The observed activities from the various elements were used to compute the relative activity for each element in the amounts found in a shale, sandstone, limestone and dolomite. The data given in table 1 was used as the basis for the average content of the common elements in the four kinds of sedimentary rocks. Table 8 gives the results of these measurements and calculations. Appreciable interference to aluminium analysis comes only from silicon and amounts to 5.7 percent in a sandstone and less than 3 percent in the other rocks. Magnesium, calcium and iron give a combined interference

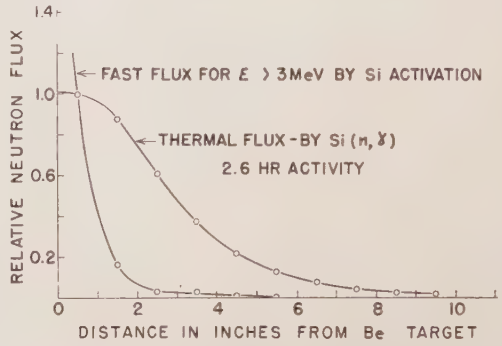

Fig. 1. Flux calibration in barrel of water.

† Other neutron energies (from the D–Be and D–D reactions) were tried for aluminum activation but were discarded because of the longer bombardment times required and the lower produced activity.

TABLE 8
Interfering elements in aluminium analysis

Sample	Observed CPM/gm	Calculated relative activity from elements in the amounts found in rocks			
		Shale	Sandstone	Limestone	Dolomite
Al	184 978	100	100	100	100
Si	723	1.3	5.7	2.2	2.2
Mg	39	0.0038	0.0059	0.23	0.65
Ca	29	0.0044	0.024	1.1	0.79
Fe	240	0.075	0.091	0.53	0.5
P	3.5	0.002	0	0	0
Cl	477	0.007	0.023	0.034	0.034
Ti	8.2	0.0026	0.003	0.005	0.005
Na	1 002	0.06	0.07	0.045	0.045
K	15	0.003	0.003	0.05	0.05

in carbonate rocks of less than 2 percent. As a further check on silicon and other interferences, a composite sample was made containing aluminium, silicon, iron, chlorine, etc., in amounts found in an average shale core sample. A pure aluminium standard was used for comparison to compute the aluminium in the composite sample, making no corrections for the contributions of silicon and other elements to the observed counting rate. The aluminium values obtained in two successive runs were 2.55 and 2.69 grams, while the actual value was 2.64 grams.

For routine analysis of core samples the procedure was to bombard four samples and an aluminium standard for one minute in a plastic container rotated at 56 rpm at 5 inches from the target, wait one minute before counting the first sample for thirty seconds, allow twelve seconds to change samples and reset the scaler, count sample # 2 for 30 seconds, etc.. The standard was counted last. A fixed-time schedule was followed so that only one set of constants was necessary to make the decay correction for successive runs. Total time for 4 cores is 6½ minutes.

Several samples of pure aluminium of about the same weight were analyzed on three repeat runs to check the reproducibility of the method. Results are given in table 9.

2.2.3. Magnesium

Fast neutron bombardment of magnesium produces three activities as shown in table 3. The $Mg^{25}(n,p)Na^{25}$ and $Mg^{26}(n,\alpha)Ne^{23}$ activities produced by 14 MeV neutron bombardment were found to be too low in intensity to be useful for magnesium analysis of rock samples. Instead, the 15-hour activity from the $Mg^{24}(n,p)Na^{24}$ reaction was used even though a long bombardment time is required. The procedure adopted for routine magnesium analysis of core

TABLE 9
Reproducibility of aluminium analysis

Weight of aluminium in sample (grams)	Aluminium weight determined by activation analysis				
	run 1	run 2	run 3	average	% error
2.8281	2.87	2.81	2.76	2.81	0.47
2.8048	2.81	2.72	2.75	2.76	1.7
4.2080	4.17	4.07	4.21	4.15	1.4
2.7308	2.66	2.63	2.66	2.65	2.8

TABLE 10

Long-lived activity from a 4-h, 14-MeV neutron bombardment of magnesium, aluminium, iron and other elements

Sample	Observed CPM/gm	Calculated relative activity from elements in the amounts found in rocks			
		Shale	Sandstone	Limestone	Dolomite
Mg	14 500	25	38	100	100
Al	10 600	100	100	6.6	2.4
Fe	276	1.5	1.8	0.7	0.25
Si	0	0	0	0	0
Ca	0	0	0	0	0
P, Cl, K, Na, Ti	30	0.1	0.1	0.1	0.1

samples uses a 4-hour bombardment with 14 MeV neutrons, a 15-hour wait to let short-lived activities from other elements decay, and a 20-minute count in a scintillation counter with 2.3 MeV integral bias. Eight core samples and two standards (one Mg and one Al) are bombarded simultaneously in an aluminium wheel rotating at 56 rpm in front of the 14 MeV neutron source. Aluminium in the samples also gives 15-hour sodium-24 activity from the (n,α) reaction. However, since the slow neutron activation method gives aluminium content, the magnesium content can be calculated. Table 10 gives the activities produced by 14 MeV neutron bombardment of magnesium, aluminium and iron. All the other common earth elements give less than 0.1% relative activity compared to aluminium and magnesium. As predicted from the data in table 3, no activity is counted from silicon and calcium because of the high gamma ray bias (2.3 MeV). The interference from iron cannot be eliminated but is small in most sedimentary rocks. Analysis of an NBS dolomite standard gave a value of 21.2 percent for the magnesium content compared to the NBS value of 21.48 percent.

3. Core Analysis Results

3.1. CORRELATION STUDIES IN THE SMACKOVER LIMESTONE

In sedimentary rocks, there are extensive vertical sections of variable lithology. The pronounced layering or "bedding" characteristic of sedimentary rocks is usually associated with variations in the clay mineral content and silica (quartz) content of these rocks. Therefore

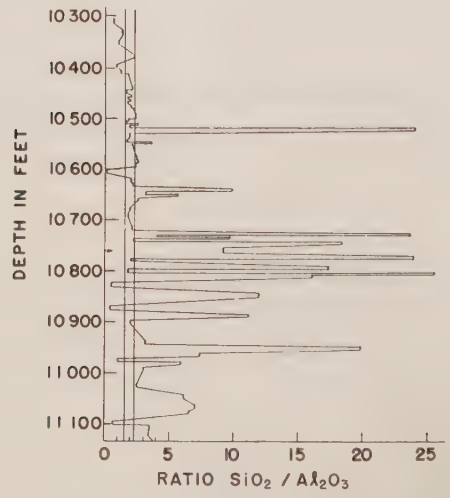

Fig. 2a. Silica Alumina "log" well A.

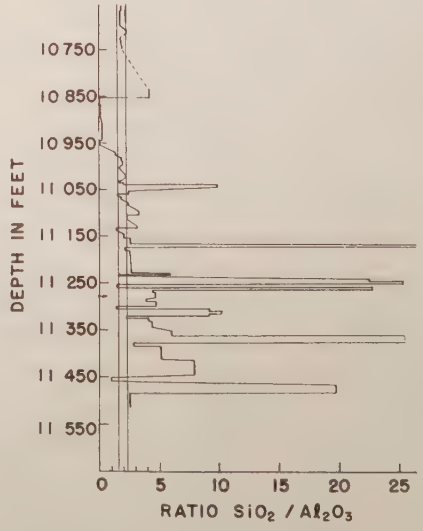

Fig. 2b. Silica alumina "log" well B.

a "log" of the aluminium and silicon content of a sedimentary section should be a useful tool for correlation as well as for such purposes as determination of the clay content of "dirty" sands.

Cores from two wells in northern Louisiana were examined by a geologist to select the more important lithological changes represented by the samples. The 135 cores selected were analyzed for silicon and aluminium; values are reported in terms of the oxides silica and alumina. The results of the analyses were plotted as "logs" of alumina content, silica content and of the silica-alumina ratio plotted against depth in the two wells. No very definite correlation between the two wells was apparent based on the logs of silica concentration or on the logs of alumina concentration. Figs. 2a and 2b are linear plots of the silica-alumina ratios of samples from the two wells. On these linear plots, the sections characterized by high silica-alumina ratios (i.e., sands and sandy shales) stand out as sharp, prominent peaks. Correlations of these two logs appears quite definite. The peak at 10 525 feet in Well A is the stratigraphic equivalent of 11 050 feet in Well B. The peak at 10 645 feet in Well A is the equivalent of 11 170 feet in Well B and the section from 10 720 to 10 970 feet in Well A correlates with that from 11 230 to 11 485 feet in Well B. This correlation agrees substantially with prior interpretations made on the basis of electric logs and core descriptions.

3.2. IDENTIFICATION OF DOLOMITE AS A CLUE TO PERMEABILITY IN THE EDWARDS FORMATION

In many carbonate reservoirs production is largely from the dolomitic facies. As early as 1886, Orton[9]) postulated that secondary dolomitization was responsible for the porosity in the Trenton limestone. This idea has been studied by geologists for years. It appears that in many reservoirs prediction of porosity can be made from the chemical composition of carbonate rocks. In certain reservoirs which did not have a clear correlation, Chilingar and Terry (1954)[10]) and Chilingar (1956)[11]) showed that the average properties of a large number of samples did indicate a correlation between chemical composition and porosity. Therefore, a magnesium "log" to differentiate dolomite and limestone is of practical interest in the development of this type of oil reservoir.

Ten core samples from a well in Texas that produces from the Edwards formation were analyzed for magnesium plus aluminium and for silicon using 14 MeV neutron bombardment. The samples were all from a carbonate section

[9]) Edward Orton, The Trenton limestone as a source of petroleum and natural gas in Ohio and Indiana, U.S. Geol. Survey 8th Ann. Report, 1886–1887, Part II (1889) 483–662.

[10]) G. V. Chilingar and R. D. Terry, Relationship between porosity and chemical composition of carbonate rocks, Petroleum Engineer **26**, No. 10 (1954) 341–343.

[11]) G. V. Chilingar, Use of Ca/Mg ratio in porosity studies, Bull. American Asso. Petroleum Geologists, Vol. **40**, No. 10 (1956) 2489–2493.

TABLE 11

Analysis of Edwards formation core samples

Depth	Dolomite expressed as % MgO		Lithology	CaO wet chem. anal. %	SiO_2 act. anal. %
	wet chem anal.	act. anal.			
1265	0.6	3.2	Limestone	52.6	1.2
1271.1	0.6	1.17	Limestone	46.3	1.81
1280.3	2.6	1.66	Limestone	50	5.3
1282.2	7.2	7.76	Limestone	54.7	0.63
1284.1	12.1	13.7	Dolomite	30.5	1.87
1297.1	19.2	17.0	Dolomite	40.3	2.69
1319.1	11.3	12.3	Dolomite	33.1	1.85
1335.0	19.1	18.6	Dolomite	33.2	2.12
1340.2	17.7	18.5	Dolomite	26.3	2.02
1594	19.5	20.1	Dolomite	32.4	2.05

in which the aluminium content was believed to be low so that the results are given as magnesia and silica content. These samples were also analyzed by wet chemistry for CaO and MgO. The combined results are given in table 11. At the lower values of MgO the activation results are high compared to the wet chemical values. At the higher values of MgO, the two methods agree favorably. In this particular well, which is characteristic of the area in which it is located, the permeable producing sections are generally high in magnesium content (10% or more dolomite). Thus, a borehole measurement of magnesium content should be useful in reevaluation of old wells in this area.

3.3. SHALE CONTENT OF CARBONATE ROCKS

It is generally recognized that the neutron log provides a measurement of hydrogen concentration. In reservoirs that are free of clay, shale or other hydrogen-containing matrices, the log response can be accepted as a measure of porosity. The porosity resolution is greater at low porosities than at high porosities, making the neutron log particularly useful in carbonate reservoirs where the porosities may be considerably lower than in many sandstone formations. In shaly sands or shaly carbonate rocks the porosity measurements may be questionable or in serious error. Thus, in some sections it is difficult to tell whether a change of neutron deflection is due to a change of porosity or shale content. Quantitative analysis of cores for aluminium, silicon and magnesium should be useful for identifying shaly sections.

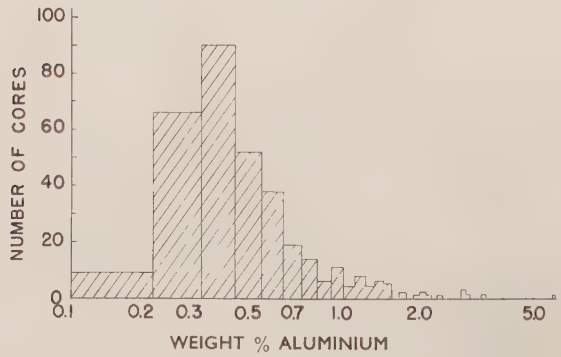

Fig. 3. Aluminium analysis of cores.

The range of aluminium concentrations in one carbonate reservoir where a large number of cores were analyzed is indicated by fig. 3. Most of the samples have aluminium concentration in the range 0.2 to 0.6 weight percent. These low values indicate an essentially shale-free reservoir. The reproducibility in routine runs for aluminium is shown in table 12.

TABLE 12

Reproducibility of aluminium analysis in routine runs

Core number	Wt. % aluminium	
	run 1	run 2
550	0.28	0.26
552	0.32	0.27
267	0.59	0.58
177	4.13	4.20
96	0.36	0.35
92	0.18	0.16
199	1.43	1.45
155	0.85	0.84
270	0.59	0.62
153	0.64	0.64
170	1.75	1.75
206	1.87	1.89

3.4. ALUMINIUM AND SILICON ANALYSIS OF SILICEOUS ROCKS OF THE MONTERY FORMATION

In California there is a type of oil reservoir that occurs in fractured rocks of the Monterey formation that are nearly pure silica (chert). The formation changes in going away from the reservoir to porcelanite to a soft shale or mudstone. Analysis of selected samples by wet chemical methods had suggested a strong gradient in the silicon-aluminium ratio of the rocks upon approaching a fractured chert reservoir. Activation analysis of forty-five outcrop samples showed a variation in the silicon-aluminium ratio from a low value of 1.5 to a high value of 110. The silica content varied from 30.4 to 96.8 percent and the alumina content ranged from 0.84 to 27.4 percent. These values can be interpreted as indicating rock types varying from nearly pure quartz (chert)to a typical shale.

Acknowledgments

The authors express appreciation to J. B. Hickman and S. E. Turner for obtaining many of the data in this paper.

NUCLEAR INSTRUMENTS AND METHODS 5 (1959) 323–326; NORTH-HOLLAND PUBLISHING CO.

EIN GERÄT ZUR SCHNELLEN REGISTRIERUNG AUSGEDEHNTER RADIOAKTIVER STRAHLER†

K. H. LAUTERJUNG und W. GRUHLE

Max-Planck-Institut für Kernphysik, Heidelberg

Eingegangen am 11. August 1959

There are two possibilities of recording the distribution of radiation intensity in an extended area. The first has a good resolution of space, but requires a recording time too long for rapid changes, while the second records with good resolution of time but with a restricted one of space.

The new method has a good resolution both of time and of space. The main feature is the use of the propagation speed of GM-counter discharge.

The area under inspection is covered by ten counters, each of which is sensitive for 1 msec all 10 msecs. The primary pulse of radiation hitting the sensitive counter starts the recording device and the arrival of the discharge in a short probe counter triggers a CRO display which gives a mapping of the radiation.

1. Einleitung

Die Methoden zur Registrierung räumlich oder flächenhaft verteilter radioaktiver Strahler lassen sich gemäss ihrer Leistungsfähigkeit in zwei Gruppen einteilen. In der einen Gruppe[1–12]) wird ein gutes *örtliches* Auflösungsvermögen erreicht, indem Detektoren die auszumessende Fläche punkt- oder zeilenweise abtasten. Dabei wird die an den jeweiligen Messorten während der Messdauer vorhandene Aktivität registriert. Diese Methode liefert nur dann ein wahres Bild der Verteilung, wenn sich die Aktivität an den einzelnen Messorten innerhalb der Gesamtmessdauer nicht ändert. Diese Methode erlaubt also keine "Momentaufnahme" der örtlichen Verteilung radioaktiver Strahler; sie hat ein niedriges zeitliches Auflösungssvermögen.

In der anderen Gruppe[13–15]) wird ein gutes *zeitliches* Auflösungsvermögen erzielt, indem eine Fläche möglichst dicht mit empfindlichen Detektoren belegt ist, von denen jeder die momentane Aktivität der von ihm erfassten Fläche registriert. Nachteilig ist dagegen der hohe apparative Aufwand und wegen der endlichen Ausdehnung der Detektoren das niedrige örtliche Auflösungsvermögen. Bei dem im folgenden zu beschreibenden Verfahren ist versucht worden, ein gutes *örtliches und zeitliches* Auflösungsvermögen zu erreichen. Dabei wird Gebrauch gemacht von den Gesetzmässigkeiten der Ausbreitung der Entladung in Auslösezählrohren[12, 16–24]).

† Vorgetragen auf der Fachausschusssitzung Kernphysik am 11.4.1957 in Bad Nauheim.

[1]) W. V. Mayneord, R. C. Turner, S. P. Newbery und H. J. Hodt, Nature **168** (1951) 762.

[2]) B. Cassen, L. Curtis, C. Reed und R. L. Libby, Nucl. **9**, No. 2 (1951) 46.

[3]) G. L. Brownell und W. H. Sweet, Nucl. **11**, No. 11 (1953) 40.

[4]) H. O. Anger, Americ. Journ. Roentgenol. Radium Therapy **70** (1953) 605.

[5]) V. Spear, Phys. Rev. **95** (1954) 308.

[6]) M. E. Jacobs, A. L. Orvis und B. B. Borrman, Nucl. **12**, No. 1 (1954) 60.

[7]) H. C. Allen und J. R. Risser, Nucl. **13**, No. 1 (1955) 28.

[8]) N. H. Horwitz und J. E. Loftstrom, Nucl. **13**, No. 7 (1955) 56.

[9]) G. R. Meneely und H. L. Jones, Nucl. **13**, No. 8 (1955) 39.

[10]) L. Holm, Rev. Sci. Instr. **27** (1956) 370.

[11]) H. O. Anger, Rev. Sci. Instr. **29** (1958) 27.

[12]) P. Kienle, Zeitsch. f. Naturf. **13a** (1958) 37.

[13]) W. Fucks und H. W. Knipping, Naturw. **42** (1955) 493.

[14]) W. Fucks, H. W. Knipping, E. Liese und W. Budde, Zeitsch. f. Naturf. **11b** (1956) 142.

[15]) W. Fucks, G. Schumacher und A. Scheidweiler, Zeitschr. f. Naturf. **12b** (1957) 250.

[16]) S. A. Korff und R. D. Present, Phys. Rev. **65** (1944) 274.

2. Prinzip

Wenn durch ein in ein Auslösezählrohr eintretendes Teilchen oder Quant in Drahtnähe eine Primärlawine ausgelöst wird, dann breitet sich von dieser Stelle eine Entladung bis zu den beiden Zählrohrenden aus. Bei vorgegebenen Zählrohrdaten ist ihre Geschwindigkeit $v = s/t$ unabhängig vom Einstrahlungsort. Die Laufzeit $t = s/v$ der Entladung vom Einstrahlungsort bis zu einem Zählrohrende ist also ein Mass für die Entfernung s des Einstrahlungsortes von diesem Zählrohrende. Sie wird in folgender Weise registriert. Die Primärlawine am Einstrahlungsort stösst den Zeilenablauf des Kathodenstrahls einer Braunschen Röhre an. Dabei ist der Strahl zunächst dunkelgesteuert. Beim Eintreffen der Entladung am einen Zählrohrende nach der Laufzeit t wird der Strahl momentan hellgesteuert. Auf dem Bildschirm entsteht ein heller Punkt, dessen Abstand vom Zeilenbeginn dem Abstand des Einstrahlungsortes s vom Zählrohrende entspricht.

Die Ankunft der Entladung am Zählrohrende wird durch ein zweites, kurzes Zählrohr registriert, das mit dem langen Zählrohr die Kathode gemeinsam hat, dessen Anodendraht aber durch eine kleine Glasperle von dem des langen Zählrohrs isoliert ist. Bei geeigneter Grösse der Glasperle und passender Arbeitsspannung der Zählrohre springt die Entladung aus dem langen in das kurze Zählrohr über.

Die auszumessende Fläche ist dicht mit solchen Zweierzählrohren belegt. Diese werden nacheinander kurzzeitig zur Registrierung eingeschaltet und geben ihre Informationen in der im nächsten Abschnitt beschriebenen Weise auf den Leuchtschirm der Braunschen Röhre.

[17]) J. M. Hill und J. M. Dunworth, Nature **158** (1946) 833.

[18]) F. Alder, E. Baldinger, P. Huber und F. Metzger, Helv. Phys. Acta **20** (1947) 75.

[19]) E. Wantuch, Phys. Rev. **71** (1947) 646.

[20]) S. G. F. Frank, Phil. Mag. **42** (1951) 612.

[21]) P. A. C. Mortier und J. F. Roose, Proc. Phys. Soc. B **67** (1954) 161.

[22]) K. H. Lauterjung und W. Gruhle, Phys. Verh. **8** (1957) 11.

[23]) E. Huster und E. Ziegler, Z. f. Phys. **146** (1956) 281; **149** (1957) 583.

[24]) K. H. Lauterjung und O. Vater, Z. f. Naturf. (im Druck).

3. Ausführung

Abb. 1 zeigt das Blockschaltbild der gesamten Anlage. In der ausgeführten Form ist die zur Registrierung ausgenutzte Fläche dicht mit 10 der im vorigen Abschnitt beschriebenen Zweierzählrohre A belegt. Jedes lange Zählrohr liefert den primären Impuls und das mit ihm verbundene kurze Zählrohr den Anzeigeimpuls über die zugehörigen Kathodenfolger B an ihre Tore C. In der Ruhe sind alle Tore gesperrt. Zur Abtastung der Fläche werden die Zweierzählrohre nacheinander (jedes für 1 msec) durch Öffnen der beiden zueinander gehörenden Tore an die Anzeigevorrichtung angeschaltet. Die Steuerimpulse hierzu werden von einem Ringzähler D geliefert, der seinerseits von einem 1000Hz-Steueroszillator E gespeist wird.

Kommt es in dem langen Teil des auf diese Weise gerade eingeschalteten Zweierzählrohres zur Bildung einer Primärlawine, dann wird der Sägezahngenerator F angetriggert. Der Kathodenstrahl der Braunschen Röhre CRT beginnt einen Zeilenablauf, der zunächst dunkelgesteuert bleibt. Der um die Laufzeit t verzögerte Anzeigeimpuls im kurzen Zählrohr triggert über sein geöffnetes Tor einen Impulsgenerator G an, der den Kathodenstrahl momentan helltastet. Der so entstandene helle Punkt hat vom Zeilenbeginn einen Abstand, der der Entfernung Einstrahlungsort-Glasperle im Zählrohr entspricht.

Damit jedes Zählrohr des Tabletts einer lagegetreuen Zeile auf dem Bildschirm der Braunschen Röhre zugeordnet ist, wird der Kathodenstrahl synchron mit der Torumschaltung schrittweise in vertikaler Richtung bewegt. Dies besorgt ein Impulsgenerator H, der einen treppenförmigen Spannungsverlauf erzeugt. Jede Treppenstufe beginnt mit dem Öffnungswechsel zweier Tore. Nach dem Durchlaufen der 10 Stufen kehrt die Vertikalablenkung wieder in die Ausgangslage (Zeile 1) zurück. Der Treppengenerator H wird ebenfalls vom Steueroszillator E gespeist.

Die Anlage arbeitet mit folgenden Zeiten: Einschaltdauer jedes Zählrohrtores 1 msec; Dauer eines Zeilenablaufes (etwas grösser als die

maximale Laufzeit einer Zählrohrenladung) 10 μsec; Umschaltdauer von Zeile zu Zeile 0.5 μsec; Dauer des Helltastimpulses 0.1 μsec.

4. Schirmbild

Die Anzeige der Verteilung radioaktiver Strahlung durch eine dauernde Folge von

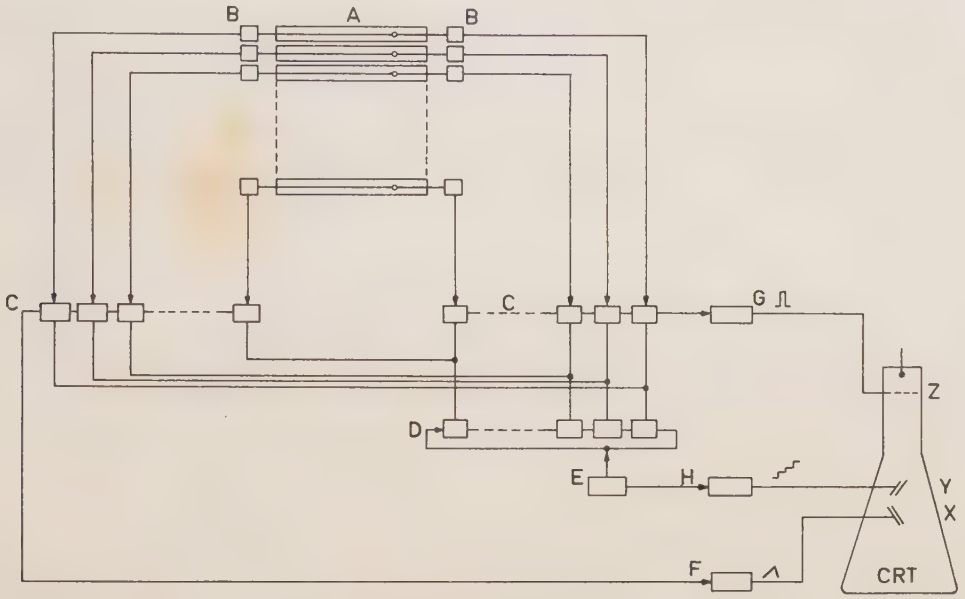

Abb. 1. Blockschaltbild. A, Zweierzählrohre; B, Kathodenfolger; C, Tor; D, Ringzähler; E, Steueroszillator; F, Sägezahngenerator; G, Impulsgenerator; H, Treppenimpulsgenerator.

Die Braunsche Röhre CRT und der Sägezahngenerator F können durch ein handelsübliches Oszilloskop ersetzt werden. Mit Ausnahme des an anderer Stelle[25]) beschriebenen Ringzählers und des Treppenimpuls-Generators H (Abb. 2) sind die Bausteine in Abb. 1 konventionell.

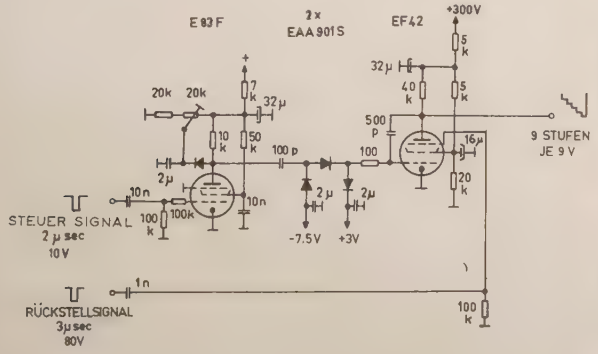

Abb. 2. Schaltung des Treppenimpulsgenerators.

Jedes Zählrohr hat eine eigene Feinregelung der Hochspannung, um kleine Unterschiede in der Ausbreitungsgeschwindigkeit der Zählrohrentladung ausgleichen zu können.

Lichtblitzen auf dem Bildschirm kann visuell unmittelbar verfolgt oder photographisch festgehalten und quantitativ ausgewertet werden. Abb. 3 gibt ein Beispiel einer Schirmbild-

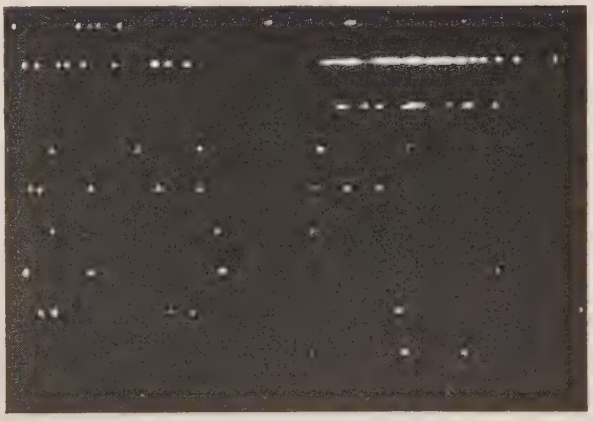

Abb. 3. Schirmbildaufnahme.

aufnahme. Dabei befand sich ein Präparat von 500 μC in der rechten oberen Ecke (Zeile 2) einer Fläche von 40 × 52 cm. Die Belichtungs-

[25]) W. Gruhle, Nuclear Instruments 3 (1958) 204.

zeit betrug 1 sec. Das örtliche Auflösungsvermögen in vertikaler Richtung ist durch den Zählrohrdurchmesser gegeben. Im vorliegenden Fall betrug er 4 cm. In horizontaler Richtung liegt die Auflösung in der gleichen Grössenordnung.

Eine falsche Anzeige entsteht dann, wenn während eines Zeilenablaufs auf das nächste Zählrohr umgeschaltet wird und dieses einen Helltastimpuls liefert. Um diesen Fall auszuschliessen, bleibt der Helltastgenerator G nach jedem Zeilenwechsel für die Dauer einer Zeilenlänge gesperrt.

Bei vorgegebener Anzahl der Zählrohre lässt sich das Auflösungsvermögen der Anlage dem jeweiligen Verwendungszweck durch Zählrohre von entsprechendem Durchmesser anpassen.

Bei Erweiterung der Anlage auf eine grössere Anzahl von Zählrohren wächst der elektronische Aufwand additiv um 6 Röhren/Zählrohr.

NUCLEAR INSTRUMENTS AND METHODS 5 (1959) 327–331; NORTH-HOLLAND PUBLISHING CO.

NUCLEAR PLATE CAMERAS FOR THE MEASUREMENT OF PROTON ENERGIES EMITTED FROM A TOROIDAL DISCHARGE IN DEUTERIUM

W. M. JONES, A. C. L. BARNARD†, K. M. YOUNG, E. D. TAYLOR, D. G. WATERS and H. B. MUNDY

Associated Electrical Industries Limited, Research Laboratory, Aldermaston Court, Aldermaston

Received 6 August 1959

Two types of nuclear plate camera used for measurement of proton energies emitted from a toroidal discharge in deuterium in SCEPTRE are discussed. One of these records energies of protons emitted normal to the discharge axis, while the other records protons emitted at about 45° or 135° to the direction of positive gas current along the axis. A later model of the second type which records at both angles simultaneously, is also described. The size of slot in the wall of the discharge vessel necessitates that the second type of camera should be very small, and should be placed close to the wall. Measures to prevent damage to the nuclear plate by shock waves or overheating are given.

The energy resolution of the cameras has also been found using a monoenergetic beam of protons from the A.E.I. electrostatic generator.

1. Introduction

The measurement of the energies of the nuclear particles emitted from the various types of equipment used in controlled thermonuclear research is of interest in helping to determine the mode of fusion which occurs.

In the case of low energy deuterons, fusion proceeds with approximately equal probability by the reactions:

$$D + D \rightarrow H^3 + n + 4\,MeV$$

and

$$D + D \rightarrow He^3 + p + 3.2\,MeV$$

(Eliot *et al.*, 1953[1])) so that, in principle, energy measurements may be carried out on any of the four reaction products. Apart from the proton energy measurements carried out in SCEPTRE, in which it was shown that the velocity of the centre-of-mass of the fusing deuterons had a velocity of about 4×10^7 cm/sec parallel to the discharge axis, (Jones *et al.*, 1958[2])) the only energy measurements which have been reported were carried out on the emitted neutrons (Rose *et al.*, 1958[3]), Hagerman and Mather, 1958[4]) and Andrianov *et al.*, 1958[5])).

Neutron energy measurements can be performed outside the discharge vessel, and the neutron energies and directions of motion are unaffected by electromagnetic fields in the discharge apparatus. The disadvantages arise from neutron scattering in the walls of the discharge apparatus and in the greater intrinsic difficulty of measuring the energy of a neutral particle. In the case of SCEPTRE III the first disadvantage is aggravated by the ½ in. water jacket which surrounds the discharge vessel. Proton energy measurement, on the other hand, is much simpler and more direct but suffers in general from the disturbance of the proton trajectories by electromagnetic fields. This effect, however, is small in SCEPTRE III where in addition it has been found possible to place nuclear plate cameras close to the wall of the torus without disturbing the discharge detectably.

The nuclear emulsion technique has been used for proton energy measurement inside SCEPTRE

† Now at the State University of Iowa, U.S.A.

[1]) Elizabeth A. Eliot, D. Roaf and P. F. D. Shaw, Proc. Roy. Soc. A **216** (1953) 57.

[2]) W. M. Jones, A. C. L. Barnard, S. E. Hunt and D. R. Chick, Nature **182** (1958) 216.

[3]) B. Rose, A. E. Taylor and E. Wood, Nature **181** (1958) 1630.

[4]) D. C. Hagerman and J. W. Mather, Nature **181** (1958) 226.

[5]) A. M. Andrianov, O. A. Bazilevskaja, S. I. Braginsky, B. G. Breznev, N. G. Kovalski, I. M. Podgorny, Yu. G. Prokhorov, N. V. Philippov, T. I. Pilippova, S. Khvaschevski and V. A. Khrabrov, Second U.N. Int. Conf. on the Peaceful Uses of Atomic Energy, A/Conf. 15/P/2301 (1958).

III and it is felt that a more detailed description of the cameras used in this work will be of interest.

2. Description of Cameras

Two types of camera have been used. The first, called type A, in which protons emitted at 90° to the discharge axis are recorded, presented few difficulties once it was found that the plate could be shielded from discharge radiation by a copper foil thin enough to transmit the protons without excessive loss of energy. In this type of camera the nuclear plate and shielding foil were set well back from the discharge, thus reducing the possibility of heat damage or shock wave rupture of the foil. In one of these cameras which has been used successfully, a 4×2 in. Ilford C2 nuclear plate is fixed about 20 in. from the discharge axis. A $2 \times \frac{1}{8}$ in. slit covered by a 0.0001 in. copper foil placed about 4 in. in front of the centre of the plate defines the direction of observation and ensures that the glancing angle of the protons at the emulsion surface is approximately 20°. A flap valve is incorporated between the defining slit and the torus and a pumping port is provided in the camera so that plates may be changed without letting the torus up to atmospheric pressure.

Two cameras of the second type, called type B, for measuring the energies of protons emitted at angles in the region of 45° and 135° to the discharge axis, were designed to fit in a long window slot $\frac{3}{4} \times 12$ in. cut in the torus wall at right angles to the discharge axis. The size of the slot dimension parallel to the discharge axis severely restricted the camera dimensions in that direction and required that it should be placed close to the wall of the discharge vessel, thereby greatly increasing the risk of damage due to overheating and shock waves.

In the first camera of this type shown in fig. 1 mounted in the torus slot, a nuclear plate 16×7 mm is held in position against a machined face and locating edge by clips bearing on its ends. The plate length is perpendicular to the plane of the figure, as is that of the 3×1 mm defining slit which is covered by a 0.005 in. thick copper foil, soft soldered in position. The camera head consists of a light shield in which the defining slit is cut, encased by a heat and electrical breakdown shield. The

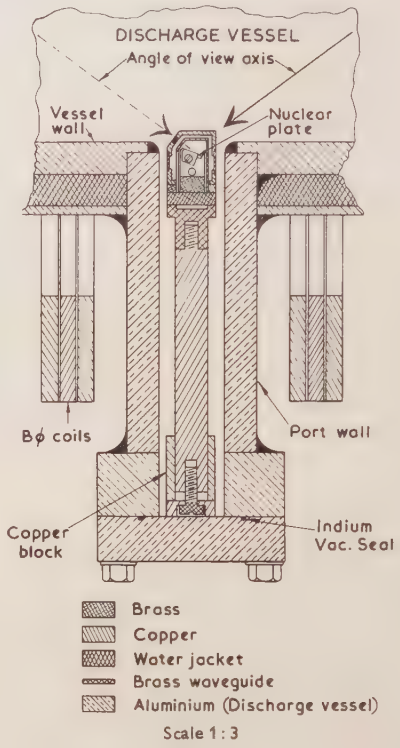

Fig. 1

light shield was constructed from a piece of rectangular brass wave guide; the protective shield, with a 11×3 mm slot cut in it, was fabricated from copper components by silver soldering. The whole projects by about $\frac{3}{16}$ in. beyond the torus walls. This composite unit, which is of fairly massive construction to assist heat dissipation, is mounted on two $\frac{1}{2}$ in. diameter copper pillars which have a sliding adjustment in a copper block which may be bolted in one of two orientations, to the window flange, depending on whether protons in the direction of the dashed or full arrow in fig. 1 are to be observed. A photograph of the arrangement is shown in fig. 2. The foil holder and protective cover are held in position on the camera body by 10 BA screws and the system is then light tight. A pumping path to the inside

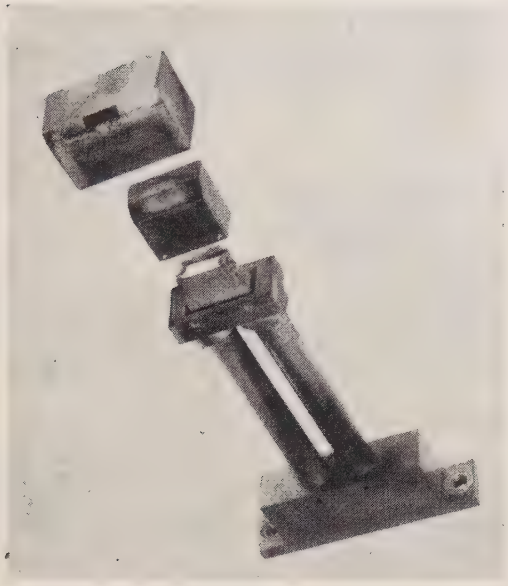

Fig. 2

of the camera is provided to equalise the pressure on each side of the foil and this path is made sufficiently tortuous to avoid any light leakage. No vacuum valve is provided so that each exposure involves the breaking of the torus vacuum. The plate is arranged to be under vacuum for at least one hour before starting the exposure in order to dry the emulsion.

A second camera, which is a development of the one just described, has also been made and used successfully. In it, two of the earlier type cameras are effectively combined by arranging two of the camera blocks shown in fig. 2 end-to-end, but facing in opposite directions, so that protons emitted at 45° and 135° to the discharge axis may be simultaneously recorded. This double camera, which accommodates two 11 × 15 mm plates, is enclosed by a foil holder and protective copper shield similar to that described for the earlier camera. The camera head is fixed by screws to a copper plate mounted on a $\frac{1}{2}$ in. stainless steel tube, which is water cooled. This tube passes out of the torus vacuum system through a seal in the flange of a loading chamber, which can be shut off from the torus by a Metropolitan-Vickers 03B vacuum valve. In this way the breaking of the torus vacuum between exposures is avoided.

3. Results

3.1. SPECIMEN RESULTS FROM EXPOSURE OF TYPE A CAMERA TO THE DISCHARGE

A histogram showing the results obtained for the energy of protons emitted from the discharge at 90° to the discharge axis in November, 1958 is shown in fig. 3. Two exposures with a total of 9000 discharges were used to obtain these results for the discharge conditions $B\phi_0 = 500$ gauss, number of primary turns = 16, deuterium pressure = 1.8 microns, condenser voltage = 25 kV and peak gas current = 75 kA. The width of the spectrum at half maximum is 150 ± 10 keV. The mean energy of the tracks shown in the figure is 3.01 ± 0.03 MeV the error being compounded of:

(a) ± 6 keV standard deviation of results.

(b) ± 10 keV estimated uncertainty in energy loss in traversing the 0.0001 in. copper foil.

(c) ± 15 keV estimated uncertainties in scanning.

(d) ± 20 keV estimated uncertainty in shrinkage of emulsion on processing.

(e) ± 15 keV error in the range energy relationship for protons in emulsion.

The errors given here refer to an absolute measurement of the energy. In the normal usage of comparing between plates observing the discharge at different angles, errors (c), (d) and

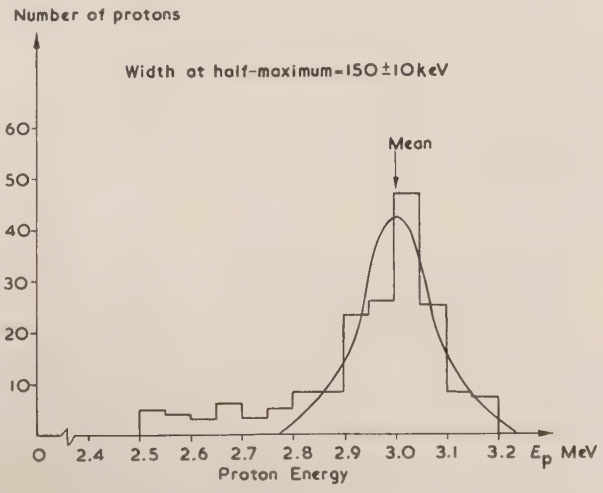

Fig. 3. Proton energy spectrum perpendicular to toroidal axis. (Conditions: $B\phi = 500$ gauss; $N = 16$, $P_{D_2} = 1.8\mu$; $V_C = 25$ kV; $I = 75$ k amp).

(e) need not be considered. In fig. 3 it can be seen that there is a fairly large excess of tracks at low energies, above the number expected for a normal distribution. A detailed consideration of the distribution seems to indicate that these tracks do not belong to a "background" extending across the distribution but rather consist of a tail due to tracks of protons of degraded energy. For this reason the mean and standard deviation of the distribution have been calculated ignoring these tracks.

3.2. SCANNING PROCEDURES

The cameras described for the measurement of proton energies at acute angles to the discharge axis were of such small dimensions that, despite the fact that they were quite accurately constructed, the dip angle of the tracks in the emulsion could not be precisely determined from the geometry of the system. The dip angle was thus determined by depth measurements in the emulsion. This procedure was adopted for the exposures made with both types of camera.

Four measurements were therefore taken for each track. These were, its position on the plate relative to a marked axis, the projected length of the track on the plane of the emulsion surface, the depth of the end of the track below the emulsion surface and the angle the projected length of the track makes with the centre-line of the plate. From these readings it is possible to estimate the small correction in energy due to the obliquity of the protons' traversal of the foil.

3.3. PROCESSING OF PLATES

Ilford C2 nuclear emulsions, in general only 100 microns thick, were used in these exposures so that the "temperature" development technique (Dilworth *et al.*, 1948[6])) was not necessary. The following processing procedure was used, care being taken to avoid excessive thermal shock which could increase emulsion distortion and hence affect the instrumental line-width.

3.3.1. Development

10–20 minutes in Ilford ID 19 developer diluted 4 to 1 at 19.5 ± 1° C.

3.3.2. Stop Bath

10 minutes in 2% acetic acid at 19.5 ± 1° C.

3.3.3. Fixing Bath

Several hours in solution consisting of 10% Kodak acid hardener and 30% saturated "hypo" solution. Initial temperature 19.5 ± 1° C.

3.3.4. Washing

A few minutes in water warmed to within 5° C below the final temperature of the fixing bath and then several hours in a bath of filtered tap water, a slow steady flow being maintained throughout.

3.4. TESTS OF CAMERAS USING MONO-ENERGETIC PROTONS

Each camera in turn was exposed to a 3.0 MeV beam of mono-energetic protons from the

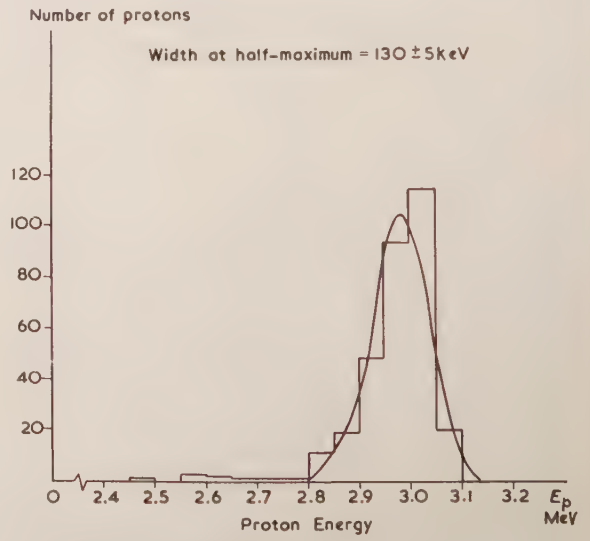

Fig. 4. Proton energy spectrum in type 'A' camera using mono-energetic protons.

A.E.I. electrostatic generator in order to find the instrumental line width of the cameras. In each case the foil was the same thickness as that used in the discharge exposures.

[6]) C. C. Dilworth, G. P. S. Occhialini and R. M. Payne, Nature **162** (1948) 102.

Figs. 4 and 5 show histograms obtained for the energy of the protons using camera type A and the first version of camera type B respectively.

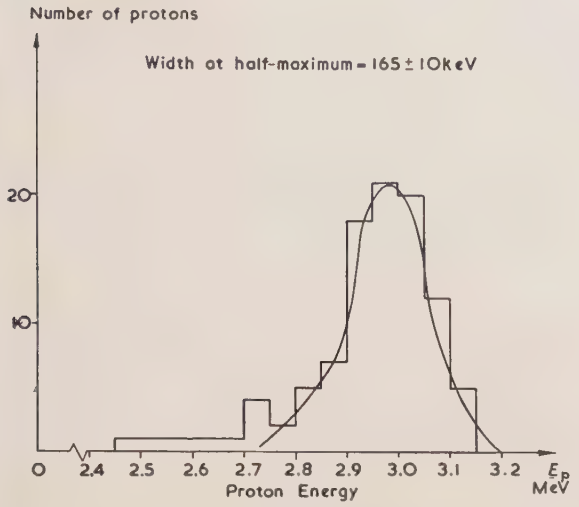

Fig. 5. Proton energy spectrum in type 'B' camera using mono-energetic protons.

The results were as follows:

Type A: Width at half-maximum = 130 ± 5 keV.

Type B: Width at half-maximum = 165 ± 10 keV.

A 0.0005 in. thick copper foil was used in the type B camera and a 0.0001 in. copper foil in the type A camera. An exposure of the type A camera without a foil produced no significant difference in line-width, thereby indicating that the thin foil used was not affecting the resolution of the camera.

Acknowledgements

The concept of measuring the proton energy differences to diagnose the mechanism of the fusion reaction was the result of discussions between Mr. D. R. Chick, Dr. S. E. Hunt and the authors. Professor J. Rotblat contributed helpful suggestions on the measurement and interpretation of the tracks.

The authors would like to thank both Miss S. J. May of this Laboratory and Miss J. Holmes of the Physics Department, St. Bartholomew's Hospital Medical College who scanned the plates.

The assistance of members of the Thermonuclear Section in particular Mr. J. E. Read in the SCEPTRE exposures is gratefully acknowledged.

Thanks are also due to Dr. T. E. Allibone, F.R.S., Director of the Research Laboratory, Associated Electrical Industries Limited, for his permission to publish this paper.

NUCLEAR INSTRUMENTS AND METHODS 5 (1959) 332–334; NORTH-HOLLAND PUBLISHING CO.

SIMPLE CORE SCALING CIRCUITS

J. C. BARTON

Northern Polytechnic, London

Received 11 August 1959

A new type of core scaler is described which requires only one transistor per stage. Details are given of a scale of ten which operates from a 6-volt supply, consumes 1.5 mW at 1000 counts per seconds, and has a resolving time of 5 μsec. It is possible to obtain a resolving time of 1 μsec with a scale of two. These circuits are not critically dependent on component values.

1. Introduction

The use of magnetic cores with rectangular hysteresis loops as the memory elements in counting circuits was first proposed by An Wang and Way Dong Woo (1950)[1]). Various circuits, using magnetic cores, have subsequently been described but the reliability of these circuits in practice proved disappointing. Recently, Franklin and James (1958)[2]) have surveyed the possible circuits and shown that, in most cases, these were dependent critically on the amplitude and length of the current pulse used to switch the cores from one remanent state to the other. They describe a circuit which avoids this difficulty but which is relatively complicated and requires two transistors per stage. The circuit described below is a simpler one which solves the problem in a different way. It uses only a single transistor and a minimum number of cores; it has proved remarkably stable in operation.

2. Basic Circuit

The essential idea of this circuit is to arrange that the cores themselves determine the length of the current pulse which switches them. This is achieved by placing the scaler components in the collector circuit of what is otherwise a conventional transistor blocking oscillator, (fig. 1). This enables a very simple circuit to be used with only a single separate winding on each core, together with a base winding which is common to both cores; the latter winding is applied after the individually wound cores have been stacked together.

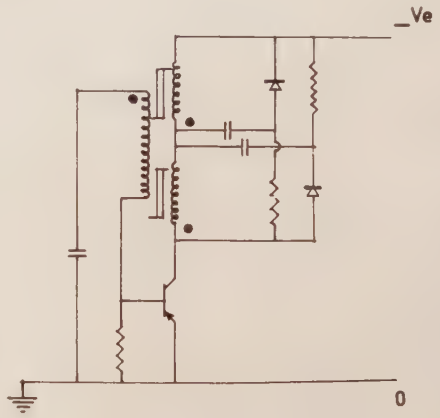

Fig. 1. Basic scale of two.

In the static state, the two cores are always magnetized in opposite directions. The only current flowing is the transistor collector cut-off current. When triggered, the circuit operates as a blocking oscillator; only the core which has to reverse its magnetisation contributes to the positive feed-back. As far as the collector current is concerned, the core which is switched presents a high impedance and the other core a much lower one. Most of the collector current is, therefore, diverted from the first core and charges a condenser via one of the diodes. As soon as the first core is completely switched, the induced voltage in the base winding rapidly falls

[1]) An Wang and Way Dong Woo, J.A.P. 21 (1950) 49.
[2]) Franklin and James, Nuclear Instruments 2 (1958) 348.

and the blocking oscillator pulse is terminated.

The condenser discharges relatively slowly through the resistance and second core, reversing its magnetisation. Thus, both cores are switched and the circuit is ready to receive the next trigging pulse. Because the circuit itself determines the length of drive pulse necessary to switch the cores, the only requirement on the trigging pulse is that it should not be long enough to disturb this action.

The same type of circuit can be used with any number of cores, although one of then will require an extra winding. The operation is always such that the main drive pulse only has to switch one of the cores, while one condenser is charged which subsequently switches the next core.

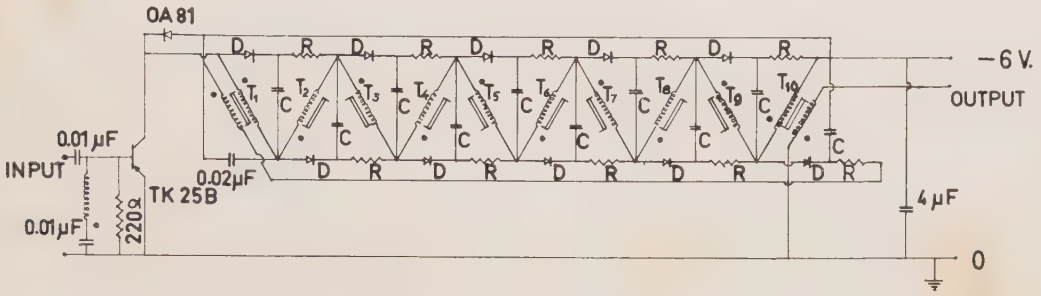

Fig. 2. Scale of ten. R: 33 Ω; C: 0.1 μF; D: OA 10; T_1–T_{10}: cores FX 1508; T_1: both windings 40 turns 47 s.w.g. Lewmex; T_2–T_{10}: 40 turns 44 s.w.g. Lewmex; T_{10}: extra winding 10 turns 47 s.w.g.; T_1–T_{10}: common winding for base circuit, 30 turns 45 s.w.g. Lewmex.

3. Guide to Design

Because of the many non-linear elements in this circuit, it is not possible to make an exact analysis. The following scheme has been evolved, partly from theoretical considerations and partly from experiments using different core sizes and component values.

1. Select the smallest practicable core size, as this minimises the power consumption.

2. Decide on required battery voltage V.

3. Choose values of C so that, when charged to 0.75 V, the stored energy W is several times the core switching energy. For Mullard 2 mm O.D. cores, (FX 1508), the switching energy is ≈ 0.1 μ joules.

Hence $$C = \frac{1.5}{V^2}\ \mu\text{F}.$$

4. Make the drive pulse length τ equal to the minimum recommended core switching time. For the FX 1508 cores, this is ≈ 1.2 μsec.

5. Choose R so that $RC \approx 2\tau$.

6. Use diodes whose forward resistance is much less than R; junction diodes meet this requirement.

7. Calculate the number of turns n from the equation: core switching voltage = diode drop + voltage on condenser.

Using the manufacturers' data for the cores, we get $0.09\ n = 0.5 + 0.75$ V.

8. Check that the drive current,

$$n\frac{\sqrt{2\ WC}}{\tau}$$

is within the transistor rating and does not lead to very large ohmic losses in the windings.

9. Use a base winding with a comparable number of turns and base components which have a time constant of about 2τ.

If the requirement 8 cannot be met, it is necessary to choose a larger value for the battery voltage.

With ferrite cores, it is obviously preferable to use fast switching transistors. For most of this work, we have used type TK 25 B, (by Standard Telephones and Cables, Ltd.,), as these have a low collector bottoming voltage for currents of ≈ 0.5 amp.

0A10 junction diodes have usually been used although their reverse impedance is unnecessarily good. It is possible to use the cheaper 0A5's, but their forward voltage drop is slightly higher.

4. Performance of Practical Circuits

Fig. 2 shows a scale of ten which has been developed with the aid of the above considerations. In addition to the components mentioned previously, there is a diode to protect the transistor from the transient at the end of the pulse and a condenser connected from the supply to the junction of the first two cores. This condenser ensures that when the circuit is first switched on, it is always the left-hand core which is magnetised in the reverse direction. In addition, for reasons which are not understood, it improves the overall performance.

An important feature of this type of circuit is that it cannot be" jammed".

As far as the circuit of fig. 2 is concerned, the battery voltage can be anything from 5 volts up to the maximum permitted for the transistor, which is 10 volts. Operation has been checked over the temperature range 0° C to 40° C. These results have been obtained using components with $\pm$ 10% tolerances.

The power consumption, using a 6 volt supply, is about 1.5 mW per 1000 counts per second. Since only a fraction of this power is dissipated in the transistor, the counting rate is not limited on this account. The resolution of this circuit is 5 μsec.

It has been found possible to obtain better resolution using the scale of two shown in fig. 3. This circuit has a rather smaller power consumption and a resolution of about 1 μsec. The improved performance is a consequence of the smaller ohmic losses as compared to the scale of ten. This illustrates the importance of choosing a wire size that will ensure optimum use of the available winding space.

These scalers can be directly coupled together. For example, two scales of ten have been connected using the output winding of one to feed via 47 Ω and 0.01 μF in series to the input of the other.

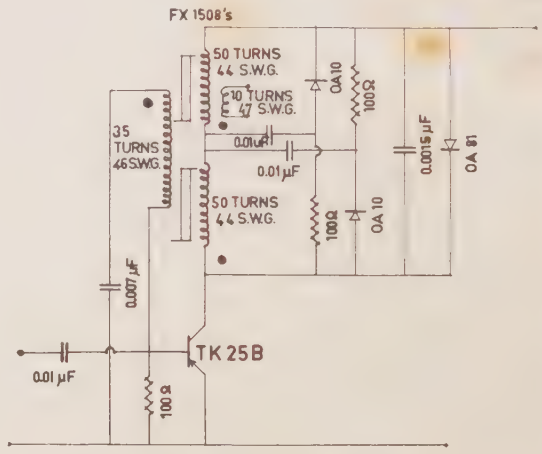

Fig. 3. High speed scale of two.

Core scalers are inherently not self-indicating and it is probable that they will be of greatest value where this is not a disadvantage. If indication is required, it should be possible to use the moving magnet system proposed by Franklin and James. Alternatively, if an output winding is added to each core, a signal is obtained on the appropriate winding when the circuit is re-set to zero. This is done by temporarily earthing the junction of T_1 and T_2 (fig. 2), either mechanically or via a transistor. For consistent operation, it is necessary to switch on this transistor rapidly and then switch it off with a decay time of a few microseconds.

NUCLEAR INSTRUMENTS AND METHODS 5 (1959) 335–336; NORTH-HOLLAND PUBLISHING CO.

STARTING UP OF THE CYCLOTRON WITH SPACE VARIATION OF THE MAGNETIC FIELD

V. I. DANILOV, YU. N. DENISOV, V. P. DMITRIEVSKY, V. P. DZHELEPOV, A. A. GLAZOV, V. V. KOLGA, A. A. KROPIN, LU NE-CHUAN, V. S. RYBALKO, L. A. SARKISYAN, A. L. SAVENKOV, D. P. VASILEVSKAYA, B. I. ZAMOLODCHIKOV and N. L. ZAPLATIN

Joint Institute for Nuclear Research, Dubna

Received 9 May 1959

In January 1959 in the Laboratory of Nuclear Problems of the Joint Institute for Nuclear Research (Dubna) the circular accelerator of the new type with azimuth and radial periodical structure of the magnetic field was put into operation. The diameter of the accelerator magnet is 1200 mm. The lines of the constant magnetic field are of the form of Archimedes spiral[1]) $r = 16.2\,\varphi$, the periodicity of the magnetic field structure is $N = 6$.

The mean value of the magnetic field increases along the radius in accordance with relativistic mass increase of the accelerating ions. As the acceleration starts in the center of the magnet the frequency of free oscillations is changed respectively from $Q_z = 0$, $Q_r = 1$ (at $r = 0$) to $Q_z = 0.2$, $Q_r = 1.01$ (at $r = 52$ cm). The working point moves through the stability region not crossing the lines corresponding to resonance frequencies. The exception is a non-linear resonance effect in the center of the accelerator. ($Q_r = 1$). This effect was investigated in detail in 1958 by using the model the magnetic field of which had the structure with periodicity $N = 4$, and a radial pitch equal to $2\pi\lambda\!\!\!^{-} = 8.47$ cm, the lines of the constant field being curved along the spiral $r = 5.4\,\varphi$ (cm).

It was theoretically shown that the necessary rise of the mean magnetic field along the radius requiring for elimination of non-linear resonance effect in the center of the accelerator reduces as $N/2^N\,(N-1)!$ with increasing N (N is the order of non-linear resonance), and as $(\lambda\!\!\!^{-}_1/\lambda\!\!\!^{-}_2)^{N-2}$ with increasing the radial pitch.

As the non-linear resonance effect at $Q_r = 1$ is equivalent to displacement of the center of instantaneous orbits with respect to the center of the magnetic field the conditions of the vertical stability were considered for displaced orbits. As a result of this consideration it was established that the shift of the instantaneous orbit centers must not exceed the value $\lambda\!\!\!^{-}$ so that the character of vertical oscillation should not be essentially changed. The analogous requirement corresponds to condition of small shifts from the resonant value of the period of particle revolution along the displaced orbit.

The results of these investigations were taken as a basis in changing the parameters of the above six spiral structure of the magnetic field with which the non-linear resonance in the center of the accelerator was not observed. The necessary variation of the magnetic field was obtained with the aid of iron shims of the rectangular cross section. The calculation of optimum shim parameters providing the necessary depth of the magnetic field variation was based on the assumption of magnetizing the shims up to the saturation. The rise of the mean magnetic field along the radius corresponding to the requirement of the constant frequency of ion rotation was obtained by means of thin cylindrical shims computed on the assumption of uniform magnetizing. To remove the effect of simple and parameter resonances ($Q_r = 1$) the shimming was made of the first and the second

[1]) D. W. Kerst, K. M. Terwilliger, K. R. Symon and L. W. Jones, Bull. Amer. Phys. Soc. **30** (1955) N1.

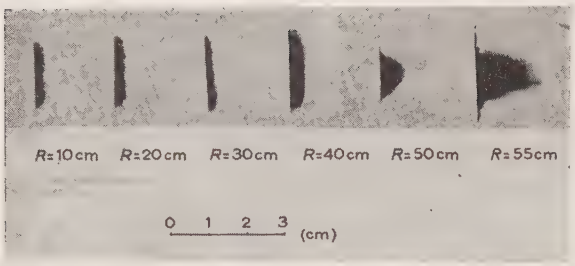

Fig. 1

harmoniques in the magnetic field structure with the aid of symmetrically placed cylinders of small diameters (8 mm). All the measurements of the magnetic field were made with the accuracy of $\pm$ 1.5 Oe by a nuclear magnetometer[2]). The time constancy of the magnetic field was provided by a nuclear stabelizer[3]).

For ion acceleration the use was made of the resonance quaterwave system with one dee. The resonance system supply was fulfilled by the generator with independent exitation providing the obtaining of the accelerating voltage up to 40 kV.

The cyclotron accelerated deutrons up to the energy of 12 MeV, α-particles up to 24 MeV when the minimum amplitude of the accelerating voltage on the dee was 8 kV. The measurement of the accelerated particle energy at the maximum radius (52 cm) was made by two methods:

(a) by measuring the mean curvature radius of the orbits by means of three probes;

(b) by measuring the accelerated deutron path in aluminium foil.

All the measurements were carried out with the intensity of the internal beam close to 1 μA; due to this fact the noticeable activity was not induced on the inner details of the chamber.

Fig. 1 represents the beam autographs at different accelerator's radii. The general view of the accelerator is shown in fig. 2.

The results of the investigations made indicate the possibility of constructing the relativistic cyclotron for the proton energy which is obtained on modern synchrocyclotrons.

[2]) Yu. N. Denisov, Pribory i tekhnika eksperim. (1958)N5
[3]) Yu. N. Denisov, Pribory i tekhnika eksperim. (1959)N1

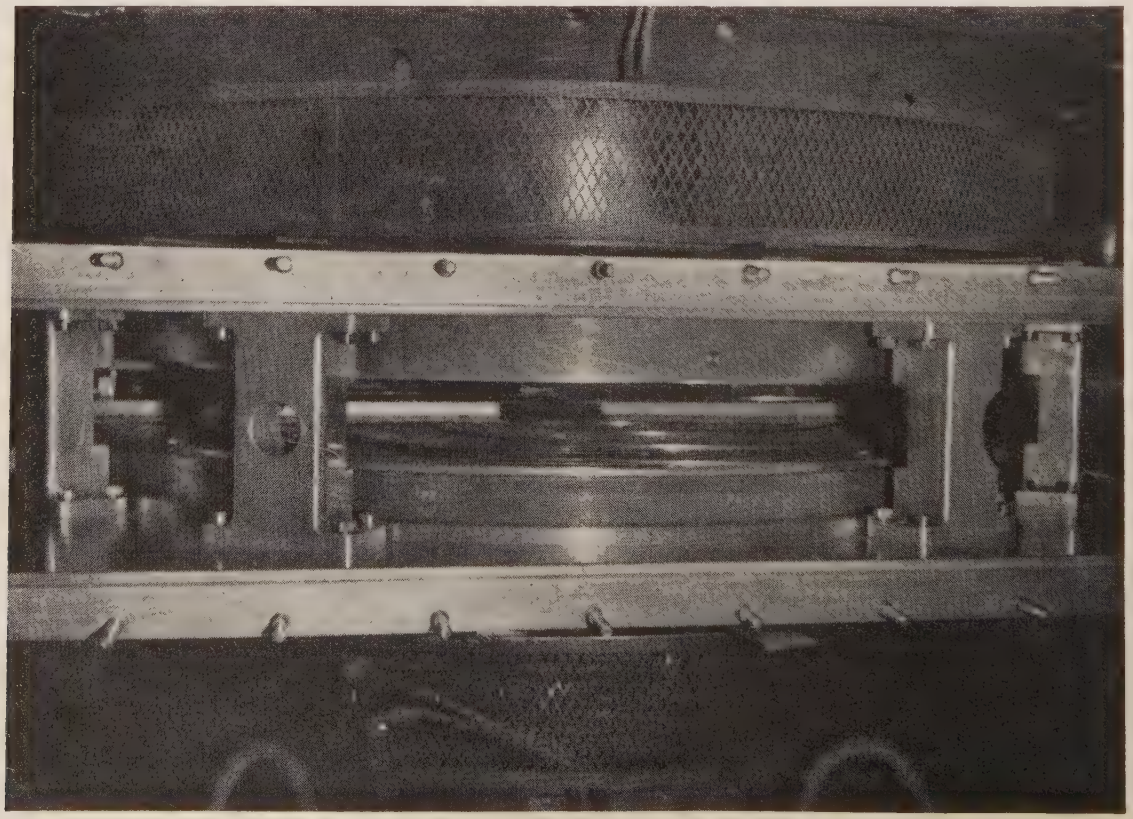

Fig. 2

NUCLEAR INSTRUMENTS AND METHODS 5 (1959) 337–338; NORTH-HOLLAND PUBLISHING CO.

WITHDRAWAL OF A BEAM OF ACCELERATED ELECTRONS OUT OF THE CHAMBER OF A CYCLICAL ACCELERATOR WITHOUT THE APPLICATION OF A LEAD-OUT DEVICE

A. A. VOROBJEV and L. S. SOKOLOV

Polytechnical Institute, Tomsk, U.S.S.R.

Received 4 February 1959

The existing methods of withdrawing an electron beam from the chamber of a betatron or synchrotron are founded on the removal of electrons out of the working zone in two stages. The first stage is the relatively slow expansioning of the electrons equilibrium orbit to the outer boundary of the working zone (translation of the orbit). The second stage is a more rapid outbound deflection of the electrons by means of electrical and magnetic fields, concentrated in a small region (withdrawal of the electrons).

In the laboratories of the Tomsk Polytechnical Institute a method of withdrawing accelerated electrons from a betatron or synchrotron was developed, by means of which they can be withdrawen in one stage, without placing any devices into the vacuum chamber of the accelerator, by one-way translation of the equilibrium electron orbit out of the range of the working zone†.

The differential equation for the movement of the electron with due regard for the non-linear focusing-force as deviation size relation can be presented as follows††:

$$\frac{\mathrm{d}^2x}{\mathrm{d}t^2} + (1 - n_0)x - \varepsilon x^3 = f_0(\tau) + f_1(\tau)\cos t\,.$$

Here x is the deflection of the electrons from the initial equilibrium orbit with the radius r_0.

n_0: the droping index of the magnetic field in the betatron along the radius on the initia equilibrium orbit (and near it);

ε: a coefficient, empirically chosen so that the function

$$F = (1 - r_0)x - \varepsilon x^3 \quad (\varepsilon \ll 1) \tag{2}$$

should sufficiently describe the relation between the real focusing forces, acting on the electron and the size of the electrons deviation from the initial equilibrium orbit. $f_0(\tau)$ and $f_1(\tau)$-functions, which describe the forces, acting on an electron in the case of a local disturbance of the controlling magnetic field in the betatron.

t: the azimuthal coordinate of the electron, $\tau = \varepsilon t$: so called "slow" time.

Equation (1) alows a rising solution which describes the oscillations of the electron with the frequency $0.5\ \omega_0$, where ω_0 is the frequency of the electrons circulation on its orbit. In equation (1) and below $\omega_0 = 1$.

The solution of equation (1) was obtained with the help of the asymptotic methods[3]).

$$x - x_0 = a\cos(\tfrac{1}{2}t + \vartheta) - h\,[1 - \varepsilon(2a^2 + h^2)]\cos t + \\ + 6\,x_0\varepsilon(a^2 + h^2) + \varepsilon\ldots \tag{3}$$

$$a = \sqrt{u^2 + v^2} \tag{4}$$

$$\vartheta = \operatorname{arc\,tg}\frac{v}{u} \tag{5}$$

† An analogical method was proposed independently by R. Wideroe, ref. [1]).

†† The working out of the movement equations in the care of a linear focusing-force as deviation-size relation is givenby Goward, ref. [2]).

[1]) CERN Symposium on high energy accelerators and pion physics, Geneva, June 1956, Proceedings, vol. 1, p.p. 155.

[2]) F. K. Groward. Proc. Phys. Soc. **61** (1948) 284.

[3]) N. N. Bogolubov and U. A. Mitropolski, Asymptotic methods in theory of non-linear oscillations. (Moscow, 1955) p. 221, 229, 276.

$$h = \frac{f_1(\tau)}{n_0 + 3\varepsilon x_0^2} \tag{6}$$

$$x_0 \approx \frac{f_0(\tau)}{1 - n_0} \tag{7}$$

$$u \approx u_0 + \tfrac{3}{2}\,\varepsilon x v_0^2 u_0 t^2 + 3\varepsilon x^2 \vartheta_0 u_0^2 t^3 + \tfrac{3}{2}\,\varepsilon \alpha^3 u_0^3 t^4 \tag{8}$$

$$v = v_0 + 2\alpha u_0 t - \tfrac{3}{2}\,\varepsilon \alpha u_0^2 v_0 - \varepsilon \alpha^2 u_0^3 t^3 \tag{9}$$

$$\alpha = \varepsilon \cdot 3 x_0 h\,. \tag{10}$$

v_0 and u_0 — initial values of v and u.

It (the solution (3) consists of the symmetrical expansion of the orbit as an addition to the value x_0, the asymetrical deviation of the orbit because of an external sinusoidal force with the frequency ω_0, radial vibrations with the frequency $0.5\omega_0$ around the deviated orbit and harmonics of higher order with a coefficient ε.

In the indicated sum the oscillations with the frequency $0.5\omega_0$ grow with the largest velocity. These oscillations are excited by the harmonic of the focusing forces with the frequency ω_0.

The reason of this excitation is that there originates such a relationship between the phase of the oscillations with the frequency $0.5\omega_0$ and the harmonic of the focusing forces with the frequency ω_0, that an oscillating electron will always move from the orbit under the effect of a smaller focusing force and to the orbit under the effect of a larger focusing force. In spite of the fact that the initial cause of the considered resonance is an external force, the immediate excitation of the oscillations depends on the periodical changing of the basic vibrational parameter n; consequently the considered resonance is parametrical.

Here n is the drooping index of the magnetic field in the accelerator on the deviated equilibrium orbit ($n \neq$ const), the focusing force is proportional to $(1 - n)$.

An analysis of the expression (3) shows that the deviated equilibrium electron orbit comes nearest of all to the outer edge of the accelerators working zone in small azimuthal ranges. In these ranges, according to the formulae (4, 5) electrons can be liberated from the influence of the focusing forces in the magnetic field with a considerable radial velocity. On other orbits, far from the point of the maximal deviation of the orbits equilibrium form, the liberation of electrons has small probability.

So if the vacuum chamber of the betatron is realized with a large enough outer diameter, larger then the diameter of the working zone, the electron beam will withdraw from the accelerator without any lead-out device in the vacuum chamber.

The electrons will come out in a focused beam, if thus hit the resonance zone with equal initial conditions (amplitudes and phases), whereby the emission angle of the beam will be the bigger the amplitude of the oscillations.

The above stated theory was satisfactorily confirmed by experiment[6]). A beam of electrons with the energy 10 MeV was lead out of a betatron constructed in the Tomsk Polytechnical Institute. Directly next to the lead-out windows the dimensions of the beam are 4×60 mm. At the distance 10 cm from the window the dimensions are 20×90 mm (the first factor is the vertical dimension of the beam, the second factor: its horizontal dimension).

The efficiency of the lead-out was 75% while the average current was 6×10^{-10} A.

The proposed method is evidently a variety of the regenerative methods[4, 5]). It is more effective and simple when used in accelerators for small and medium energies.

The authors make there sincere acknowledgements to the junior research worker of the FIAN USSR, com. I. S. Danilkin for his critical remarks regarding the form of account and the contents of this paper.

[4]) S. E. Barden, Rev. Sci. Instr. **25** (1954) 587.

[5]) K. I. Le Couteur and S. Lipton, Phil. Mag. **46** (1955) 1265.

[6]) L. S. Sokolov, News of Polytechnical Institute, Tomsk, USSR **87** (1957) 314.

BOOK REVIEWS

Proceedings of the Second United Nations International Conference on the Peaceful Uses of Atomic Energy. Vol. 8: Nuclear Power Plants. Part 1. United Nations, Geneva, p. 584, $ 14.00.

Is devoted people who are concerned with projecting, design and construction of nuclear power plants. It contains the 54 papers of the sessions on Experience with Nuclear Power Plants (G-3), Use of Nuclear Energy for Purposes Other Than Generation of Electricity (G-6) and Plans for Construction of Nuclear Power Plants (G-7).

Session G-3 reports the experience with the UK reactor Calder Hall, the French reactor G 1, the USA PWR and different reactor experiments and the Russian atomic power station.

In session G-6 which does not cover any reactors in operation is reported plans for ship propulsion. Of special interest there is the atomic ice breaker Lenin, now in operation. Further is reported stations for process and space heating. As more future projects comes proposals of non military uses of nuclear explosions.

Session G-7 deals with projects which are authorised, designed and under construction and are expected to come into operation within some years. Among them should be mentioned NPD-2, the different Stage I power reactors in UK and US power stations as Dresden, Yankee, and Enrico Fermi.

At the end of the volume is compiled a catalogue of nuclear reactors in operation with important data on power, type and main design features.

This volume should be compared to the corresponding volume 3 from Geneva '55. Power reactors as PWR and Calder Hall was then reported as projects under construction and comparison can be made with respect to predicted and acutal performance and time schedules. The volume from '55 did contain a lot of optimistic projects which have not been realized. Even this volume does contain some reactors which probably will meet the same destiny.

M. STRÅAT

Proceedings of the Second United Nations International Conference on the Peaceful Uses of Atomic Energy. Vol. 30: Fundamental Physics. United Nations, Geneva 1958, p. 329

Volume 30 of the Proceedings is devoted to Fundamental Physics. It contains 53 papers. Most of these cover the field of elementary particle physics both theoretically and experimentally. Many papers are of general interest and are written as introductions to or reviews of a chosen subject. One can find excellent papers on strange particles, pions and antinucleons and on weak and strong interactions. Some aspects of cosmic ray physics are dealt with, such as the origin of cosmic rays and the elementary particles in cosmic radiation. To mention is also a paper on nucleon structure and one on nucleogenesis by fusion processes in stars.

The developments of high energy accelerators in various parts of the world are described in seven papers as is also the development of particle detectors, especially bubble chambers. All these papers are written by leading experts.

There are also some twenty-odd papers of interest to the specialists. Most of these deal with limited detailed problems and are not of the review character expected in a volume of this kind.

GÖSTA EKSPONG

Directory of Nuclear Reactors, Vol. I, Power reactors. International Atomic Energy Agency, Vienna, 1959. Price: U.S. $ 3.50; U.K. 21/—.

Volume I of the Directory of Nuclear Reactors appeared in June 1959 as one of the first major scientific publications of the International Atomic Energy Agency. In this volume are listed actual power producers, experimental as well as fully developed, but the treatment does not include small-scale reactor experiments. In all, 36 stations are described. Because of the international character of the undertaking it has been possible to present a very comprehensive set of data with no undue emphasis on any particular national program. Further, the data are impressively up to date, some of the information being collected as late as April 1959.

The presentation of the data is very clear and as detailed as can be expected. Direct comparison between different stations is facilitated by a similar layout of the tables throughout the volume. Where information is not available, this is explicitly stated. The tables are supplemented by detailed drawings of core and fuel element geometries as well as steam cycle flow diagrams.

The reviewer noted with satisfaction that core parameters are given wherever possible. An indication of whether the parameters are based on measurements or theoretical calculations might have been of value in some cases. However, this criticism is modified by the extensive bibliography accompanying each description.

The volume is bound in such a way that the pages can be easily extracted and placed in folders. This is of particular value in view of the supplements that will be issued in the future to keep the work up to date. In an appendix the present volume contains a number of nomograms for the conversion of units.

The reviewer is convinced that the directory will prove to be of very great value to the scientists directly concerned with reactor design, as well as to persons wishing to keep informed on the general status of nuclear power development.

E. SOKOLOWSKI

Proceedings of the Second United Nations International Conference on the Peaceful Uses of Atomic Energy. Vol. 19: The use of isotopes, Industrial use. United Nations, Geneva 1958.

This "Geneva-58" volume comprises all aspects of the industrial use of radioisotopes. It covers uses of gamma and beta rays for control of various properties and tracers in all fields of industry, such as metallurgy, chemistry etc. and also applied radiation chemistry.

The volume reflects the fact that the field has grown very fast quantitatively. More than 50 papers are published here, despite the short time after the UNESCO conference 1957 (although the latter had a somwehat different character). The surveys from USA (Libby) and USSR (Topchiev) and by Spinks and Simnad give a concentrated view of the broadness of the field now and the extent of the applications. At the same time the publications show the fact that no country yet fully utilizes the isotope.

It was questioned during the conference if the industrial isotope field is still original enough. The reading of this volume shows according to the reviewer, that behind the impression of broadness there is still an apparently uninterrupted flow of methodological news which show how many variants that exist of the old principles found by Hevesy and others. To mention just a few examples: the catalysis by Kr^{85}-radiation of reactions between organic molecules (Turton), the extension of the flow rate measuring methods (Hull), the beautiful studies of weldings (Brook *et al.*), the impact of tracers on technical electrochemistry (Saito, Bozóky).

No one interested in the isotopic field, he may be an isotope specialist or an industrial user of isotopes can neglect this volume. It will take a long time for the interested reader to digest everything useful. The great number of references in many papers gives it a key function to some of the literature which is difficult to trace normally.

TORBJÖRN WESTERMARK

Turning Points in Physics. A series of lectures given at Oxford University in Trinity Term 1958, North-Holland Publishing Co. 20 shilling

This book contains the text of six lectures given at Oxford University by senior members of the University to an audience composed mainly by philosophers and scientists. The lectures deal mainly with the philosophical aspects of physical science. A. C. Crombie has written a brief introduction.

The six lectures are as follows: "The end of mechanistic philosophy and the rise of field physics" by R. J. Blin-Stoyle, "The quantum nature of matter and radiation" by D. ter Haar, "Probability enters physics" by K. Mendelssohn, "From the relative to the absolute" by G. Temple, "The decline and fall of causality" by F. Waismann and "Towards new concepts. Elementary particles" by D. H. Wilkinson. With the exception of certain problems discussed by Wilkinson there is nothing really new in this book. It deals with questions that have been subject to a great deal of discussion among philosophers and physicists during the last decades. But the authors have added to their reviews of these problems, the special touch of the outstanding expert's personal point of view. This makes their lectures very stimulating and the book can therefore be recommended to all those who take an interest in the fundamental aspects of physical science.

It is wellknown that discoveries in physics always have had a great impact on philosophy. To what extent physics can contribute to the solution of philosophical problems is a delicate question to answer. Mistakes have been made in the past. We do not know what physics of tomorrow will look like. But it will very probably be quite different from our present day concepts. It therefore seems wise to exercise a great deal of care when trying to draw more general conclusion of epistemological or logical nature from our present day picture of the physical world around us. When reading F. Waismann's lecture on causality and determinism the reviewer can not avoid feeling that a somewhat less dogmatic attitude eventually may turn out to have been wiser. However, one must admit that Waismann's point of view agrees with what seems to be the generally accepted attitude among the majority of modern physicists.

D. H. Wilkinson has given an excellent and stimulating review of our present day knowledge of the elementary particles and he calls the attention to some of the challenging problems these particles present. T. R. GERHOLM

Analytical Chemistry in Nuclear Reactor Technology. Instrumentation, Remote Control Techniques and Nucleonics (USAEC Report TID-7568 Pt 2)

This is a report containing papers presented at the Second Conference on Nuclear Technology held at Gatlinburg, Tennessee, on September 29 to October 1, 1958. As is to be expected in a publication with this title, a majority of the contributions concern the application of ordinary physical and chemical analytical methods to the special needs and conditions found in nuclear reactor work.

In the first section on instrumentation papers about potentiometric and coulometric titrations, analytical applications of radiofrequency techniques, polarography, oxide monitoring for sodium systems and X-ray diffraction are presented. This section also contains a paper by G. H. Rieck *et al.* about an automatic analysing monitor for reactor waste using combination of γ-spectroscopy and radiochemical separations.

Remote control techniques are treated in papers about the general design and operation of remote control chemical laboratories by G. A. Huft *et al.*, R. P. Larson *et al.* and U. Koskela *et al.* In other contributions special operations, as optical spectroscopy, titration etc. are described.

In the last section, with the title nucleonics, about half of the contributions describe the use of γ-spectroscopy in combination with radiochemical separations for routine analysis of radioactive materials, the remainder is about such things as determination of U^{235} by neutron activation and of boron in graphite by reactivity measurements.

K. EDVARSON

AUTHOR INDEX

Alberigi-Quaranta, A., C. Bernardini, C. Infante and I. F. Quercia, A logarithmic, constant percent error, pulse height analyzer 120
Apter, J., J. Roussel, J. M. Tissier et R. Wahl, Sélecteur 1000 canaux temps de vol 300

Barbier, M. and A. Schoch, Study of two-dimensional non-linear oscillations by means of an electromechanical analogue model, applied to particle motion in circular accelerators 211
Barnard, A. C. L., *see* Jones
Barton, J. C., Simple core scaling circuits 332
Behman, Gerald A., List of particle-accelerator installations: addenda and errata 129
Bernardini, C., *see* Alberigi-Quaranta
Birge, Robert W., Robert E. Lanou Jr., Marian N. Whitehead and Hans Courant, A new use of counter control in cloud chamber operation 161
Bjørnholm, S., Ph. Dam, H. Nordby and N. O. Roy Poulsen, A method for the preparation of cyclotron targets of rare-earth oxides by electrophoresis 196
Brown, W. L., The electron Van de Graaff in semiconductor research 234

Caldwell, Richard L. and William R. Mills Jr., Activation analysis in petroleum exploration research 312
Candy, C. J. N., *see* Chaplin
Castagnoli, C., M. Ferro-Luzzi, F. Lepri and G. Pizzella, Automatization of photometric measurements in nuclear emulsions 101
Chaplin, G. B. B. and C. J. N. Candy, A transistor circuit for fast coincidence measurements . . . 242
Chick, D. R., S. E. Hunt, W. M. Jones and D. P. R. Petrie, A Van de Graaff accelerator tube of very low retrograde electron current 205
Christiansen, Jens, Ein elektronisches Koinzidenzverfahren hoher Auflösung 115
Courant, Hans, *see* Birge

Dam, Ph., *see* Bjørnholm
Danilov, V. I., Yu. N. Denisov, V. P. Dmitrievsky, V. P. Dzhelepov, A. A. Glazov, V. V. Kolga, A. A. Kropin, Lu Ne-Chuan, V. S. Rybalko, L. A. Sarkisyan, A. L. Savenkov, D. P. Vasilevskaya, B. I. Zamolodchikov and N. L. Zaplatin, Starting up of the cyclotron with space variation of the magnetic field 335
Daum, C., A current integrator with digital output 75
De Lange, P. W., *see* Du Plessis
De Pangher, J., Double moderator neutron dosimeter 61
Denisov, Yu. N., *see* Danilov
De Vries, Hl., M. Stuiver and I. Olsson, A proportional counter for low level counting with high efficiency 111
Dmitrievsky, V. P., *see* Danilov
Dolmatova, K. A. and V. M. Kelman, A longitudinal β-spectrometer with compensated spherical aberration 269
Ducros, G., *see* Sarazin
Du Plessis, I. D., P. W. de Lange and W. Weidemann, Multirange delay line for application in beta-gamma coincidence studies 127
Dzhelepov, V. P., *see* Danilov

Elliott, David, *see* Robertson
Erman, Peter and William Parker, Vacuum deposition of uranium on thin organic backings for nuclear spectroscopic use 124

Fazzini, T., G. Fidecaro and H. Paul, A synchrocyclotron pulse simulator for testing electronic circuits 156
Ferro-Luzzi, M., *see* Castagnoli
Fidecaro, G., *see* Fazzini
Fischmann-Arbel, Arieh, Precision Schmitt trigger 56

Gabriel, R., E. L. Garwin and C. M. York, A high energy gamma ray spectrometer. 247
Garwin, E. L., *see* Gabriel
Glazov, A. A., *see* Danilov
Gruhle, W., *see* Lauterjung

Hammerschlag, M., *see* Kowalewski
Hayashi, I., *see* Suwa
Hunt, S. E., *see* Chick

Infante, C., *see* Alberigi-Quaranta

Jones, W. M., A. C. L. Barnard, K. M. Young, E. D. Taylor, D. G. Waters and H. B. Mundy, Nuclear plate cameras for the measurement of proton energies emitted from a toroidal discharge in deuterium 327
Jones, W. M., *see* Chick

Karasawa, T., *see* Suwa
Kelman, V. M., *see* Dolmatova
Kikuchi, S., *see* Suwa
King, W. G., *see* Vincent
Klein, A. G., *see* Pryor
Kockum, J. and N. Starfelt, Measurement of photonuclear absorption cross sections 37
Kolga, V. V., *see* Danilov
Kowalewski, V. J., C. A. Mayans and M. Hammerschlag, On some properties of the radio frequency ion source with longitudinal magnetic field . . . 90
Krienen, Frank, The tuningfork frequency modulator of the CERN synchro-cyclotron. Part. I General design 208

Krienen, Frank, The tuningfork frequency modulator of the CERN synchro-cyclotron. Part II. Mechanics of tuningfork 292
Kropin, A. A., *see* Danilov
Kumagai, H., *see* Suwa

Lanou Jr., Robert E., *see* Birge
Lauterjung, K. H. und W. Gruhle, Ein Gerät zur schnellen Registrierung ausgedehnter radioaktiver Strahler 323
Lepri, F., *see* Castagnoli
Loeffler, F. J., T. R. Palfrey and G. W. Tautfest, The energy dependence of the Cornell thick-walled ionization chamber 50
Lohmann, W., Apparatus for the development of nuclear emulsion plates 194
Luckey, David, The use of electrostatic generators as injectors for electron synchrotrons 266
Lu Ne-Chuan, *see* Danilov

Marin, P. C., An accurate photo-neutron standard 26
Matsuda, K., *see* Suwa
Mayans, C. A., *see* Kowalewski
Meunier, R. et J. Teiger, Circuit de coïncidence rapide à trois diodes 148
Mills Jr., William R., *see* Caldwell
Mundy, H. B., *see* Jones

Neher, Leland K., Notes on the design of glow discharge voltage stabilizers for photomultiplier tube power supplies 95
Neyret, G. et J. Parain, Les circuits correcteurs du synchrotron "Saturne" 259
Nisimura, K., *see* Suwa
Nordby, H., *see* Bjørnholm

Ogawa, H., *see* Suwa
Olsson, I., *see* De Vries

Palfrey, T. R., *see* Loeffler
Parain, J., *see* Neyret
Parker, W., An apparatus for the vacuum deposition of radio active materials 142
Parker, William, *see* Erman
Paul, H., *see* Fazzini
Paulin, A., Eine möglichkeit der Stromintensitäts- und Energieerhöhung des Mikrotrons 107
Petrie, D. P. R., *see* Chick
Pizzella, G., *see* Castagnoli
Pryor, A. W. and A. G. Klein, (Letter to the Editor) Modification to: Statistical design basis for fast scaling systems (Nuclear Instruments **4** (1959) 1) 199

Quercia, I. F., *see* Alberigi-Quaranta

Robertson, David S. and David Elliott, Magnetic losses in cores of various shapes 133
Rosenblatt, Jorge, Design of alternating gradient quadrupole lenses 152
Roussel, J., *see* Apter
Rowles, J. B., *see* Vincent
Roy Poulsen, N. O., *see* Bjørnholm
Rubin, Sylvan, Surface analysis by charged particle spectroscopy 177
Rybalko, V. S., *see* Danilov

Saji, Y., *see* Suwa
Samueli, J., *see* Sarazin
Sanada, J., *see* Suwa
Sarazin, A., J. Samueli et G. Ducros, Mesure de temps de montée d'impulsions électriques inférieures à la millimicroseconde 44
Sarkisyan, L. A., *see* Danilov
Saudinos, J., *see* Thirion
Savenkov, A. L., *see* Danilov
Schérer, M., *see* Séguinot
Schoch, A., *see* Barbier
Séguinot, J., M. Schérer et J. Teiger, Efficacité et dispersion du temps de collection de la lumière d'un détecteur de Čérenkov à parois réflechissantes 170
Slätis, Hilding, On bubble chambers (survey article) 1
Sokolov, L. S., *see* Vorobjev
Starfelt, N., *see* Kockum
Stuiver, M., *see* De Vries
Suwa, S., J. Sanada, T. Karasawa, A. Suzuki, H. Ogawa, H. Yamaguchi, Y. Saji, S. Kikuchi, H. Kumagai, I. Hayashi, K. Matsuda and K. Nisimura, Efficient beam extraction from a synchro-cyclotron at $n = 1$ 189
Suzuki, A., *see* Suwa
Szabó, P., On the optimum dimensions of collimators for neutron diffraction 184

Tautfest, G. W., *see* Loeffler
Taylor, E. D., *see* Jones
Teiger, J., *see* Meunier
Teiger, J., *see* Séguinot
Thirion, J. et J. Saudinos, Aimants de focalisation et d'analyse du cyclotron de Saclay 165
Tissier, J. M., *see* Apter

Vasilevskaya, D. P., *see* Danilov
Vincent, C. H., W. G. King and J. B. Rowles, A modification of the nuclear resonance method for measurements of non-uniform magnetic fields 254
Vorobjev, A. A. and L. S. Sokolov, Withdrawal of a beam of accelerated electrons out of the chamber of a cyclical accelerator without the application of a lead-out device 337

Wahl, R., *see* Apter
Waters, D. G., *see* Jones
Weidemann, W., *see* Du Plessis
Whitehead, Marian N., *see* Birge

Yamaguchi, H., *see* Suwa
York, C. M., *see* Gabriel
Young, K. M., *see* Jones

Zaccheroni, E., The 2.5 MW H.F. amplifier of the CERN linear accelerator 78
Zamolodchikov, B. I., *see* Danilov
Zaplatin, N. L., *see* Danilov

SUBJECT INDEX

Accelerators

The 2.5 MW H.F. amplifier of the CERN linear accelerator, E. Zaccharoni . . . 78
On some properties of the radio frequency ion source with longitudinal magnetic field, V. J. Kowalewski, C. A. Mayans and M. Hammerschlag . . . 90
Eine Möglichkeit der Stromintensitäts- und Energieerhöhung des Mikrotrons, A. Paulin . . . 107
List of particle-accelerator installations: addenda and errata, Gerald A. Behman . . . 129
Magnetic losses in cores of various shapes, David S. Robertson and David Elliot . . . 133
Design of alternating gradient quadrupole lenses, Jorge Rosenblatt . . . 152
A synchro-cyclotron pulse simulator for testing electronic circuits, T. Fazzini, G. Fidecaro and H. Paul . . . 156
Aimants de focalisation et d'analyse du cyclotron de Saclay, J. Thirion et J. Saudinos . . . 165
Efficient beam extraction from a synchro-cyclotron at $n = 1$, S. Suwa, J. Sanada, T. Karasawa, A. Suzuki, H. Ogawa, H. Yamaguchi, Y. Saji, S. Kikuchi, H. Kumagai, I. Hayashi, K. Matsuda and K. Nisimura . . . 189
A van de Graaff accelerator tube of very low retrograde electron current, D. R. Chick, S. E. Hunt, W. M. Jones and D. P. R. Petrie . . . 205
Study of two-dimensional non-linear oscillations by means of an electromechanical analogue model, applied to particle motion in circular accelerators, M. Barbier and A. Schoch . . . 211
Les circuits correcteurs du synchrotron "Saturne", G. Neyret et J. Parain . . . 259
The use of electrostatic generators as injectors for electron synchrotrons, David Luckey . . . 266
The tuningfork frequency modulator of the CERN synchro-cyclotron. Part I. General design, Frank Krienen . . . 280
The tuningfork frequency modulator of the CERN synchro-cyclotron. Part II. Mechanics of tuningfork, Frank Krienen . . . 292
Starting up of the cyclotron with space variation of the magnetic field, V. I. Danilov, Yu. N. Denisov, V. P. Dmitrievsky, V. P. Dzhelepov, A. A. Glazov, V. V. Kolga, A. A. Kropin, Lu Ne-Chuan, V. S. Rybalko, L. A. Sarkisyan, A. L. Savenkov, D. P. Vasilevskaya, B. I. Zamolodchikov and N. L. Zaplatin . . . 335
Withdrawal of a beam of accelerated electrons out of the chamber of a cyclical accelerator without the application of a lead-out device, A. A. Vorobjev and L. S. Sokolov . . . 337

Detectors

The energy dependence of the Cornell thick-walled ionization chamber, F. J. Loeffler, T. R. Palfrey and G. W. Tautfest . . . 50
Double moderator neutron dosimeter, J. de Pangher . . . 61
A proportional counter for low level counting with high efficiency, Hl. de Vries, M. Stuiver and I. Olsson . . . 111
A new use of counter control in cloud chamber operation, Robert W. Birge, Robert E. Lanou Jr., Marian N. Whitehead and Hans Courant . . . 161
Efficacité et dispersion du temps de collection de la lumière d'un détecteur de Čérenkov à parois réflechissantes, J. Séguinot, M. Schérer et J. Teiger . . . 170
Ein Gerät zur schnellen Registrierung ausgedehnter radioaktiver Strahler, K. H. Lauterjung und W. Gruhle 323

Errata

E. Gatti *et al.*, Nuclear Instruments **4** (1959) 189–201 . . . 199

Instruments and Methods for Nuclear Spectroscopy

An accurate photo-neutron standard, P. C. Marin . . . 26
Measurement of photonuclear absorption cross sections, J. Kockum and N. Starfelt . . . 37
A logarithmic, constant percent error, pulse-height analyzer, A. Alberigi-Quaranta, C. Bernardini, C. Infante and I. F. Quercia . . . 120
Vacuum deposition of uranium on thin organic backings for nuclear spectroscopic use, Peter Erman and William Parker . . . 124
An apparatus for the vacuum deposition of radio-active materials, W. Parker . . . 142
Surface analysis by charged particle spectroscopy, Sylvan Rubin . . . 177
On the optimum dimensions of collimators for neutron diffraction, P. Szabó . . . 184

A method for the preparation of cyclotron targets of rare-earth oxides by electrophoresis, S. Bjørnholm, Ph. Dam, H. Nordby and N. O. Roy Poulsen 196
The electron Van de Graaff in semiconductor research, W. L. Brown 234
A high energy gamma ray spectrometer, R. Gabriel, E. L. Garwin and C. M. York 247
A modification of the nuclear resonance method for measurements of non-uniform magnetic fields, C. H. Vincent, W. G. King and J. B. Rowles 254
A longitudinal β-spectrometer with compensated spherical aberration, K. A. Dolmatova and V. M. Kelman 269
Selecteur 1000 canaux temps de vol, J. Apter, J. Roussel, J. M. Tissier et R. Wahl 300
Activation analysis in petroleum exploration research, Richard L. Caldwell and William R. Mills Jr. . . . 312

Instruments and Methods for High Energy Physics

On bubble chambers (survey article), Hilding Slätis 1
Automatization of photometric measurements in nuclear emulsions, C. Castagnoli, M. Ferro-Luzzi, F. Lepri and G. Pizzella 101
Apparatus for the development of nuclear emulsion plates, W. Lohmann 194
Nuclear plate cameras for the measurement of proton energies emitted from a toroidal discharge in deuterium, W. M. Jones, A. C. L. Barnard, K. M. Young, E. D. Taylor, D. G. Waters and H. B. Mundy 327

Nuclear Electronics

Mesure de temps de montée d'impulsions électriques inférieures à la millimicroseconde, A. Sarazin, J. Samueli et G. Ducros 44
Precision Schmitt trigger, Arieh Fischmann-Arbel 56
A current integrator with digital output, C. Daum 75
Notes on the design of glow discharge voltage stabilizers for photomultiplier tube power supplies, Leland K. Neher 95
Ein elektronisches Koinzidenzverfahren hoher Auflösing, Jens Christiansen 115
Multirange delay line for application in beta-gamma coincidence studies, I. D. du Plessis, P. W. de Lange and W. Weidemann 127
Circuit de coïncidence rapide à trois diodes, R. Meunier et J. Teiger 148
(Letter to the Editor) Modification to: Statistical design basis for fast scaling systems (Nuclear Instruments 4 (1959) 1), A. W. Pryor and A. G. Klein 199
A transistor circuit for fast coincidence measurements, G. B. B. Chaplin and C. J. N. Candy 242
Simple core scaling circuits, J. C. Barton 332

BOOK REVIEWS

Flügge, S. (Editor), Encyclopedia of Physics, Vol. XLV, Nuclear Instrumentation II (T. R. Gerholm). . 132
Flügge, S. (Editor), Encyclopedia of Physics, Vol. 38-1, External Properties of Atomic Nuclei (T. R. Gerholm) 200
Proceedings of the Sixth Scintillation Counter Symposium (N. H. Lazar) 201
Flügge, S. (Editor), Encyclopedia of Physics, Vol. XLII, Nuclear Reactions III (T. R. Gerholm) 202
Endt, P. M. and M. Demeur (Editors), Nuclear Reactions, Vol. I, (T. R. Gerholm) 203
Rose, M. E., Internal Conversion Coefficients (T. R. Gerholm) 203
Wapstra, A. H., G. J. Nijgh and R. van Lieshout, Nuclear Spectroscopy Tables (T. R. Gerholm) 203
Proceedings of the Second United Nations International Conference on the Peaceful Uses of Atomic Energy. Vol. 31: Theoretical and Experimental Aspects of Controlled Nuclear Fusion (Lars Högberg) 203
Blanc, Daniel, Détecteur de Particules (Gunnar Bäckström) 204
Walton, G. N., Glove Boxes and Shielded Cells (W. Parker) 204
Proceedings of the Second United Nations International Conference on the Peaceful Uses of Atomic Energy. Volume 8: Nuclear Power Plants, Part I (M. Strååt) 339
Proceedings of the Second United Nations International Conference on the Peaceful Uses of Atomic Energy. Vol. 30: Fundamental Physics (Gösta Ekspong) 339
Directory of Nuclear Reactors. Vol. I: Power Reactors. (E. Sokolowski) 339
Proceedings of the Second United Nations International Conference on the Peaceful Uses of Atomic Energy Volume 19: The use of isotopes: Industrial use (Torbjörn Westermark) 340
Turning Points in Physics. A series of lectures given at Oxford University in Trinity Term 1958 (T. R. Gerholm) 340
Analytical Chemistry in Nuclear Reactor Technology. Instrumentation, Remote Control Techniques and Nucleonics (K. Edvarson) 340

Spotlight on Industry

This section appears each month and features various happenings of interest in the nuclear industrial world and objective information on products of the nuclear manufacturers. It is offered entirely as a service and all nuclear manufacturers are cordially invited to submit clearly objective and descriptive material on their endeavours and product developments for consideration for use in this section.

SCALER 1700

Isotope Developments Limited, Beenham Grange, Aldermaston Wharf, Nr. Reading, Berks., England

Specification

Scaler

The first stage employs a trochotron tube for fast counting.

This is followed by five dekatron stages.

Count Capacity. 1 000 000. Glow-tube indication.

Resolution Time. Better than 3 micro-seconds.

Counting Loss. 1% loss at 3 000 counts per second random pulses.

Electronic Timer

Capacity. 100 000 seconds in steps of 0.1 seconds. Six stages with dekatron indication.

Drive. The Timer is normally driven internally from the power supply frequency, but facilities are provided for feeding in 1 second pulses from an external clock, or 100 cycles per second from an external standard frequency.

Automatic Operation

Autocount. The Scaler may be pre-set to stop counting after recording 100, 400, 1 000, 4 000, 10 000, 40 000, 100 000, 400 000 or 1 000 000 counts. The Timer then indicates the number of seconds taken for the count.

Auto-time. The Timer may be pre-set to stop counting after an elapsed time of 10, 40, 100, 400, 1 000, 4 000, 10 000, 40 000 or 100 000 se onds. The count is then indicated by the Scaler. These automatic facilities may be switched off when not required.

Ratemeter

Ranges. 0–100, 0–1 000, 0–10 000 counts per second.

Indication. Selected by push button and indicated on the front panel meter.

Recording. Ratemeter output available to operate external Recorder.

Time constants: Short 1.5 seconds. Long 15 seconds.

Inputs

(a) *Geiger-Muller Tube.* Through 50 pF to input amplifier. HV fed to counter through 4.7 megohms.

(b) *Scintillation Counter.* Through 50 pF to input amplifier HV to counter via 22 000 ohms.

(c) *Direct.* Switched (a) negative pulse via internal amplifier; (b) positive pulse direct to discriminator or Pulse Height Analyser.

(d) *Probe Input.* Switched as for Direct Input.

(e) *External Frequency Standard.* Input from external clock or frequency standard 1 or 100 cycles per second for operating Timer. Minimum amplitude 20 volts peak pulse.

High Voltage Supply

Polarity Positive Only

Ranges. 1. "Off".

Indicated on the front panel meter:

2. 250–1 000 V, 3. 500–12000 V.

Current. Up to 1 500 volts: 0.2 mA. 1 500–2 000 volts: 0.1 mA.

Stability. 0.25% for mains change, + 5% to — 15%.

Ripple. Less than 50 mV peak to peak.

Amplifier

Gain. Switched × 10. × 100. × 1 000.

Input Impedance. 1 megohm.

Band Width. 3 dB down at 50 Kc/s and 1 Mc/s.

Stability. 1%.

Input Polarity. Negative going pulses only.

Output. 60 volts, maximum.

Discriminator

Only pulses of amplitude exceeding a pre-set bias level will be counted.

Range. 5–50 volts.

Indication. Bias level indicated on the front panel meter.

Polarity. Positive going pulses only.

Single Channel Pulse Height Analyser. Only pulses whose amplitude falls within a pre-set channel will be counted.

Channel Width. Continuously variable 1–50 volts by calibrated knob.

Threshold. Continuously variable 5–50 volts indicated on front panel meter.

Stability. For mains change + 5% to — 15%: Channel width ± 0.25 volts. Threshold level ± 0.25 volts.

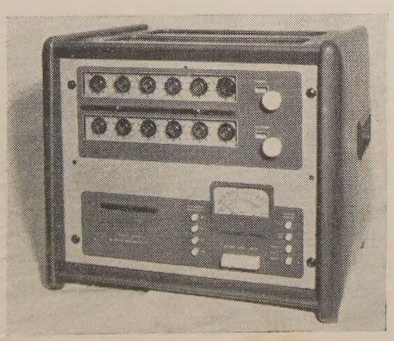

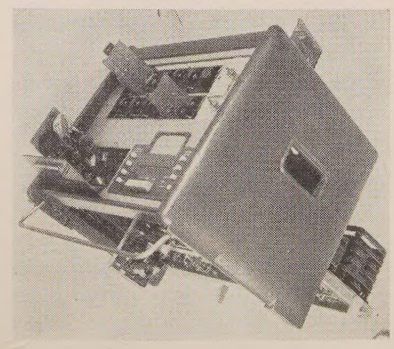

Polarity†. Positive going pulses only.

Test Facilities

A test signal is provided and can be switched direct to either first or fourth decades of Scaler and Timer.

Note†. When the discriminator or Single Channel Pulse Height Analyser is used with the in-built amplifier, the input polarity is reversed—thus becoming negative.

PARTICLE ACCELERATORS

SAMES, 99 Avenue Félix-Viallet, Grenoble, Isère, France
British Representative: Miles Hivolt Limited, Sussex, England

A

1. *Types H and V*

The type H accelerator is recommended for ion accelerators, the type V for electrons. Both can be equipped so as to accelerate electrons or ions as required.

2. *Mains voltage input power*

Power consumption 15 kVA.

3. *Electrostatic generator CD 600-5, CDS 600-5.*

Maximum voltage: 600 kV.

Maximum current at 600 kV: 5 mA.

Voltage stability (CD 600-5) medium ± 1%. (CDS 600-5) high: ± 0.1%.

Internal capacitance generator and tube: CD 600-5: 300 $\mu\mu$F. CDS 600-5: 1200 $\mu\mu$F.

4. *Accelerator tube. 4 lens*

H.F. ion source supply 100 Mc/s.

Maximum current in the beam: Ions: 1 mA.

Electrons: inside tube: 3 mA. outside tube: 2 mA.

5. *Vacuum System*

Backing pump: 450 l/mn.

Diffusion pump: 1 500 l/s at 10^{-4} mm Hg.

Refrigerated baffle.

Gauge for backing pressure: Pirani.

Gauge for high vacuum: Penning.

6. *Protective devices*

Overload and overvoltage cut-outs are provided. In case of internal sparking the voltage is automatically returned to zero and then raised again to the working value at a predetermined rate.

7. *Control panel*

Interlocks are provided in order to prevent damage due to carrying out operations in the wrong sequence.

8. *Performance*

As ion accelerator:

Reaction p/Li giving 17 Mev rays.

Reaction D/D giving 10^9 neutrons/s.

Reaction D/Be giving 2×10^{10} neutrons/s.

As electron accelerator:

Electron beam: 10^9 rad/s.

X Rays between 500 and 1000 r/s at a few cm from the target on the axis of the beam.

This accelerator is capable of supplying extremely strong radiation doses.

B

1. *General layout*

The electrostatic generator and accelerator are placed inside a pressure vessel in order to limit the overall size of the installation. The gas used is a mixture of nitrogen and freon at a pressure of 10 kg/cm² (10 atmospheres) The equipment is able to accelerate both electrons and ions as required.

2. *Mains input power*

Power consumption: 40 kVA.

3. *High voltage generator*

Maximum voltage: 1.3 MeV.

Maximum current: 6 to 8 mA.

Stability: ± 1%.

4. *Accelerator tube*

High frequency ion source supplied at 20 Mc/s.

Three lens injection.

Constant field acceleration.

Maximum beam current: 4 mA.

5. *Vacuum system*

Backing pump: 1 000 l/mn.

Diffusion pump: 3 000 l/s at 10^{-4} mm Hg.

Backing pressure measured by thermocouple gauge.

Three vacuum gauge heads.

High vacuum pressure measured by ionisation gauge.

6. *Protective devices*

As for other types of accelerator.

7. *Control panel*

As for other types of accelerator.

8. *An optical system* is provided permitting the operator to observe the ion source discharge and various ion source instruments from the remote control desk.

9. *Performance*

As ion accelerator: D/Be: 1.2×10^{12} neutrons/s.

As electron accelerator: Electron beam: 4×10^8 rad/s. Beam on anticathode: 5 000 to 8 000 r/s.

C

1. *The tube is normally horizontal, but can be supplied mounted vertically if required.*
2. *Mains input power*

Power consumption: 8 kVA.

3. *High voltage generator*

Type K 150-2.

Maximum voltage: 160 kV.

Maximum current at 160 kV: 2.5 mA.

Voltage stability: ± 1%.

Internal capacitance: 150 $\mu\mu$F.

4. *Accelerator tube. 2 lens*

High frequency ion source supplied at 100 Mc/s. The ion source power is supplied by an isolating transformer.

Maximum beam current: 1 mA.

A voltage divider is mounted outside the tube.

5. *Vacuum system*

Backing pump: 150 l/mn.

Diffusion pump: 300 l/s at 10^{-4} mm Hg.

Gauge for backing pressure: Pirani.

Gauge for high vacuum: Penning.

6. *Protection*

See accelerators type S.

7. *Performance*

D/T Reaction: The neutron output depends on the targets used. With tritium targets as supplied by certain nuclear research centers neutron rates > 10^9 neutrons/s have been attained.

D/D Reaction: 10^8 neutrons/s are obtained. (1 Curie of Radium-Beryllium = 10^7 neutrons/s).

'CLEANER' METALS FOR NUCLEAR REACTORS

Nuclear Science and Engineering Corporation, Pittsburgh 36, Pennsylvania

The development of a method, called Activation Analysis, is announced by which uranium-235 can be detected in quantities of one thousandth of one part per million parts in hafnium, zirconium, aluminum, stainless steel, graphite, and beryllium metals which are used to clad nuclear fuel elements. Also, it is possible to determine 0.005 parts per million of uranium with an accuracy of ± 5%.

The process consists of irradiating surface and interior samples of the cladding materials. These samples may consist of shavings, borings, chips, etc., which are then analyzed for uranium content by comparative neutron activation.